Novel mechanism of inhibition of the proteasome by Bruton's Tyrosine Kinase inhibitors

by

Olasubomi Atinuke Akintola

A dissertation submitted to the Graduate Faculty of
Auburn University
in partial fulfillment of the
requirements for the Degree of
Doctor of Philosophy

Auburn, Alabama
December 9, 2023

Keywords: Proteasome, Proteasome inhibitor,
BTK inhibitor, snoRNA

Approved by

Dr. Alexei Kisselev, Chair, Professor of Drug Discovery and Development
Dr. Forrest Smith, Professor of Drug Discovery and Development
Dr. Jianzhong Shen, Professor of Drug Discovery and Development
Dr. Nancy Merner, Associate Professor of Pathobiology

Abstract

Bruton's tyrosine kinase (BTK) inhibitor Ibrutinib has been shown to synergize in vitro with proteasome inhibitors (PIs) in reducing the viability of cells derived from B-cell malignancies. This synergy was also observed in cells that do not express BTK and in cells that do express BTK, synergy was observed at concentrations much higher than the concentration at which BTK activity was completely inhibited; however, the mechanism responsible for synergy is not known. We report here that an off-target effect of Ibrutinib causes synergy and another BTK inhibitor, CGI-1746, showed even stronger synergy. We reveal through inhibition of the degradation of a model substrate by a purified 26S proteasome as well as inhibition of classical fluorescent proteasome substrates and inhibition of ATP hydrolysis by the 19S subunit of the proteasome, that CGI-1746 allosterically inhibits the proteasome's ATPase and peptidase activities. We show that the inhibition of the proteasome by CGI-1746 is responsible for the synergy with proteasome inhibitors by comparing the cytotoxic mechanisms governing cell death due to CGI-1746 with FDA-approved proteasome inhibitors. We thereby demonstrate a conceptually novel mode of inhibition that may aid the development of more potent proteasome inhibitors and improve response in solid tumors clinically. We also demonstrate, using CRISPR mutated cell lines, that multi-site inhibition of the proteasome is more efficacious in reducing cancer cell viability compared to single-site inhibition and allows for significant dose reduction which may mitigate off-target adverse events. In addition, through knockdown of small nucleolar RNAs and proteomic analysis, we elucidate a previously unknown non-coding RNA mechanism that regulates proteostasis and modulates the response of cancer cells to proteasome inhibition.

Acknowledgments

To God be the glory.
I would not have been able to get here on my own. And so, I would like to say a big thank you to all the people who supported me.
To my advisor, Dr. Alexei Kisselev, for his sound mentorship throughout this program and for making me a better scientist, I'd like to say a very big "Thank You!".
To my committee members, Dr. Smith, Dr. Shen, and Dr Merner. I sincerely appreciate all the sound advice and encouragement right from the beginning.
To my family for their interest, support, and encouragement during these years.
To my friends who provided distractions when I most needed it.
To the faculty and staff of Harrison College of Pharmacy who shared their knowledge and greased the wheels of this whole process.
To the members of the lab, Sriraja, Ibby, Tyler, and Andrey. The members of the lab make or break one's graduate experience, and you made all this so much easier than it could have been otherwise. Thank you for listening, thank you for sharing, thank you for helping.

Table of Contents

List of Tables

List of Figures

List of Abbreviations

AMC	7-Amino-4-methylcoumarin
ATF6	Activating Transcription Factor 6
ATP	Adenosine Triphosphate
Bcl-2	B-Cell Lymphoma 2
BH3	Bcl-2 Homology 3
BID	BH3 Interacting-Domain Death Agonist
BIK	Bcl-2-Interacting Killer
BIM	Bcl-2 Interacting Mediator of Cell Death
BiP	Binding Immunoglobulin Protein
BTK	Bruton's Tyrosine Kinase
BTZ	Bortezomib
CFZ	Carfilzomib
CLL	Chronic Lymphocytic Leukemia
D	Aspartic Acid
DNA	Deoxyribonucleic Acid
DUB	Deubiquitinating enzyme
E	Glutamic Acid
EGFR	Epidermal Growth Factor Receptor
eIF2α	Eukaryotic Initiation Factor 2 Alpha
ER	Endoplasmic Reticulum
HA	Hemagglutinin

HSP	Heat Shock Protein
HSR	Heat Shock response
IκB	Inhibitor of NFκB
IRE1α	Inositol-Requiring Protein 1
K	Lysine
L	Leucine
M	Methionine
MCL	Mantle Cell Lymphoma
MDM2	Mouse Double Minute 2 Homolog
MOMP	Mitochondrial Outer Membrane Permeabilization
mRNA	Messenger RNA
NFκB	Nuclear Factor Kappa-Light-Chain-Enhancer of Activated B Cells
nL	norLeucine
NSCLC	Non-Small Cell Lung Cancer
PCNSL	primary central nervous system lymphoma
PERK	RNA-like ER kinase
PH	Pleckstrin Homology
PI	Proteasome Inhibitor
PIP_3	Phosphatidylinositol (3,4,5)-trisphosphate
R	Arginine
RNA	Ribonucleic Acid
ROS	Reactive oxygen Species
SC	SRC Homology

siRNA	Short interfering RNA
SYK	Spleen Tyrosine Kinase
TH	TEC homology
tRNA	Transfer RNA
Ub/Ubi	Ubiquitin
UPR	Unfolded Protein Response
V	Valine
XLA	X-linked agammaglobulinemia
Y	Tyrosine

Chapter 1: Introduction

Overview

A healthy body is a tightly controlled system that exists in perfect homeostasis. A shift in any one direction is quickly counterbalanced by signaling pathways, which restore the system to regular operation. Cancer is defined as the malignant uncontrolled proliferation of cells. This proliferation is due to genetic changes that overrule the standard checks and balances that aid cells in growing normally. In 2023, there will be approximately two million new cancer cases and over 600,000 deaths due to cancer[1]. In general, two classes of drugs are used to treat cancer: traditional chemotherapy, which disrupts the proliferation of any dividing cell in the body, and more recently, targeted chemotherapy, which specifically attacks molecules preferentially expressed by malignant cells or molecules malignant cells exhibit greater dependence on, killing these cells and sparing normal proliferating cells in the process.

The first targeted cancer therapy, tamoxifen, which targets the estrogen receptor, was approved in the 1970s[2]. Since the Human Genome Project was completed in 2003, many more cancer targets have been identified.

Nearly all the cells in the body can become malignant. This includes cells of the immune system. The most common hematologic malignancies are B-cell malignancies. In B-cells, a host of different cancers can develop depending on the stage of development at which mutations in genes controlling proliferation arise and the type of mutation. Common to these neoplasms is Bruton's Tyrosine Kinase (BTK), a protein kinase central to all the pathways important in B-cell

maturation and proliferation. Activation of BTK results in proliferation genes being switched on[3,4]. As such, BTK is an attractive target in B-cell cancers, as inhibiting BTK will result in proliferation genes being switched off[5–7]. BTK inhibitors have been approved for the treatment of relapsed mantle cell lymphoma (MCL) and chronic lymphocytic leukemia (CLL). Acalabrutinib (Calquence), zanubrutinib (Brukinsa), and pirtobrutinib (Jaypirca) are approved for relapsed MCL[8–10]. Ibrutinib was granted accelerated approval for the treatment of MCL in 2013. This approval was withdrawn in 2023[11] due to an increase in adverse events and the lack of prolongation of overall survival[12]. Ibrutinib (Imbruvica)[13], acalabrutinib (Calquence)[14], and zanubrutinib (Brukinsa)[15] are approved for CLL. These drugs are now first-line therapy in these diseases; unfortunately, they are not a cure, and patients eventually succumb to their illnesses.

Cancers can also develop in antibody-producing B-cells, called plasma cells. These cancers are called multiple myeloma[16]. Because these cells have a large load of proteins within them due to their constant immunoglobulin production, they are especially reliant on the protein quality control machinery, particularly the protein recycling plant of the cell, the proteasome[17,18]. Inhibiting the proteasome in multiple myeloma causes a buildup of proteins within the cells, eventually resulting in apoptosis[19–23]. Due to the reliance on the protein quality control machinery in multiple myeloma and cancer cells in general compared to normal cells, a therapeutic window can be exploited with proteasome inhibitors. Proteasome inhibitors bortezomib (Velcade)[24], carfilzomib (Krypolis)[25], and ixazomib (Ninlaro)[26] are approved for the treatment of multiple myeloma. However, as with BTK inhibitors, these cells either have intrinsic resistance to proteasome inhibitor treatment or eventually acquire resistance[27–31].

Combination therapies are often required to improve sensitivity and achieve complete remission in cancer[32–34]. For efficient therapy combinations, the targets of each therapy must be adequately elucidated to achieve maximum synergy. Off-target effects of drugs confound this effort and contribute to adverse events in patients. This dissertation delves into the mechanisms of BTK inhibitors' potential off-targets that explain their efficacy and elucidates the mechanism of a heretofore unknown modulator of cancer cells' response to proteasome inhibition.

Bruton's Tyrosine Kinase

Bruton's tyrosine kinase (BTK) is a non-receptor tyrosine kinase of the Tec family that is a core component of B-cell receptor signaling mechanisms that govern B-cell proliferation and survival (Figure 1.1)[35–37]. BTK was originally identified as the defective tyrosine kinase in X-linked agammaglobulinemia (XLA), one of the most frequently inherited immunodeficiency diseases[38,39]. BTK is ubiquitously expressed in hematopoietic cells, including B cells, macrophages, neutrophils, mast cells, eosinophils, and platelets. BTK activation governs signaling in various pathways such as BCR signaling, chemokine receptor signaling, TLR signaling, and FcR signaling[40,41]. These signaling pathways, once activated, lead to the activation of genes that drive B-cell proliferation and survival (Fig. 1.1).

BTK, a 659 amino acid protein consists of five domains from the N-terminus to the C-terminus: the pleckstrin homology (PH) domain, the proline-rich TEC homology (TH) domain, the SRC homology (SH) domains – SH3 and SH2, and the catalytic domain[35–37]. Each domain serves its own function. The PH domain mediates interactions with phospholipids and other proteins. The TH domain is responsible for protein activity and stability and contains a zinc finger motif. The SH3 domain contains the Y223 residue, an autophosphorylation site. Meanwhile, the catalytic domain contains two important sites - Y551, the phosphorylation site in the catalytic domain, and C481, the binding site for covalent inhibitors of BTK (Fig. 1.2)[37,42].

BTK is typically located in the cytoplasm but, when activated, can temporarily be recruited to the cell membrane[37,43]; BTK has also been found to translocate to the nucleus transiently[44]. The PH domain mediates this recruitment by binding to the phosphatidylinositol lipids (PIP_3) on the cell membrane[37]. Following translocation, BTK can be activated with two steps:

- Y551 site phosphorylation by spleen tyrosine kinase (SYK) or SRC family kinase
- Y223 site autophosphorylation, a consequence of Y551 phosphorylation, fully stimulates the kinase activity of BTK and stabilizes its active conformation.

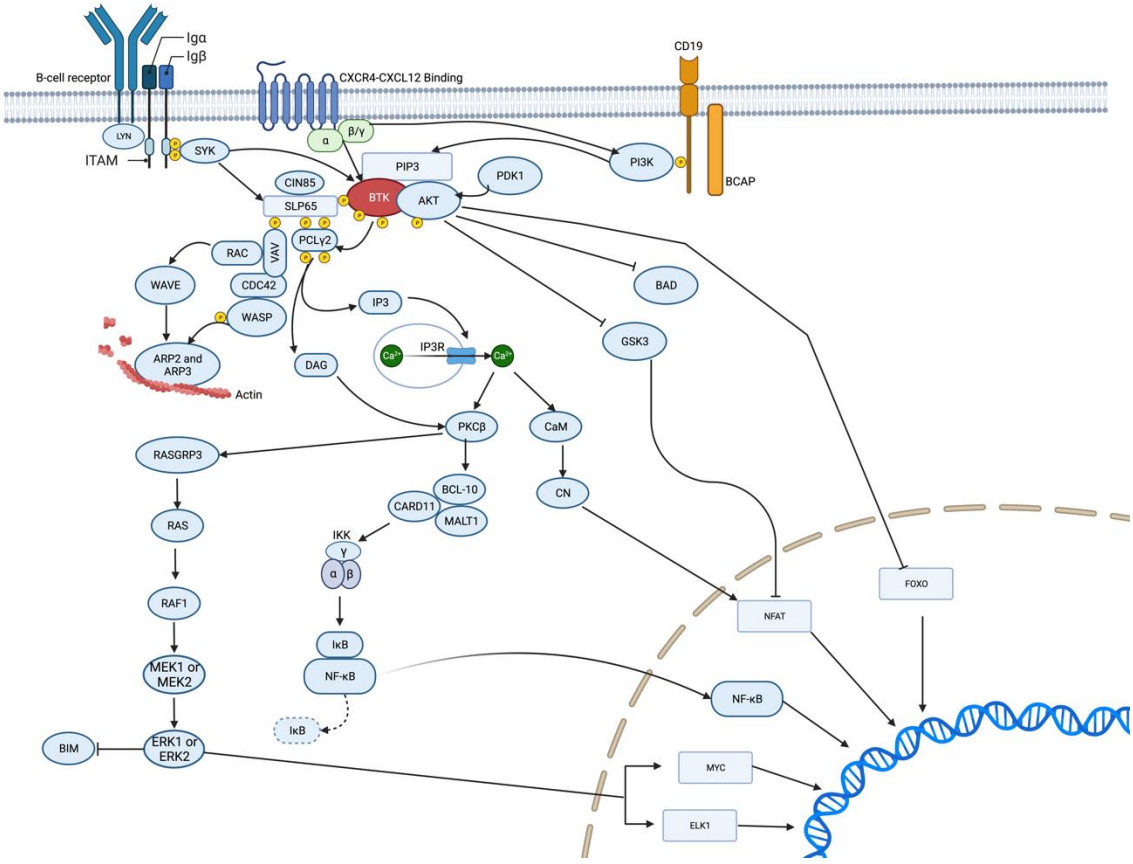

Figure 1. 1 BTK activation.
An overview of BTK activation and its downstream pathways. B cell receptor (BCR), CXC chemokine receptor 4 (CXCR4), and B-lymphocyte antigen CD19 (CD19) signaling results in the activation of BTK. Relevant to this work is BCR signaling which results in the formation of a multiprotein signaling complex that is composed of Bruton's tyrosine kinase (BTK), VAV, Phosphoinositide 3-kinase (PI3K), SH2 domain-containing leukocyte protein of 65 kDa (SLP65) and phospholipase Cγ2 (PLCγ2). Activation of PLCγ2 by BTK causes an influx of calcium ions

(Ca^{2+}) which subsequently causes the activation of the transcription factors nuclear receptor of activated T cells (NFAT) and nuclear factor-κB (NF-κB), as well as ERK1 or ERK2 activation (which activates Myc and ETS Like-1 protein (ELK1) and prevents Bcl-2 interacting mediator of cell death (BIM)-induced apoptosis) through the Ca^{2+} induced activation of calmodulin (CaM) and protein kinase C β (PKCβ). Independently of Ca^{2+}, Protein kinase B (PKB/Akt) is activated via PI3K, blocking pro-apoptotic protein BH3-only protein BCL-2 antagonist of cell death (BAD), thereby releasing it from BCL-XL and stabilizing MCL1. Akt also phosphorylates forkhead box O (FOXO) transcription factors, inhibiting their transcriptional functions. BTK activation causes the activation of Wiskott–Aldrich syndrome protein (WASP), which regulates actin polymerization, driving the generation of branched actin filaments that support cell migration associated with BCR activation. Figure created with Biorender.com.

BTK inhibitors

BTK inhibitors acalabrutinib, zanubrutinib, and pirtobrutinib, are approved for relapsed MCL[8–10], and Ibrutinib, acalabrutinib, and zanubrutinib are approved for CLL[10,13–15,45]. Other approved inhibitors are orelabrutinib (approved in China for MCL and CLL)[46], and tirabrutinib (Velexbru, ONO-4059; given orphan drug status by the FDA for primary central nervous system lymphoma (PCNSL) and approved in Japan for the treatment of PCNSL)[47]. In addition to these inhibitors, there are BTK inhibitors that are currently in clinical trials: spebrutinib (CC-292)[48], branebrutinib (BMS-986195)[49], SHR-1459[50], tolebrutinib (SAR 442,168)[51], evobrutinib (M2951)[52], elsubrutinib (ABBV-105)[53], nemtabrutinib (ARQ 531, MK-1026)[54], fenebrutinib (GDC-0853)[55,56], vecabrutinib (SNS-062)[57], rilzabrutinib (PRN1008)[58], atuzabrutinib (SAR444727)[59], remibrutinib (LOU064)[60]. There are also BTK inhibitors which have failed trials, and inhibitors which are strictly experimental tools. While some inhibitors are approved for the treatment of MCL, CLL, and PCNSL, BTK inhibitors are also in clinical trials for a range of diseases including other leukemias and lymphomas as well as autoimmune diseases such as Rheumatoid Arthritis, Multiple Sclerosis, and Myasthenia Gravis[61].

BTK inhibitors can generally be divided into two groups based on their mode of inhibition of BTK: covalent and allosteric/ noncovalent. The BTK inhibitors which have already been approved have a Michael acceptor moiety able to form a covalent bond with the conserved C481 residue in the ATP binding site. The allosteric inhibitors aim to target BTK mutations particularly those which result in the replacement of the cysteine residue at position 481 with serine and result in resistance to the approved BTK inhibitors. Allosteric inhibitors bind to a specific pocket in the SH3 domain through weak reversible reactions (hydrogen bonds or hydrophobic

interactions), forcing the enzyme to remain in an inactive conformation[61,62]. To date, only one allosteric BTK inhibitor has been approved for the treatment of relapsed or refractory MCL, pirtobrutinib (Jaypirca, LOXO-305).

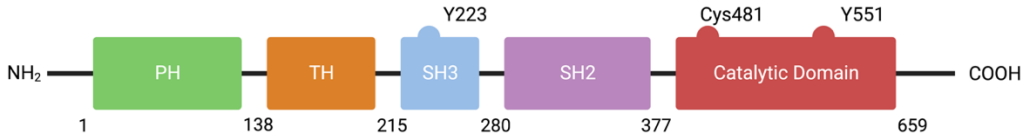

Figure 1. 2 BTK domains.
The domain organization of BTK protein. The two tyrosine phosphorylation sites are highlighted (Y223 and Y551), as well as the cysteine residue which is the binding site for covalent BTK inhibitors. Figure created with Biorender.com.

More recently, other classes of BTK inhibitors have come into play; a new BTK inhibitor has emerged – able to bind BTK through C481 in a reversible covalent manner, temporarily inactivating the enzyme. This inhibitor combines the advantages of covalent and non-covalent inhibitors while being highly potent and selective. Rilzabrutinib (PRN1008), one such inhibitor is in clinical development for Immune Thrombocytopenic Purpura (ITP)[63,64]. Additionally, proteolysis-targeting chimeras (PROTACs) targeting BTK have been developed including the first-in-human BTK degrader, NX-2127[65]. Such PROTACs typically use ibrutinib, acalabrutinib, or their derivatives as the warhead[12,66–71].

In this work, we use the two most established classes of BTK inhibitors: the covalent and allosteric inhibitors[72,73]. The covalent inhibitors we use are ibrutinib (first-in-class BTK inhibitor), acalabrutinib (which was based on ibrutinib), and spebrutinib (CC-292). The major disadvantage of the covalent inhibitors is their promiscuity in inhibiting other kinases, which, in patients, cause adverse effects as several other kinases possess C481-like residues. Ibrutinib, for example, is a potent inhibitor of epidermal growth factor receptor (EGFR)[74,75]. Acalabrutinib was actually synthesized as an improvement of ibrutinib to create a more specific inhibitor that would theoretically elucidate fewer side effects. The allosteric inhibitors we use are Fenebrutinib (GDC-0853) and CGI-1746 (strictly a research tool). These inhibitors are more specific to BTK and weakly inhibit only a few other kinases. In fact, CGI-1746 does not inhibit any other kinase at a 1μM concentration in enzymatic assays testing 205 other kinases [76]. GDC-0853, a CGI-1746 derivative is slightly less specific and is in clinical trials for the treatment of immune diseases (Fig. 1.3)[77,78].

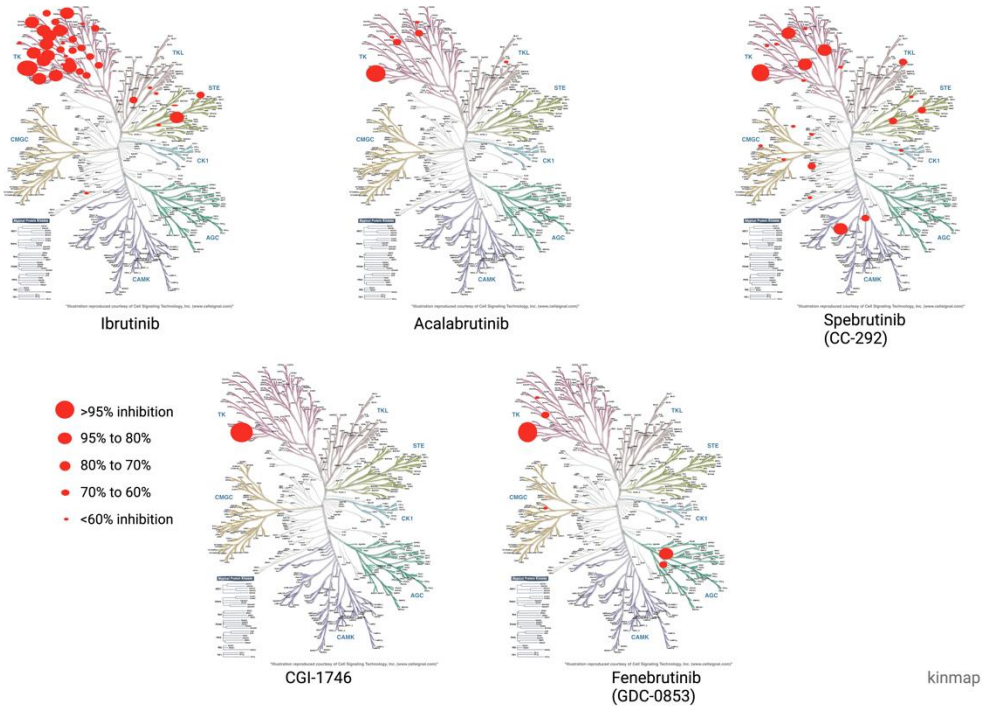

Figure 1. 3 Kinome trees denoting the selectivity of BTK inhibitors for the inhibition of BTK.

A red circle on the tree indicates the inhibition of a kinase by the BTK inhibitor based on known inhibition In the literature. The size of the red circles corresponds to the degree of inhibition of a single kinase. Kinome tree obtained from KinMap (http://www.kinhub.org/kinmap/). Figure created with Biorender.com.

The proteasome

The proteasome is a major multi-subunit protein complex responsible for maintaining protein homeostasis in mammalian cells[79–81]. The protein substrates of the proteasome are misfolded proteins or proteins that are no longer needed by the cell. The proteasome catalyzes the degradation of proteins into short peptides which are then further broken down into amino acids by other proteases. These amino acids can then be used to make more proteins. As such, the proteasome system can be described as the protein recycling factory of the cell[81].

The 20S catalytic core of the proteasome is a cylindrical structure consisting of two heteroheptameric β-rings that contain the catalytic β subunits (β1, β2, and β5) sandwiched between two heteroheptameric α-rings. The α-rings are responsible for proteasome gating and, therefore, entry of protein substrates into the core particle. The catalytic β subunits cleave polypeptides after specific residues, β1(caspase-like) cleaves after acidic residues, β2 (trypsin-like) cleaves after basic residues, and β5 (chymotrypsin-like) cleaves after hydrophobic residues. The specificity of each catalytic subunit for its substrate has allowed for the development of specific probes to study their function, and inhibitors specific for each site[81–84].

The vast majority of 20S proteasomes are catalytically inactive on their own in cells. For the small percentage of 20S proteasomes that are catalytically active, ATP hydrolysis is not required. Due to the lack of energy requirement for degradation, and the closed compartmentalized structure of the 20S core particle, constitutive proteolytic activity is limited to already denatured or unstructured proteins and small peptides.[85–87] Larger, more complex proteins are degraded

upon recruitment of activators to the 20S core to enable substrate access to the active sites, termed 'unfoldase-assisted-proteolysis'[87].

It has been shown that there are several core particle activators that cap the 20S proteasome at one or both ends, positioning the 20S gate controlled by the α-ring gating residues into an open conformation. These activators are ATP-dependent (19S particle/ PA700) or ATP-independent (PA28α and PA28β in the cytoplasm and PA200, and PA28γ in the nucleus). For the degradation of folded proteins, steps other than gate opening are necessary to allow cleavage of the substrate; substrate unfolding and translocation are two energy-dependent steps that are necessary. Therefore, ATP-dependent activators are essential.

The form of the proteasome responsible for the majority of the protein degradation in cells is the 26S proteasome which consists of the 20S core particle linked to a 19S regulatory particle (Fig. 1.4). 26S proteasomes with two 19S particles are also referred to as the 30S proteasome.

The 19S regulatory particle consists of a lid and a base. The base is in direct contact with the core particle and consists of ten subunits in total; three subunits can recognize and bind to ubiquitin chains – Rpn1 (through its toroid repeat region), the main ubiquitin receptor, Rpn10 (through Ubiquitin Interacting Motif domains, UIM), and Rpn13 (through Pleckstrin-like Receptor for Ubiquitin domains, PRU). These subunits also serve as receptors for ubiquitin-like (UBL) domains of UBL-UBA proteins and can bind substrates indirectly and so are also referred to as Ub/UBL receptors. Rpn1 also binds the UBL of the deubiquitinating enzyme (DUB) Ubp6 at a separate T2 site[88]. Rpn1 is located on top of Rpn2, and functions as a docking site for a

substrate-recruitment factor with Rpn2 interfacing with the 20S particle. In addition to these four subunits are six AAA-ATPase subunits, Rpt1-Rpt6. The ATPases are required to unfold proteasome substrates and open the channel on the α-rings before the translocation of the unfolded substrate into the core particle.

The lid component of the 19S particle comprises nine non-ATPase subunits bound to one side of the base: Rpn3, Rpn5–Rpn9, Rpn11, Rpn12, and Sem1. The main purpose of the lid is the deubiquitination of proteasome substrates by the deubiquitinating enzyme (DUB) Rpn11. Rpn11 catalyzes the deubiquitination of substrates which is coupled to substrate feeding into the catalytic core by the AAA-ATPase motor [81–84,89,90].

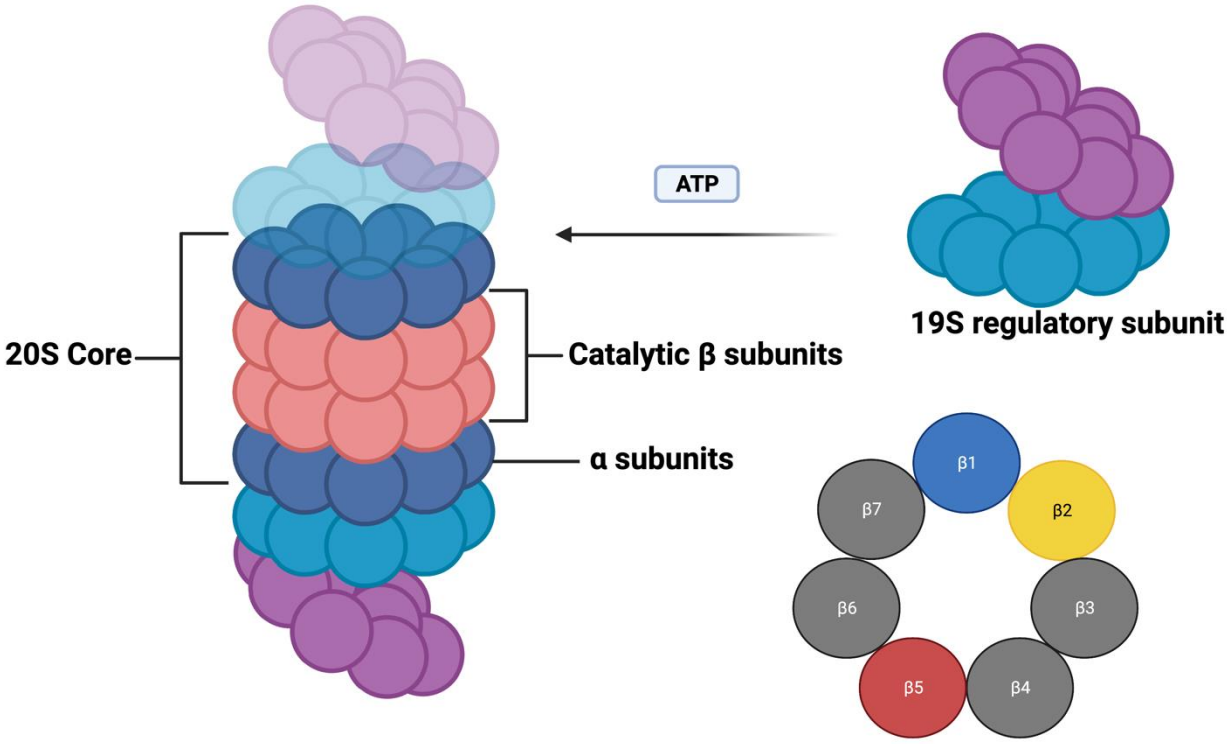

Figure 1. 4 A schematic of the structure of the 26S proteasome.
The 26S proteasome (left) consists of the 20S core – two β rings that consist of the catalytic β subunits sandwiched between two α rings that house the proteasome gate. One or two 19S regulatory subunits (top right) that house the proteasome's ATPases and non-ATPase regulatory subunits assemble onto the 20S core to form the 26S proteasome (an energy-dependent process). On the bottom right is a top-down view of one of the β rings with the catalytic subunits,β1, β2, and β5 highlighted. Figure created with Biorender.com.

Proteins that are degraded by the proteasome are marked for destruction by a signal that consists of four or more repeats of a protein, ubiquitin (Ub), attached to the protein substrate, called a polyubiquitin chain. Ubiquitin chains are attached to protein substrates (involves the formation of a covalent bond between the α-carboxyl group of the terminal glycine residue of ubiquitin, and typically, the ε-amino group of an internal lysine residue of the substrate) through an energy-dependent process involving multiple enzymes, called the ubiquitination cascade (Fig. 1.5)[91].

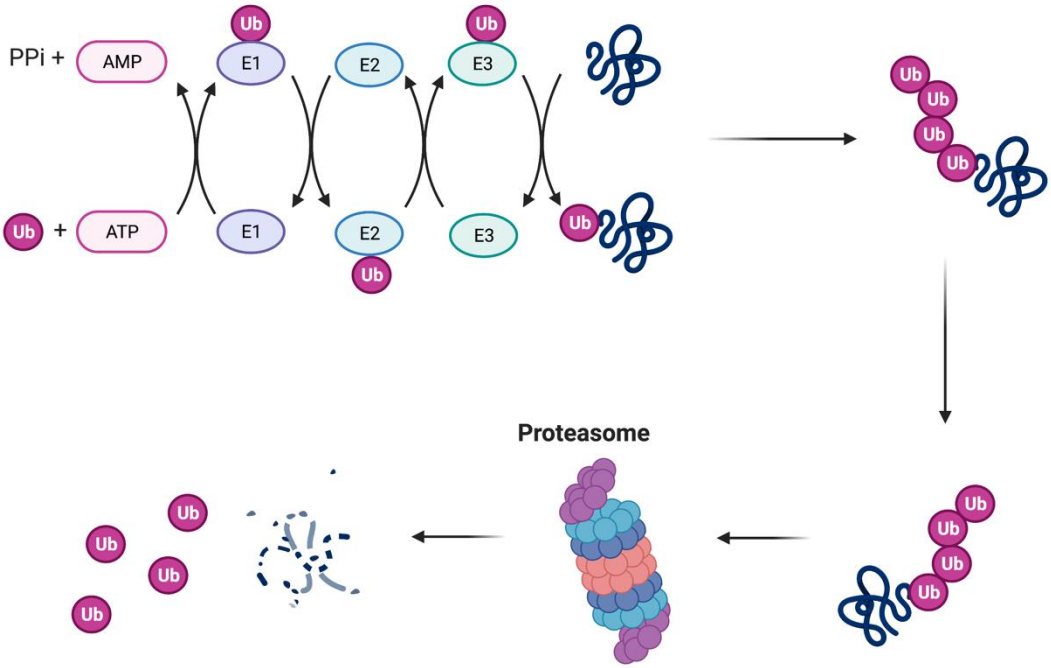

Figure 1. 5 The ubiquitination and degradation of a proteasome substrate.
Clockwise from the top-left, the ubiquitination cascade results in the ubiquitination of a proteasome substrate with at least four ubiquitin chains with lysine (K) – 48 linkages. The ubiquitinated substrate is recognized by the ubiquitin receptors of the 26S proteasome. The substrate is then deubiquitinated, unfolded, and degraded by the proteasome. Figure created with Biorender.com.

Ubiquitin is activated via an ATP-dependent process by a ubiquitin-activating (E1) enzyme and subsequently transferred to the cysteine residue in the active site of a ubiquitin-conjugating (E2) enzyme, followed by the attachment of the active ubiquitin to a substrate – a final step mediated by a ubiquitin ligase (E3). In this step, ubiquitin is transferred to the ε-amino group of a target lysine. To form a ubiquitin chain of variable length, linkage, or configuration, any of the eight amino groups of ubiquitin (M1, K6, K11, K27, K29, K33, K48, K63) can be attached to the C terminus of another ubiquitin[91–96]. Protein substrates that are marked for degradation by the proteasome are typically tagged with polyubiquitin chains with K48 linkages though substrates with K63 ubiquitin chains have also been described[97]. Ubiquitination can be reversed by more than 100 deubiquitinating enzymes (DUBs), which hydrolyze peptide bonds and result in ubiquitin deconjugation from the ubiquitinated protein[98].

Proteasome inhibition

In multiple myeloma, a cancer of immunoglobulin-producing plasma cells, there is a high protein load within cells due to immunoglobulin production[16–18]. Other types of cancer may not produce immunoglobulins. Nonetheless, cancer cells have an intrinsically higher protein load than normal cells due to a higher proportion of misfolded proteins caused by mutations or aneuploidy, hypoxia, and glucose deprivation among other factors[99–102]. Due to the critical function of the proteasome in the protein quality control machinery in cancer cells, especially when compared to normal cells, there is a therapeutic window that can be exploited by the use of proteasome inhibitors in the treatment of cancer[103,104]. Proteasome inhibitors (PIs) have been approved and are an effective treatment for hematologic malignancies like multiple myeloma and mantle cell lymphoma. The proteasome inhibitors which have FDA approval, bortezomib (Velcade),

carfilzomib (Krypolis), and Ixazomib (Ninlaro), target the β5 site of the proteasome, which is the most catalytically active site, although, at higher concentrations of these inhibitors, other sites are inhibited as well – bortezomib and ixazomib also inhibit the β1 site, and carfilzomib inhibits the β2 site[103–106]. In conjunction with our collaborators at Leiden University, our lab has developed an inhibitor specific for the β2 site of the proteasome, LU-102 (Fig. 1.6)[107–112].

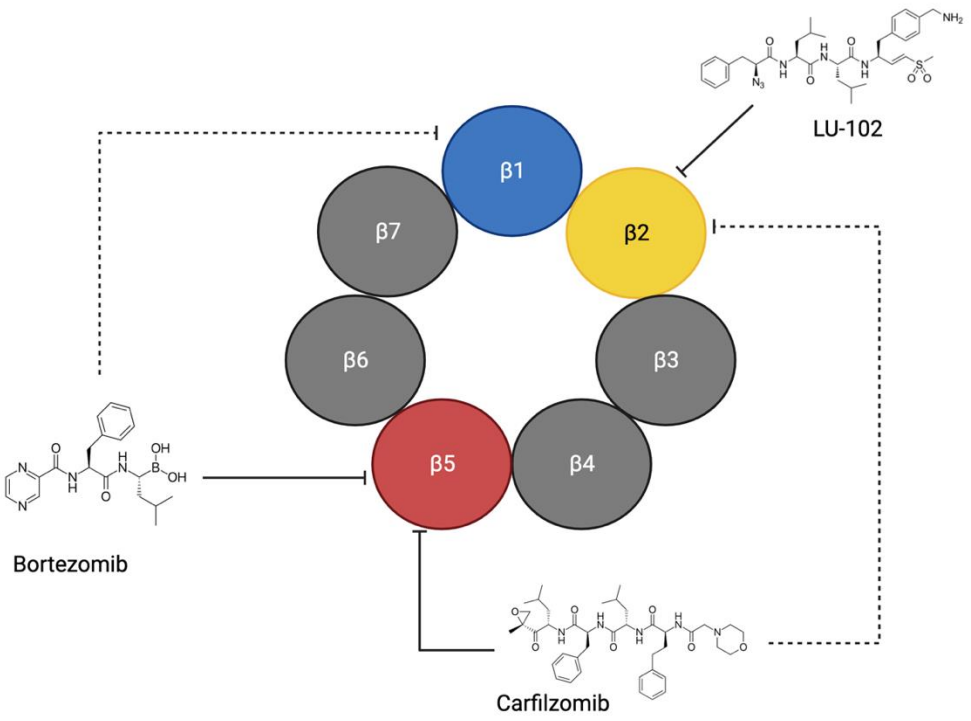

Figure 1. 6 A top-down view of the 26S proteasome's β ring and site-specific inhibitors. A top-down view of the 26S proteasome's β ring reveals the binding sites of the proteasome inhibitors discussed in this work. Bortezomib and carfilzomib, both β5 site-specific inhibitors also inhibit other sites at high concentrations, bortezomib β1, and carfilzomib β2. LU-102 is considered specific for the β2 site of the proteasome. Figure created with Biorender.com.

Mechanisms of anti-neoplastic activity of proteasome inhibitors

As mentioned above, the ubiquitin-proteasome system (UPS) is the major protein quality control mechanism within the cell. As a result, proteasome inhibition is pleiotropic in nature. Several different mechanisms result in cancer cell death due to proteasome inhibition.

Inhibition of NF-κB

Proteasome inhibitors were first developed in an effort to mitigate cancer-related cachexia (weight loss as a result of muscle wasting) due to the role of the UPS in protein turnover in a wasting muscle[113–115]. The interest in their potential as chemotherapeutics was piqued by the emergence of studies showing that small-molecule proteasome inhibitors induced apoptosis in cultured cell lines and murine cancer models. One of the early hypotheses driving the study of proteasome inhibitors as chemotherapeutic agents was the inhibition of NF-κB signaling[116–120]. NF-κB is a transcription factor that regulates the expression of cytokine, chemokine, and other genes, regulating inflammation, immune response, cell survival, proliferation, and apoptosis. Normally, a family of inhibitors called IκBs sequester NF-κB dimers in the cytoplasm. NF-κB inhibitor, IκB, is a substrate for degradation by the proteasome. Stimulation causes phosphorylation and subsequent ubiquitination of IκB, leading to IκB degradation[121]. Proteasome inhibitors cause the buildup of IκB, thereby preventing nuclear translocation of NF-κB. Inhibition of the proteasome means IκB is not degraded and continues to constitutively inhibit NF-κB causing down-regulation of the genes activated by NF-κB including genes involved in cell proliferation, invasion, metastasis, and angiogenesis. This rationale led to the development of bortezomib, a first-generation proteasome inhibitor in 1994 which then gained FDA approval for the treatment of relapsed or refractory multiple myeloma in 2003.

Though the NF-kB pathway was initially thought to be main mechanism by which proteasome inhibitors exerted their anti-cancer activity, since the pathway plays a role in cell proliferation, invasion, metastasis and angiogenesis, a potent IκB kinase inhibitor, PS-1145, that blocks NF-kB activation by inhibiting IκB phosphorylation and subsequent degradation, was found to not elicit the cellular toxicity profile of proteasome inhibitors, suggesting other mechanisms are equally, if not more responsible for causing toxicity in cancer cells[120,122].

Depletion of free ubiquitin and amino acids

Inhibition of the proteasome means proteins tagged for degradation with ubiquitin chains are not degraded. Despite the action of deubiquitinases (DUBs), the majority of these proteins will continue to be tagged with polyubiquitin. Given that a product of protein degradation is recycled ubiquitin which then becomes available for use within the cell, inhibition of the proteasome causes depletion of free ubiquitin in the cell which can signal apoptosis. It has been shown that ubiquitin overexpression rescues cells from death under conditions in which free ubiquitin is normally depleted[123]. In a similar vein, the degradation of unneeded and misfolded proteins by the proteasome replenishes the store of free amino acids available to the cell for additional protein synthesis. Inhibition of the proteasome causes depletion of this store of amino acids which has been shown to lead to the induction of signaling of both the integrated stress response and autophagy; failure of both to replenish the amino acid store leads to cell death[124].

Accumulation of BH3-only proteins

The fate of a cell hinges on the ratio of pro-apoptotic signaling to anti-apoptotic signaling. A higher proportion of anti-apoptotic signals pushes the cell toward survival, while a higher

proportion of pro-apoptotic signals pushes the cell toward death. These signals are governed by the Bcl-2 family of proteins that serve as sensors of cellular conditions that determine cell fate[125]. Of the Bcl-2 family, there is a subset of proteins that contain only a Bcl-2 homology 3 (BH3) domain. These are pro-apoptotic proteins called BH3-only proteins. Under normal cellular conditions, Bcl-2 anti-apoptotic proteins are bound to BAX and BAK, effectors of apoptosis which exert their effects by pore formation in the mitochondrial outer membrane causing mitochondrial outer membrane permeabilization (MOMP) thus causing the release of cytochrome c from the mitochondria and caspase activation (apoptosis). Anti-apoptotic proteins of the Bcl-2 family sequester BAX and BAK and prevent them from exerting their effects[126]. Pro-apoptotic BH3-only proteins such as BIM, BIK, BID, or NOXA compete with BAX and BAK for interaction with anti-apoptotic Bcl-2 proteins and cause the release of BAX and BAK, allowing them to effect apoptosis. BH3-only proteins are regulated by rapid ubiquitination and degradation, interference with their degradation causes their accumulation, out-competing the sequestration of BAX and BAK, thus promoting apoptosis[127–129]. Inhibition of the proteasome causes these proteins to accumulate, triggering caspase activation and cell death[130,131].

Stabilization of p53

The expression of p53, a known tumor suppressor, regulates apoptosis, senescence, and cell cycle progression. p53 stabilization is important in inducing cell death under diverse circumstances. p53 is normally regulated by polyubiquitination by the ubiquitin ligase, MDM2, and subsequent proteasomal degradation. Inhibition of the proteasome causes stabilization and accumulation of p53 leading to cell death[132]. A lot of cancers are deficient in p53 however, due to mutations that result in p53 losing its ability to check progress through the cell cycle, block the

proliferation of cancerous cells, and induce apoptosis[133]. In these cancers, other mechanisms of cell death due to proteasome inhibition take precedence.

Endoplasmic reticulum stress, heat shock response, and the unfolded protein response

Proteins are synthesized on ribosomes in the cytosol; however, the endoplasmic reticulum (ER) is where most secretory protein folding and assembly occurs before either being retained in the ER for ER-resident proteins or translocated out of the ER[134–136]. Cancer cells, in general, and multiple myeloma, in particular, in which plasma cells produce large quantities of immunoglobulins, produce high amounts of misfolded proteins, resulting in a high protein burden for the ER. Misfolded proteins in the ER that cannot be properly folded are targeted for degradation by the proteasome[137–140]. Protein chaperones assist in the folding of proteins. A subtype of protein chaperones called BiPs are normally bound to ER-resident stress sensors, part of the native ER a quality control mechanism to monitor for misfolded proteins. These ER-resident stress sensors: are inositol-requiring protein 1α (IRE1α), protein kinase RNA-like ER kinase (PERK), and activating transcription factor 6 (ATF6). These sensors mediate adaptive responses that maintain proteostasis through both transcriptional and non-transcriptional responses, causing changes in protein synthesis and the secretory pathway, including protein folding, ribosome biogenesis, ER-associated degradation (ERAD), protein entry to the ER, and autophagy among others[141–144].

When the cell produces large amounts of misfolded proteins, the ER becomes stressed. This ER stress initiates the unfolded protein response (UPR). BiPs which are normally bound to the ER-resident stress sensors are released and bind to misfolded proteins, causing activation of the

stress sensors, in turn, activating intracellular signal transduction pathways to maintain proteostasis in the ER by reducing protein synthesis, a pro-survival mechanism.

Of note with proteasome inhibitor-based therapy, is the PERK arm of the UPR. BiP dissociation from PERK results in the autophosphorylation of PERK, activating it. Activated PERK phosphorylates the eukaryotic initiation factor 2 alpha (eIF2α). eIF2α is a subunit of the eIF2 complex that catalyzes the binding of methionyl-tRNA (Met-tRNA$_i$), the translation initiator tRNA, to the 40S ribosome subunit, thus initiating protein translation. Phosphorylation of eIF2α deactivates the protein causing inhibition of translation. Thus, eIF2α phosphorylation is considered an adaptive response of cells to excess protein load, such as occurs with proteasome inhibition[145–149]. Alternatively, the UPR can cause cell cycle arrest and induce apoptosis, when ER protein load and thus, ER stress cannot be mitigated[150–152]. Proteasome inhibitors prevent the degradation of misfolded, ubiquitinated proteins. The accumulation of misfolded proteins in the ER causes increasing ER stress and activates the UPR, causing cell cycle arrest, and the cell undergoes apoptosis as a result[153].

Another cytoprotective stress response involving protein chaperones is the heat shock response (HSR). The HSR is governed by heat shock factor (HSF) proteins, which are transcription factors that, when activated, result in the upregulation of heat shock proteins (HSPs). HSPs, so named as they were first discovered as a cellular defense mechanism against heat shock in Drosophila, are molecular chaperones that assist in protein folding when the cell undergoes stresses, including heat, cold, ultraviolet light, starvation, hypoxia, and oxidative damage[154–156]. HSPs have been found to be upregulated by proteasome inhibition. Proteasome inhibition causes the

accumulation of misfolded proteins to which HSPs bind to assist in folding. In this way, chaperone upregulation is an attempt to relieve the misfolded protein load in cells. Failure of this mechanism to restore protein homeostasis leads to apoptosis[157–159].

Generation of reactive oxygen species (ROS)

Treatment of cancer cells with proteasome inhibitors results in the generation of reactive oxygen species (ROS). Though catastrophic protein load and the failure of pro-survival mechanisms to relieve that load are thought to be the main mechanisms that cause death in multiple myeloma, the generation of ROS is believed to be the mechanism that causes cell death in other cancers, including mantle cell lymphoma (MCL) for which proteasome inhibitors are approved as a treatment. Mitochondrial impairment, leading to ROS generation, has been shown to be a consequence of treatment with proteasome inhibitors in Chinese Hamster Ovary (CHO) cells and in non-small cell lung cancer (NSCLC)[160,161]. ROS scavengers and inhibitors have been shown to prevent proteasome inhibitor-induced cell death[162].

Despite the clinical success of proteasome inhibitors in the treatment of multiple myeloma, and although there is evidence that other solid tumors may be candidates for proteasome inhibitor therapy, proteasome inhibitors are still only used in the clinic for hematologic malignancies. Even in hematologic cancer patients, some cancers have innate resistance to proteasome inhibition. In addition, it is almost inevitable that cancers previously sensitive to PIs acquire resistance to PI therapy, causing relapse, which is associated with a worse prognosis.

Overcoming intrinsic and acquired resistance to proteasome inhibitor therapy

Various mechanisms have been documented by which cancers become resistant to proteasome inhibitor therapy. Notably, efforts to replicate the cause of resistance in vitro do not directly mirror the mechanisms reported in multiple myeloma patients. For example, treating multiple myeloma cells in vitro according to the same treatment regimen for patients in the clinic may lead to resistance to PI therapy due to mutations of the binding site of the PI on the β5 subunit of the proteasome. However, no such mutations have been seen in patients.

Mechanisms by which cells are resistant to proteasome therapies include:

(i) **Increasing the expression of efflux pumps** – Efflux pumps are an enormous contributor to multi-drug resistance in cancer and other therapies. Efflux pumps allow regulation of the cellular internal environment. Some cancer cells overexpress these pumps, expelling chemotherapeutic drugs out of the cell, and leading to multi-drug resistance. Efflux pumps in cancers are generally multi-drug resistance proteins (MDR, P-glycoprotein/Pgp) and multi-drug resistance-associated proteins (MRP)[163]. It has been shown that overexpression of MDR and Pgp causes resistance to proteasome inhibitors in multiple myeloma and other cancers[164–166]. Blocking these efflux pumps is also able to resensitize resistant cells to proteasome inhibitors[167].

(ii) **Altered apoptotic protein accumulation** – It has been shown that in hepatocellular carcinoma cells resistant to proteasome inhibitors, upon treatment with bortezomib, these cells fail to accumulate pro-apoptotic BH3-only proteins[168], accumulation of which is one of the mechanisms through which proteasome inhibitors exert their cytotoxic effects. Resistant multiple myeloma

cells also increase the ratio of antiapoptotic Bcl-2 proteins to proapoptotic Bcl-2 proteins which suppresses apoptosis upon proteasome inhibitor treatment[169].

(iii) **Increased protein chaperone expression** – Accumulation of misfolded proteins and the resulting stress response-induced apoptosis is the main mechanism of death in multiple myeloma cells treated with proteasome inhibitors. Cells resistant to proteasome inhibitors have been shown to have an increased expression of protein chaperones and more efficient protein folding which reduces the build-up of misfolded proteins by proteasome inhibitors[170–172]. Inhibitors of protein chaperone activity have been shown to overcome resistance to proteasome inhibitors in resistant cells[173,174].

(iv) **Increase in autophagy** – The ubiquitin-proteasome pathway is the major pathway of protein quality control in mammalian cells. Another pathway involved in protein quality control is the autophagic pathway. It has been shown that proteasome inhibition in cells causes the induction of autophagy as a compensatory mechanism[175–178]. Cells that are resistant to proteasome inhibitors are more reliant on autophagy as the main mechanism for protein quality control. Dual targeting of the proteasome and autophagy overcomes the resistance to proteasome inhibition[179–181].

(v) **Increase in antioxidant levels** – One of the mechanisms by which proteasome inhibitors exert their cytotoxic effects is the generation of ROS as a result of mitochondrial impairment. Cells that have been made resistant to proteasome inhibitors have been shown to upregulate the pathways that fuel the generation of glutathione, pyruvate dehydrogenase (PDH), and NAD(P)H, thereby increasing

antioxidant capacity. Furthermore, these cells also have increased expression of nuclear factor erythroid 2-related factor 2 (Nrf2), the transcriptional regulator of antioxidant responses in cells[171,172,182–184]. Targeting redox has been shown to overcome proteasome inhibitor resistance in multiple myeloma[185].

(vi) **Increase in cell survival signaling** - Interleukin-6 (IL-6) activates many cell survival and proliferation signaling pathways in multiple myeloma. Its overexpression has been shown to induce resistance in multiple myeloma[186,187]. This resistance mechanism has been attributed to the ability of IL-6 to reestablish intracellular redox homeostasis[188]. Inhibition of IL-6 signaling has been shown to enhance the cytotoxic activity of proteasome inhibitors in multiple myeloma[189]. The hepatocyte growth factor HGF/c-MET (HGF's receptor tyrosine kinase) axis hyperactivation is associated with multiple myeloma pathogenesis (cell motility survival and proliferation) and resistance to proteasome inhibitors[190]. c-MET inhibitors have been shown to overcome drug resistance in multiple myeloma both in vitro and in clinical trials[191–193]. NF-κB inhibition by proteasome inhibitors was the reason behind the development of proteasome inhibitors for the treatment of cancer, as a means to block cancer cell proliferation. It has been reported that constitutive NF-κB activity renders multiple myeloma cells resistant to high doses of proteasome inhibitors[194]. The phosphoinositide 3-kinase (PI3K)/ protein kinase B (AKT) / mammalian target of rapamycin (mTOR) pathway activation in multiple myeloma leads to the increased transcription of genes that drive proliferation and survival and protects against apoptosis, causing resistance to chemotherapy. Inhibition of this pathway impedes myeloma proliferation and

sensitizes cells to proteasome inhibitors[195–197]. Tight junction protein 1 (TJP1) has been reported to modulate proteasome capacity and proteasome inhibitor sensitivity in multiple myeloma by suppressing epidermal growth factor (EGFR) / Janus kinase (JAK) / signal transducer and activator of transcription (STAT) signaling by suppressing the expression of proteasome subunits and so TJP1 is a sensitizer of multiple myeloma cells to proteasome inhibition[198]. Therefore, lower levels of TJP1 and more EGFR/JAK/STAT signaling indicate resistance to proteasome inhibitors.

(vii) **Changes in the bone marrow microenvironment** – multiple factors consist of the niche that is the multiple myeloma microenvironment. Soluble factors such as interleukin-6 (IL-6)[199,200], vascular endothelial growth factor (VEGF)[201,202], hepatocyte growth factor (HGF)[203,204], insulin-like growth factor 1 (IGF-1)[205,206], interleukin-8 (IL-8)[207], and stromal cell-derived factor 1 (SDF-1)[208,209] are upregulated in multiple myeloma and are secreted into the microenvironment, upregulating pathways which inhibit apoptosis, promote vascular permeability, invasiveness, migration, and adhesion[210]. Cell-adhesion factors include adhesion interactions with bone marrow stromal cells through intercellular adhesion molecule-1 (ICAM-1), CD38, vascular cell adhesion molecule-1 (VCAM-1), lymphocyte function-associated antigen-1 (LFA-1), mucin-1 antigen (MUC-1), and various integrins[211–214]. These adhesion interactions increase in multiple myeloma cells resistant to proteasome inhibitors; a consequence of this increase is the upregulation of PD-L1[215], increasing proliferation and resistance to immune responses. Other factors that change the bone marrow microenvironment are

microRNAs (miRNAs), exosomes, and cancer-associated fibroblasts. Altered miRNA expression in the microenvironment is associated with increased cell survival signaling in multiple myeloma[216,217]. Contents of exosomes from resistant and sensitive multiple myeloma cells and bone marrow stromal cells have been shown to differ, with exosomes from resistant cells able to activate cell survival pathways and downregulate apoptosis[218–220]. Cancer-associated fibroblasts parallel the disease – cancer-associated fibroblasts from bortezomib-resistant patients are also resistant to bortezomib. Furthermore, cancer-associated fibroblasts modify the bone marrow stroma and influence the malignancy of multiple myeloma cells through cell-to-cell contact[221–224]. Targeting these factors has been shown to improve the response to proteasome inhibitors in multiple myeloma.

(viii) **Plasma cell dedifferentiation** which is achieved by X-box binding protein 1 (XBP1)[225], cell division cycle 37 (Cdc37)[226], and DEP domain-containing mTOR-interacting protein (DEPTOR)[227] suppression results in immature cells, which, unlike mature multiple myeloma cells, do not produce immunoglobulins and so are less dependent on the proteasome[228,229]. As stated above, immature B-cells express BTK which makes BTK an attractive target for combination therapy.

Preliminary data and research objectives

Due to the fact that the proteasome is responsible for the degradation of the majority of cellular proteins, it is a critical component of almost all cellular processes. And so, even as the proteasome has been found to be a dependency of several cancers, all the varied mechanisms by which cells react to inhibition of the proteasome are yet to be completely elucidated.

As stated above, the development of resistance of multiple myeloma to treatment with proteasome inhibitors is almost inevitable. One of the mechanisms that govern resistance is, as stated, the dedifferentiation of plasma cells to a more 'stem-like' state[230,231]. These 'stem-like' cells are de-facto immature B-cells that become reliant on BTK signaling for growth and proliferation[232,233]. Herein lies the rationale for the combination of BTK inhibitor therapy with proteasome inhibitor therapy in multiple myeloma – to improve response and mitigate resistance.

Kraus et al in 2015[234] reported their finding that BTK inhibitor ibrutinib was highly synergistic with a specific inhibitor of the β2 site of the proteasome, LU-102, in killing hematologic malignancies in vitro. Though ibrutinib also synergized with FDA-approved inhibitors of the β5 site of the proteasome, bortezomib and carfilzomib, these synergies were surprisingly far less than the synergy seen with LU-102. Even more surprising was that synergy was found between ibrutinib and LU-102 in the in vitro killing of hematologic cancer cell lines with little to no BTK expression. This brought about the reasoning that the synergy between proteasome inhibitors and ibrutinib is due to an off-target effect of ibrutinib. Furthermore, ibrutinib was found, in that study, to potently inhibit BTK activity at 0.1 μM of ibrutinib; however, the synergy between LU-102 and ibrutinib in the reduction of cell viability was only seen at 10 μM of ibrutinib, from the

high BTK-expressing cells to the no BTK-expressing cells. In other words, synergy was seen at a concentration of BTK inhibitor that was 100 times higher than the concentration needed to inhibit BTK activity. This was further evidence that the synergy between ibrutinib and LU-102 is due to an off-target effect of ibrutinib.

When we began this study, we proposed to answer the following questions: Is the synergy between ibrutinib and LU-102 really due to an off-target effect of ibrutinib? If it is, what is the 'off-target' responsible for synergy? Do other BTK inhibitors synergize with LU-102 in the same way? If the 'off-target' is not specific to BTK-expressing hematologic cancer cells, will the BTK inhibitor + LU-102 combination be efficacious in other types of cancer?

In this work, we show that the synergy between BTK inhibitors and proteasome inhibitors is due to an off-target effect of BTK inhibitors. We provide evidence for the need to screen kinase inhibitors for potential inhibition of cellular ATPases and reveal a novel mode of inhibition of the mammalian proteasome. In addition, we shine a light on a heretofore unknown mechanism of the response of cancer cells to proteasome inhibition governed by non-canonical functions of non-coding regulatory RNAs.

Chapter 2: Experimental model and subject details

Cell culture

MDA-MB-231, Raji, NCI-H929, and MDA-MB-468 cells were obtained from ATCC. INA-6 cells were obtained from DSMZ, and SUM149 cells were obtained from Asterand. MM1.S cells were a kind gift from Dr. Steven Rosen[235]. All cell lines were validated by short tandem repeat (STR) DNA fingerprinting[236]. MDA-MB-231 and SUM149 cells were cultured in DMEM/F12 50:50 media supplemented with 5% fetal bovine serum (FBS). In addition, SUM149 media was supplemented with 1 mg/mL hydrocortisone, 4.8 μg/mL human recombinant insulin, 10 mM HEPES (pH 7.3), and 4 mM L-glutamine. Multiple myeloma and lymphoma cells were cultured in RPMI-1640 media supplemented with 10% FBS, and INA-6 cells media was supplemented with 1 ng/ml IL-6 and 50 μM β-mercaptoethanol. All media used was further supplemented with penicillin, streptomycin, amphotericin-B (0.25 μg/ml), and ciprofloxacin (0.2 μg/ml). Cell viability was assayed with resazurin (Alamar Blue, Thermo Fisher) after cells were treated for the times and concentrations indicated. Combination indices were calculated using CalcuSyn software. Apoptosis was measured by flow-cytometry on BD Accuri C6 Plus flow-cytometer using CellEvent™ Caspase-3/7 Green Detection Reagent and SYTOX cell viability dye (Thermo). Data were analyzed using BD CSampler Plus software. Alternatively, caspase-3,7 activity was measured in extracts using Ac-DEVD-AMC as described by Britton et al[237].

Immunoblotting and antibodies used

Frozen cell pellets were resuspended in CHAPS lysis buffer (0.5% CHAPS, 10% glycerol, 5 mM $MgCl_2$, and 1 mM EDTA in 50 mM Tris-HCl (pH 7.5)), incubated for 5 min on ice, and centrifuged at 20,000 × g for 15 min. 1X PhosSTOP™ (Roche) was added to the lysis buffer in experiments requiring the study of phosphorylation. Samples were quantified using Bradford assay, and 20 μg of total protein per sample was heated for 15 minutes with LDS buffer (Novex NP0007) at 72°C, fractionated on Bis-Tris gels (Genscript) using MES electrode buffer, and transferred to 0.2μm PVDF membrane (Immobilon, ISEQ00010). Blots were blocked with either 2% or 5% non-fat milk. The membrane was incubated with primary antibodies overnight at 4°C and with the secondary antibodies for 1h at room temperature, and imaged on Azure c600, directly if fluorescently labeled secondary antibodies were used, or after brief incubation with Pierce SuperSignal West Femto Maximum Sensitivity Substrate if HRP-conjugated secondary antibodies were used.

Inhibitors and substrates

Carfilzomib and bortezomib were obtained from LC Laboratories. BTK inhibitors were obtained from MedChemExpress. Suc-LLVY-AMC was obtained from Bachem, Ac-RLR-AMC, and Ac-nLPnLD-AMC were custom synthesized by ChinaPeptides. LU-102 and EK-LU-102 were synthesized as described by Geurink et al[238]. VS-less-LU-102 was synthesized by Dr. Alexandre Pletnev, Dartmouth College. Ac-LU-102 was synthesized through the acetylation of LU-102 by Dr. Alexei Kisselev.

Affinity-based probe assay

MDA-MB-231 cells were treated with compounds at the indicated concentrations and times. Cells were lysed as described above, and lysates (at normalized concentrations) were incubated with 1μM of MV151 (for proteasome activity) for 30 minutes at 37°C. The resulting samples were run on SDS-PAGE and detected by direct fluorescent in-gel readout using the RGB Cy3® setting on the Azure 600 Imaging System (λ_{ex} 532, λ_{em} 560). For deubiquitinase activity, lysates were incubated with 1μM of HA-tagged ubiquitin vinyl sulfone for 30 minutes at 37°C. The resulting samples were run on SDS-PAGE followed by western blotting to probe for HA.

RNA sequencing

MDA-MB-231 cells were treated for four hours with CGI-1746, LU-102, a combination of the two, or bortezomib as a control for pathways changed by proteasome inhibition. RNA was extracted using the Qiagen RNeasy Mini Kit according to the manufacturer's protocol, frozen, and shipped on dry ice to LCSciences (Houston, TX) for total RNA sequencing (150 bp PE, 40 million reads per sample). RNAseq data analysis was performed using a command-line-based analysis pipeline. Briefly, raw reads were pre-processed and mapped to the hg38 human genome build using the STAR Aligner tool. Next, mapped read counts were normalized, and differential gene expression analysis was performed between the Gene Expression Profiles (GEP) of each treatment group using GSA, as described earlier[239]. Ingenuity Pathway Analysis (IPA) software tool was used to predict pathways and upstream regulators potentially regulated by the top differentially expressed genes for each treatment/condition. RNA-seq data has been deposited at GEO and is publicly available as of the date of publication. Accession numbers are listed in the key resources table.

Methods related to Chapter 3

Protein isolation

Proteasome isolation

Human 26S proteasomes were isolated from mammalian cells via the UBL-affinity purification method[240]. HeLa cells were collected by centrifugation and lysed by sonication in affinity purification buffer (APB), 25 mM HEPES-KOH (pH 7.4), 10% (v/v) glycerol, 5 mM $MgCl_2$, 1 mM ATP, and 1 mM DTT, using six ten-second bursts (12-micron amplitude) with at least ten-second recovery periods on ice. Lysates were cleared by centrifugation at 4°C, 100,000g for 30 minutes. The supernatant was then further centrifuged for 3 hours at 4°C, 150,000g. The supernatant was collected for future analysis, and the proteasome-rich pellet was suspended in APB and then incubated with GST-UBL[241] and pre-equilibrated Glutathione-Sepharose for two hours at 4°C. Following the incubation period, the Glutathione-Sepharose resin was washed with APB. Bound proteasomes were eluted by fifteen-minute incubation with His_{10}-UIM[241] in APB. His_{10}-UIM was removed from eluted proteasomes by incubation with pre-equilibrated Ni-NTA resin for twenty minutes, followed by resin removal by centrifugation. Rabbit 20S and 26S proteasomes were purified from frozen muscles as described[242,243]. 19S were isolated from bovine erythrocytes as described[244].

$Sic1^{PY}$ isolation and labeling

pET vector containing His_6-tagged $Sic1^{PY}$ was a kind gift from Dr. Yasusi Saeki. $Sic1^{PY}$ was expressed and purified according to their published protocol[245,246]. Briefly, BL21 (DE3) cells were plasmid-transformed and grown to an OD_{600} of 0.7 in LB medium with 50 μg/ml ampicillin. Thereafter, the culture was cooled to 30°C and $Sic1^{PY}$ synthesis was induced by the

addition of isopropyl β-D-1-thiogalactopyranoside (IPTG) to 0.5 mM. After three hours, cells were collected by centrifugation (3,000g, 10 min), and suspended and lysed by sonication in 50 mM phosphate buffer (pH 7.0) containing 300 mM NaCl, 10% glycerol, 1 mM DTT, 0.2% Triton X-100 and 1× protease inhibitor cocktail. The lysate was centrifuged (15,000g, 30 min) and the resulting supernatant was then incubated with pre-equilibrated Ni-NTA resin for two hours at 4 °C. The resin was washed with 20 column volumes of 50 mM phosphate buffer (pH 7.5) containing 100 mM NaCl, 10% glycerol, and 1 mM DTT. $Sic1^{PY}$ was then eluted with the same buffer containing 150 mM imidazole. Imidazole was removed from the eluate via three-round dialysis with the wash buffer. To further purify the $Sic1^{PY}$ product, we used a T7·Tag Affinity Purification Kit (EMD Millipore) according to the manufacturer's protocol. To increase the sensitivity of $Sic1^{PY}$ detection and simply quantification on the gel by avoiding interference from other components of the reaction, we fluorescently labeled $Sic1^{PY}$ by incubating it with 5/6-carboxy-tetramethyl-rhodamine succinimidyl ester at a 1:1 molar ratio for two hours at room temperature (21-25°C). The reaction was quenched with 25 mM Tris-HCl (pH 7.5). Excess 5/6-carboxy-tetramethyl-rhodamine was removed by passing the reaction through a PD-10 desalting column (Cytiva) and labeled $Sic1^{PY}$ was eluted using the wash buffer.

WW-HECT isolation

pET vector containing GST-tagged WW-HECT was also a kind gift from Dr. Sasaki. WW-HECT was obtained according to their published protocol[245]. Briefly, BL21 (DE3) cells were grown to an OD_{600} of 0.5 in LB medium with 50 μg/ml ampicillin. The culture was then cooled to 20 °C and WW-HECT synthesis was induced by the addition of IPTG to 0.2 mM. Cells incubated for fifteen hours after the addition of IPTG and lysed as above for $Sic1^{PY}$. The

supernatant was incubated with pre-equilibrated Glutathione-Sepharose resin for two hours at 4 °C. The resin was washed with 20 column volumes of washing buffer (50 mM Tris-HCl, pH 7.5) containing 100 mM NaCl, 10% glycerol, and 1 mM DTT). WW-HECT was released by incubation with GST-tagged PreScission protease (GenScript) with the same buffer for twelve hours at 4°C. The protease, bound to the resin, was removed by centrifugation.

Sic1^{PY} ubiquitination

To ubiquitinate Sic1^{PY}, 40 μg/ml of Rhodamine-Sic1^{PY}, 500 nM UBE1 (R&D Systems/Biotechne), 2 μM UBCH5C (a gift from Drs. Edit Tarcsa and Alfred Goldberg, Harvard Medical School), 100 μg/ml WW-HECT and 1 mg/ml ubiquitin (R&D Systems/Biotechne) were incubated in reaction buffer (50 mM Tris-HCl [pH 7.5], 100 mM NaCl, and 10% glycerol, 2 mM ATP, 10 mM $MgCl_2$, and 1 mM DTT) for three hours at room temperature (21-25°C). The reaction was incubated with pre-equilibrated Ni-NTA resin for two hours at 4 °C. The resin was then washed with 20 column volumes of the wash buffer (50 mM Tris-HCl (pH 7.5), 100 mM NaCl, 10% glycerol), and polyubiquitinated Sic1^{PY} (Ub-Sic1^{PY}) was eluted with the same buffer containing 150 mM imidazole. The eluate was concentrated, and imidazole was removed by centrifugation with an Amicon ultrafiltration device with a 50kDa molecular weight cut-off. The ubiquitination reaction was examined by Coomassie staining of an SDS-PAGE gel. Rhodamine modification did not affect the rate of ubiquitylation and the length of the ubiquitin chains, as would be expected if rhodamine-modified lysine side chains, probably because the pH of the reaction and Rhodamine:Sic1^{PY} molar ratio favored a selective N-terminal modification.

Activity assays

Proteolytic activity in purified proteasomes

Peptidase activities of proteasomes were determined from the slope of the reaction progress curve obtained by continuously following the fluorescence of 7-amino-4-methyl coumarin (AMC), released upon cleavage of Suc-LLVY-AMC (β5 sites), Ac-RLR-AMC (β2 sites), or Ac-nLPnLD-AMC (β1 sites)[237], by ~580 pM of purified proteasome in the presence or absence of inhibitors. Each substrate was at 100 μM unless stated otherwise. The reaction buffer was 50 mM Tris-HCl (pH 7.5), 1 mM DTT for 20S measurements, supplemented with 5 mM $MgCl_2$ (unless otherwise stated), 100 μM ATP, 2 mM EDTA, and 40 mM KCl for 26S activity.

ATPase assays were conducted using Promega ADP-Glo™ Kinase Assay according to the manufacturer protocol using 14 nM 19S, 3 nM 26S proteasome, and 80 nM VCP and the indicated concentration of compounds and ATP to test for inhibition of the ATPases. Compounds were incubated with the kinase reaction containing purified 26S proteasomes for two hours in 1X kinase assay buffer (40 mM Tris (pH 7.5), 20 mM $MgCl_2$, 0.1 mg/ml BSA), and then tested for inhibitory activity.

Ubiquitinated Sic1^{PY} degradation assays. 3 nM 26S proteasome in 50 mM Tris-HCl (pH 7.5), 100 mM NaCl, 10% glycerol, 2 mM ATP, 10 mM $MgCl_2$, and 1 mM DTT was incubated with CGI-1746 for one hour at room temperature, after which ~360 nM Ub-Sic1^{PY} was added, and the reaction was incubated at 37°C. Aliquots were withdrawn at times indicated, and immediately mixed and heated with LDS sample and analyzed by SDS-PAGE. Rhodamine-labeled proteins were imaged on Azure c600 and quantified using Image Studio Lite.

ROS assay

2000 MDA-MB-231 cells/ well were plated on a 96-well plate for 24 hours after which cells were treated with 10 μM of CGI-1746, 3 μM of LU-102, a combination of 10 μM of CGI-1746 and 3 μM of LU-102, 50 nM of bortezomib, and 0.05% of vehicle (DMSO/MOCK) for 3 and 8 hours. GSH/GSSG-Glo™ Assay from Promega was used to obtain the results for the ratio of reduced glutathione to oxidized glutathione and was performed according to the manufacturer's protocol.

Cell growth assay

100,000 MDA-MB-231 and 231CL.R cells were seeded in seven 10 cm plates each. 24 hours after seeding, on Day 1, cells were harvested by trypsinization, and cells were counted using an automated cell counter. This was repeated on Days 2 through 7. The average cell count for four samples per plate was recorded for each cell line.

Native polyacrylamide gel electrophoresis (NATIVE-PAGE)

Cells were lysed as above, and 20 – 40 μg total protein was loaded onto Tris-Acetate gels and separated in 1X Tris-Glycine buffer. Western blotting was performed as described above.

Resistant cell line generation

MDA-MB-231 cells were grown in media containing increasing concentrations of a combination of CGI-1746 and LU-102 for a period of 365 days. The starting concentration was 10 μM of CGI-1746 and 3 μM of LU-102. Cells were treated for 24 hours after which surviving cells were replated in fresh media and allowed to recover for one week (with regular passaging) then the

same treatment was repeated until greater than 50% of cells survived, after which the concentration of the drugs was increased. 231CL.R cells were created with treatment at a final concentration of 80 μM of CGI-1746 and 6 μM of LU-102.

Methods related to Chapter 5

Reverse transcriptase quantitative PCR (RT-QPCR)

RNA isolation

Cells were treated and collected as indicated. Cells were lysed with TRIzol™ reagent from ThermoFisher. RNA extraction was done according to the manufacturer's protocol. In brief, chloroform was added to promote phase separation between RNA, DNA, and proteins. Isopropanol was added to the aqueous phase containing the RNA to precipitate the RNA out of the solution. 70% ethanol was used to wash the precipitated RNA, allowed to evaporate, and the RNA pellet was solubilized in nuclease-free water. RNA was quantified using a NanoDrop and 1 μg total RNA per sample was used for downstream applications.

Reverse transcription

cDNA was obtained using the SuperScript™ III First-Strand Synthesis System from ThermoFisher using 1 μg total RNA, obtained as above, according to the manufacturer's protocol.

Quantitative PCR (qPCR)

cDNA obtained above was amplified at genes of interest (SNORA71D, and β-Actin and U6 loading controls) using PerfeCTa SYBR® Green FastMix from QuantaBio according to the manufacturer's protocol.

Primers used:

SNORA71D. Forward – ACCTGTATTCGAAAGTGATCGT. Reverse – GAAGCACTTTCCGCGATTTC.

β-Actin. Forward – CCAACCGCGAGAAGATGA. Reverse – CCAGAGGCGTACAGGGATAG.

U6. Forward – GCTTCGGCAGCACATATACTAAAAT. Reverse – CGCTTCACGAATTTGCGTGTCAT.

Relative RNA abundance was detected using a CFX96 Touch Real-Time PCR Detection System thermocycler from Bio-Rad. SNORA71D expression was calculated relative to the reference gene by the Bio-Rad CFX Manager 3.1 software using ΔΔCq analysis. Data represented on bar graphs are mean ± SEM of ≥ 3 biological replicates unless otherwise stated.

Cell fractionation

Cells were treated as indicated and then lysed using the Ambion™ PARIS™ kit from ThermoFisher according to the manufacturer's protocol. RNA obtained from nuclear and cytoplasmic fractions was reverse transcribed as described above, and qPCR was performed.

snoRNA knockdown

MDA-MB-231 cells were seeded in serum-free media. 24 hours post-seeding, cells were transfected with SNORA71D siRNA (25 nM) or control siRNA (25 nM) in DharmaFECT 1 Transfection Reagent (0.3%) from Horizon Discovery and Opti-MEM media (20%) from ThermoFisher for 48 hours after which cells were harvested and downstream processes were performed.

Proteomics analysis

MDA-MB-231 cells were transfected with SNORA71D or control siRNA for 48 hours and then pulse-treated with 600 nM bortezomib or DMSO (MOCK) for one hour. Cells were harvested six hours after the start of treatment, flash-frozen in liquid nitrogen, and shipped to the proteomics core at the University of Alabama at Birmingham. Four biological replicates were performed.

Quantification and Statistical Analysis

Band intensities on gels and western blot membranes were quantified using Image Studio Lite. Statistical analysis was done using GraphPad Prism and CalcuSyn.

Table 1. Key Resources Table

REAGENT or RESOURCE	SOURCE	IDENTIFIER
Antibodies		
K-48 Polyubiquitin	Cell Signaling Technologies	Cat#12805S
HSP70	Cell Signaling Technologies	Cat#4876S
α-Tubulin	Cell Signaling Technologies	Cat#3873S
GAPDH	Abcam	Cat#AC027

Cleaved PARP	Cell Signaling Technologies	Cat#5625S
Proteasome α6	Purified from hybridoma provided by Tanaka laboratory	Clone Mab 2-17
HA Tag Monoclonal Antibody	Thermo Fisher	Cat#32-6700
CellEvent™ Caspase 3/7 Green Detection Reagent	Thermo Fisher	Cat#C10423
SYTOX™ Red Dead cell stain	Thermo Fisher	Cat#S34859
Anti-rabbit IgG, HRP-linked Antibody	Cell Signaling Technologies	Cat#7074S
Anti-mouse IgG, HRP-linked Antibody	Cell Signaling Technologies	Cat#7076S
Alexa Fluor 647, Goat anti-rabbit IgG (H+L)	Thermo Fisher	Cat#A21245
IRDye 800 CW, Goat anti-mouse	LI-COR Biosciences	Cat#926-32210
Bip	Cell Signaling Technologies	Cat#3177S
eIF2α	Cell Signaling Technologies	Cat#2103S
p-eIF2α	Cell Signaling Technologies	Cat#3398S
Cleaved PARP	Cell Signaling Technologies	Cat#5625S
SQSTM1/p62 polyclonal antibody	Thermo Fisher	Cat#PA5-20839
p-SQSTM1/p-p62 polyclonal antibody	Thermo Fisher	Cat#PA5-78267
Bacterial and Virus Strains		
Rosetta™(DE3) competent cells	Millipore Sigma	Cat#70954
NEB 5-alpha	New England Biolabs	Cat#C2987H
Chemicals, Peptides, and Recombinant Proteins		
LU-102	Provided by Overkleeft laboratory	
Bortezomib	LC Laboratories	Cat#B-1408
Carfilzomib	LC Laboratories	Cat#C-3022
Ibrutinib	MedChemExpress	Cat#HY-10997
Acalabrutinib	MedChemExpress	Cat#HY-17600
ONO-4059	MedChemExpress	Cat#HY-15771
CC-292	MedChemExpress	Cat#HY-18012
CGI-1746	MedChemExpress	Cat#HY-11999
GDC-0853	MedChemExpress	Cat#HY-19834
Evobrutinib	MedChemExpress	Cat#HY-101215
Zanubrutinib	MedChemExpress	Cat#HY-101474A

Resazurin sodium salt (Alamar Blue)	Millipore Sigma	Cat#R7017
Ac-DEVD-AMC (N-Acetyl-Asp-Glu-Val-Asp-7-amido-4-Methylcoumarin)	Bachem	Cat#I-1660
Suc-LLVY-AMC	Bachem	Cat#1-1395
Ac-RLR-AMC	ChinaPeptide	Custom synthesis
Ac-nLPnLD-AMC	ChinaPeptide	Custom synthesis
UbcH5c	Provided by Dr. A. Goldberg and E.Tarcsa	
UbE1	R&D Systems	Cat#E-305-025
NMS-873	Selleckchem	Cat#S7285
5(6)-TAMRA, SE caboxyteramethylrhodamine	Thermo Fisher	Cat#C1171
HA-Ub-VS	Enzo Life Sciences	Cat#BML-UW0155-0025
PreScission Protease	GenScript	Cat#Z02799
SuperSignal™ West Femto Maximum Sensitivity Substrate	Thermo Fisher	Cat#34095
Critical Commercial Assays		
Alamar Blue	Thermo Fisher	Cat#DAL1025
ADP-Glo™ Kinase Assay	Promega	Cat#V6930
T7•Tag Affinity Purification Kit	Millipore Sigma	Cat#69025-3
Phosphostain	Thermo Fisher	Cat#P33301
GelCode^{TM} Blue Safe Protein Stain	Thermo Fisher	Cat#1860957
RNeasy Mini Kit	Qiagen	Cat#74104
GSH/GSSG-Glo™ Assay	Promega	Cat#V6611
Ambion™ PARIS™	ThermoFisher	Cat#AM1921
Deposited Data		
Raw and analyzed RNA sequencing data	https://dx.doi.org/10.2139/ssrn.4536762	GSE239482
Experimental Models: Cell Lines		
MDA-MB-231	ATCC	RRID:CVCL_0062
MDA-MB-468	ATCC	RRID:CVCL_0419
SUM149	Asterand	RRID:CVCL_3422
INA-6	DSMZ	RRID:CVCL_5209
MM1.S	Dr. Steven Rosen	RRID:CVCL_8792
Raji	ATCC	RRID:CVCL_0511
NCI-H929	ATCC	RRID:CVCL_1600

231CL.R	This dissertation	
Recombinant DNA		
pET21a-Sic1^{PY}	Dr. Yasusi Saeki	
pGEX6P1-WWHECT	Dr. Yasusi Saeki	
pDEST15-UBL-hHR23B	Dr. Alfred Goldberg	
pET26b-His10-UIM2-hS5a	Dr. Alfred Goldberg	
Oligonucleotides		
ON-TARGETplus Non-targeting siRNA #1	Horizon Discovery	Cat#: D-001810-01-20
SNORA71D Silencer® Select siRNA, n267617	ThermoFisher	Cat# 4390771
Software and Algorithms		
Prism	GraphPad	
CalcuSyn	Biosoft	
Image Studio Lite	LI-COR Biosciences	

Chapter 3: Allosteric inhibition of proteolytic and ATPase activities of the proteasome by the BTK inhibitor CGI-1746

Sections of this chapter have been submitted for publication with the following authorship:

Olasubomi A. Akintola[1], Mitchell B. Patterson[1], John G. Smith[1], George N. De Martino[2], Amit K. Mitra[1], Alexei F. Kisselev[1]*

1- Department of Drug Discovery and Development, Harrison College of Pharmacy, Auburn University, 720 S. Donahue Dr., Auburn AL

2-Department of Physiology, University of Texas Southwestern Medical Center, Dallas, TX

Abstract

Bruton's tyrosine kinase (BTK) inhibitor ibrutinib has been shown to synergize in vitro with proteasome inhibitors (PIs) in reducing the viability of cells derived from B-cell malignancies, but the mechanism is unknown. We report here that an off-target effect of ibrutinib causes synergy because not all BTK inhibitors exhibited the synergistic effect, and those that synergized did so even in cells that do not express BTK. The allosteric BTK inhibitor CGI-1746 showed the strongest synergy. Co-treatment of cells with CGI-1746 increased PI-induced expression of heat shock proteins and accumulation of ubiquitin conjugates. CGI-1746 inhibited protein degradation by a purified 26S proteasome and allosterically inhibited its ATPase and peptidase activities. Although the effect is observed at concentrations too high to contribute to clinical anti-

neoplastic activity, this conceptually novel mode of inhibition may be useful for mechanistic studies and future drug development.

Introduction

The 26S proteasome is essential for maintaining protein homeostasis in every eukaryotic cell, including the quality control of nascent polypeptides[247–250]. Multiple myeloma cells are highly dependent on proteasome activity because these malignant plasma cells synthesize and secrete large amounts of immunoglobulins, which are complex four-chain molecules that contain multiple disulfide bridges. Partial inhibition of the proteasome causes selective apoptosis of myeloma cells, and proteasome inhibitors bortezomib, carfilzomib, and ixazomib[251–253] are approved by the FDA for the treatment of multiple myeloma. The initial response rates are high, but many patients develop resistance.

De-differentiation into stem-like plasma cell precursors that do not produce immunoglobulins is one of the mechanisms of myeloma resistance to proteasome inhibitors[254,255]. These cells express Bruton's tyrosine kinase (BTK), an essential kinase in the development and proliferation of immature B-cells and many B-cell leukemias and lymphomas[256–258]. Three BTK inhibitors, ibrutinib, acalabrutinib, and zanubrutinib, are approved for the treatment of various B-cell neoplasms [8,259]. BTK inhibitors have been clinically tested for the treatment of multiple myeloma as a proposed therapy, which in combination with proteasome inhibitors, should overcome resistance to proteasome inhibitors in multiple myeloma[260].

Previous experiments by the Driessen lab showed that the combination of proteasome inhibitors with a BTK inhibitor, ibrutinib, causes synergistic cell death in cells derived from myeloma and mantle cell lymphoma[261]. This pronounced synergy was seen regardless of BTK expression levels. Additionally, the synergy was seen at a hundred times the concentration of ibrutinib needed to completely inhibit BTK activity. These data suggested an off-target effect of the BTK inhibitor but attempts to identify a target responsible for the synergy were unsuccessful. The goal of this study was to obtain additional evidence to support an off-target effect of BTK inhibitors and identify the target.

The 26S proteasome consists of a 20S proteolytic core and one or two 19S regulatory complexes. The 20S core contains three pairs of proteolytic active sites, β5 (PSMB5, or chymotrypsin-like), β2 (PSMB2 or trypsin-like), and β1 (PSMB1 or caspase-like). β5 sites are the most important for protein degradation and the prime targets of FDA-approved proteasome inhibitors[262]. Inhibitors of β2 and β1 sites have also been developed[263] and were found to potentiate the anti-neoplastic effects of β5 inhibitors while having little effect on cell proliferation, viability, and protein breakdown when used as single agents[238,264,265]. Surprisingly, the synergy with ibrutinib was more pronounced with the specific inhibitor of proteasome β2 sites, LU-102, than with FDA-approved β5 inhibitors, bortezomib, and carfilzomib[261]. To the best of our knowledge, this is the only example where the biological effect of a β2-specific inhibitor is stronger than that of β5 inhibitors.

The 19S regulatory complex (PA700) contains ubiquitin receptors, deubiquitylating enzymes, and six ATPases, which unfold protein substrates and control access to the proteasome[245,266].

While several inhibitors of the isopeptidases[267–270] and three ATPase binders[271–273] have been described, it has not been reported whether these ATPase binders inhibit 19S ATPase activity. Here we describe how an effort to identify an off-target of ibrutinib led to a surprising discovery that a non-competitive BTK inhibitor CGI-1746, but not other BTK inhibitors, is an allosteric inhibitor of both the 19S ATPase activities and all three proteolytic sites of the proteasome.

We demonstrate in this chapter that the mechanisms by which the CGI-1746 – LU-102 combination treatment causes cell death via the same mechanisms by which FDA-approved inhibitors of the β5 site of the proteasome cause cell death: ER stress, ROS generation, and accumulation of NOXA. Finally, we show that a cell line resistant to the CGI-1746 – LU-102 combination treatment is also resistant to FDA-approved inhibitors of the β5 site of the proteasome.

Results

The majority of, but not all, BTK inhibitors synergize with proteasome inhibitors in BTK-expressing myeloma cells. Ibrutinib inhibits many different kinases[75,274–276], and if synergy with proteasome is due to the inhibition of one of these kinases, more specific second-generation BTK inhibitors should not synergize. Therefore, we determined whether other BTK inhibitors with different kinome specificity profiles synergize with proteasome inhibitors in various cell lines, starting with BTK-expressing cells. We have chosen two irreversible inhibitors, acalabrutinib and CC-292 (spebrutinib), which, similar to ibrutinib, covalently bind to the cysteine in the active site, and two reversible allosteric inhibitors, CGI-1746 and GDC-0853 (fenebrutinib). Of the irreversible inhibitors, acalabrutinib is more selective than ibrutinib, CC-292 is less

selective[277], while the allosteric inhibitors, CGI-1746 and GDC-0853 are much more selective[278,279]. Specifically, CGI-1746 does not inhibit any other kinase at 1 μM[278]. We focused on the β2-specific inhibitor, LU-102, because it showed stronger synergy than bortezomib and carfilzomib**.** Cells were co-treated with various concentrations of LU-102 and BTK inhibitors for 48hrs, and their viability was measured by the Alamar Blue mitochondrial dye conversion assay (Fig. 3.1 and Fig. S3.1). Ibrutinib, acalabrutinib, CGI-1746, and GDC-0853 exhibited various degrees of synergy, while CC-292, which was more cytotoxic when used as a single agent, was less synergistic. We confirmed that combinations reduced cell viability because of apoptosis (Fig. 3.1).

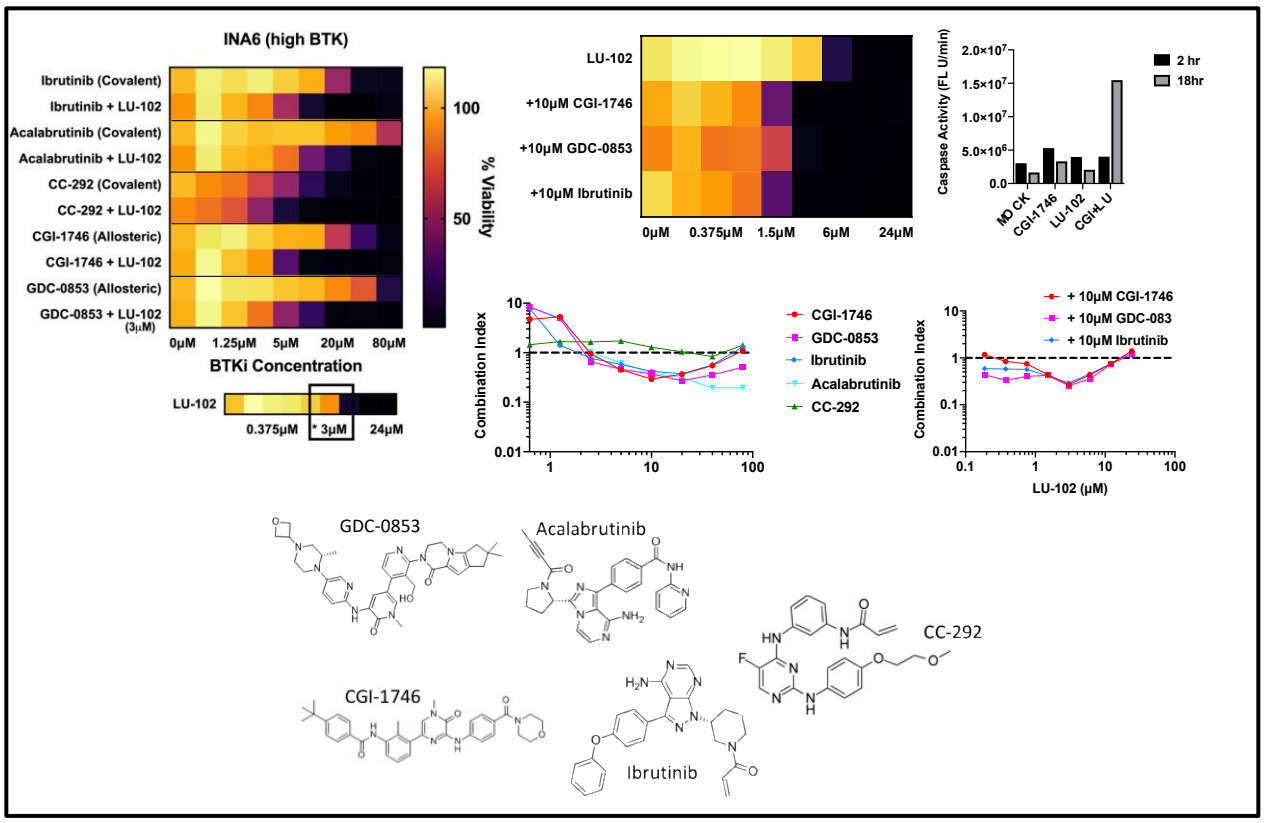

Figure 3. 1 Some BTK inhibitors synergize with specific proteasome β2 site inhibitor, LU-102, in a BTK expressing multiple myeloma cell line.
INA-6 BTK-expressing cells were treated with BTK inhibitors (ibrutinib, acalabrutinib, CC-292, CGI-1746, and GDC-0853) alone and in combination with a sub-toxic concentration (3 μM) of β2-site specific proteasome inhibitor, LU-102 for 48 hours, or indicated concentrations of LU-102 with sub-toxic doses of CGI-1746, GDC-0853, and ibrutinib, after which viability was determined by Alamar Blue dye conversion assay, and expressed as % of mock-treated controls. The bottom row demonstrates the results of single-agent LU-102 treatment, and a square shows the concentration used in combination experiments. All data are averages of repeated biological experiments (n>3). Synergy was determined by the Chou-Talalay method[280] using CalcuSyn (Synergy < 1, Antagonism > 1, Additive = 1). Apoptosis was determined by caspase 3/7 activity in cell extracts using Ac-DEVD-AMC. Raw data for heat maps are presented in Fig. S3.1. On the bottom are structures of the BTK inhibitors used in this work.

BTK inhibitors exhibited similar synergy with bortezomib and carfilzomib (Fig. 3.2a and Fig. S3.2a)[261], and similar patterns of synergy were observed in a BTK-expressing lymphoma cell line, Raji (Fig. S3.2b). While the strong synergistic activity of the highly specific inhibitor CGI-1746 can be interpreted as synergy caused by BTK inhibition, complete inhibition of BTK was observed at a concentration at least 100-fold lower than the 10 μM concentration (Fig. 3.2b and Fig. S3.2c) at which maximal synergy was observed (Fig. 3.1 and Fig. S3.2b), strongly suggesting that an off-target effect is responsible for synergy.

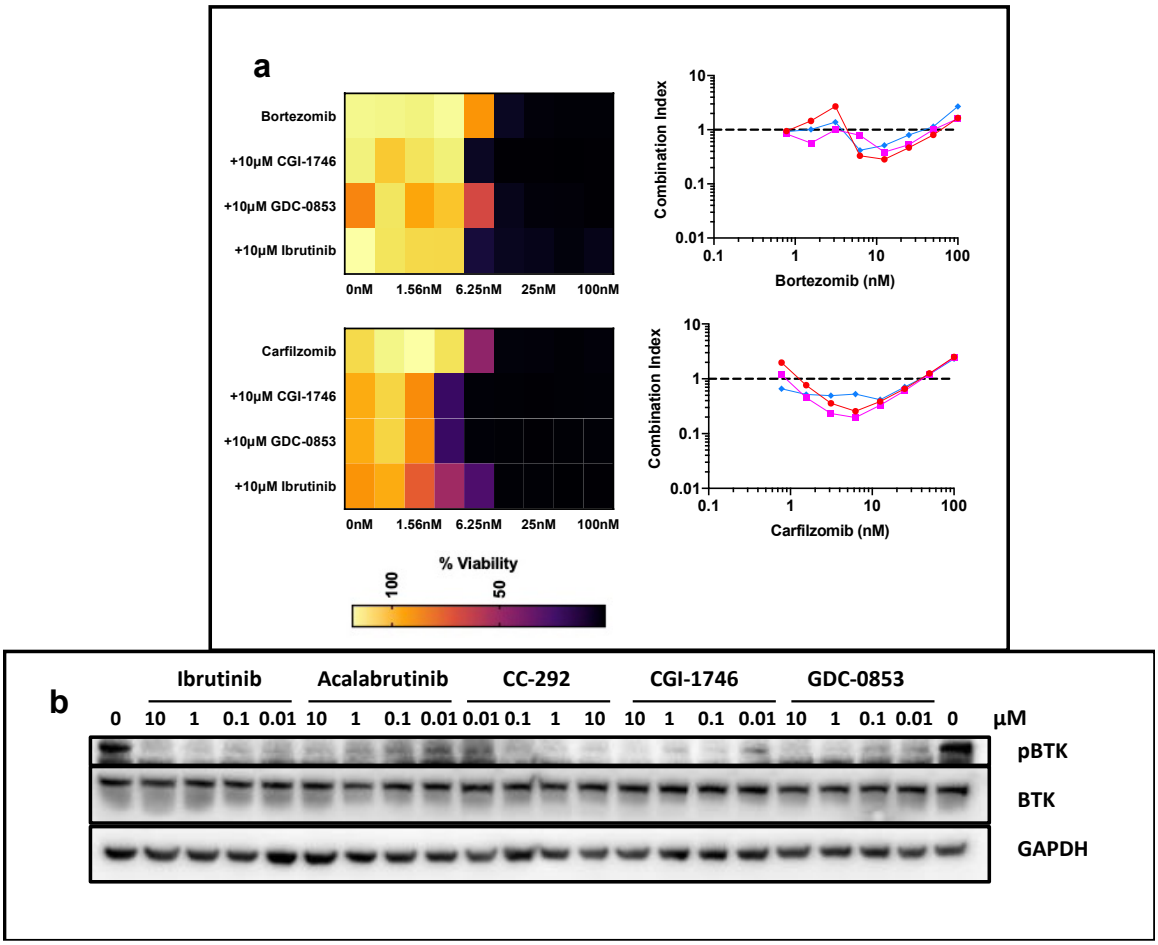

Figure 3. 2 BTK inhibitors synergize with specific proteasome β5 site inhibitors in a BTK expressing multiple myeloma cell line

(A) INA-6 cells were treated with inhibitors of proteasome β5 sites, bortezomib, and carfilzomib, alone or with sub-toxic doses of CGI-1746, GDC-0853, and ibrutinib. Viability and synergy were determined as in (A). Raw data is presented in Fig. S3.2a.

(B) Western blot showing the inhibition of BTK (reduction in autophosphorylated BTK) by indicated concentrations of BTK inhibitors in INA-6 cells treated for one hour.

BTK inhibitors synergize with LU-102 in cells that do not express BTK. If synergy between ibrutinib/other BTK inhibitors and LU-102 is caused by an off-target effect of BTK inhibitors, the effect will be observed in cells that do not express BTK. To investigate the possibility, we performed the previous experiments in MM1.S multiple myeloma cells, which have very low BTK expression and no phosphorylated (active) BTK expression, as well as in two triple-negative breast cancer cell lines, MDA-MB-231, and SUM149, which have no BTK expression (Fig. 3.3a) but are very sensitive to proteasome inhibitors[236,281,282]. The results of these experiments are summarized in Fig. 3.3b (Raw data is in Fig. S3.3).

Similar to INA-6 and Raji cells, CC-292 was cytotoxic to all cell lines with IC50 in the 10 μM range but did not show any synergy with LU-102. Ibrutinib appeared to be less synergistic in MM1.S and MDA-MB-231 cells. Acalabrutinib was not synergistic in these cells. Two allosteric inhibitors, GDC-0853 and CGI-1746, maintained synergy.

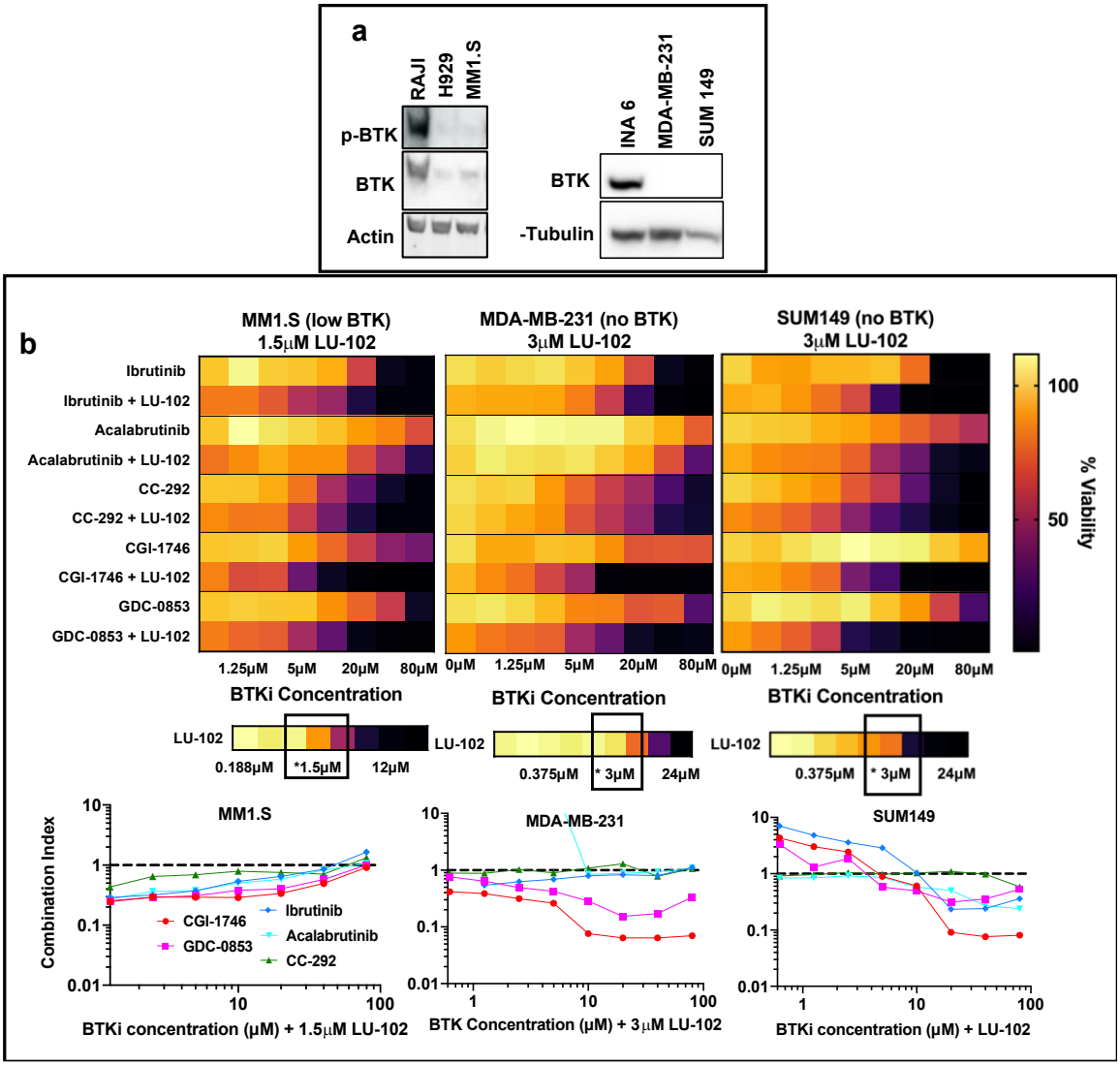

Figure 3. 3 Some BTK inhibitors synergize with specific proteasome β2 site inhibitor, LU-102, in cell lines that do not express BTK.

(A) The expression of active (phosphorylated) BTK and total BTK was determined by western blots.

(B) Heatmaps and Combination Index graphs show viability and synergy, respectively, in MM1.S, MDA-MB-231, and SUM149 cells treated with BTK inhibitors and sub-toxic concentrations of LU-102 (indicated by a square in the bottom row of the heat maps), as in Figure 1a (n>3). Raw data is presented in Fig. S3.3.

The effect of CGI-1746 on breast cancer cells was the most remarkable because, unlike in INA-6 cells, this compound was not cytotoxic to breast cancer cells yet essentially showed synthetic lethality when combined with LU-102 (Fig. 3.4a), leading to robust apoptosis within 18-24hrs of exposure. We also analyzed LU-102 combinations with three other covalent BTK inhibitors, zanubrutinib, evobrutinib, and ONO-4053 in MDA-MB-231 cells (Fig. S3.4), and identified synergy which was similar to ibrutinib. Finally, carfilzomib showed synergy with ibrutinib, CGI-1746, and GDC-0853 in MDA-MB-231 cells (Fig. 3.4b). We concluded that the synergy between ibrutinib, CGI-1746, and GDC-0853, and proteasome inhibitors is caused by an off-target effect of BTK inhibitors.

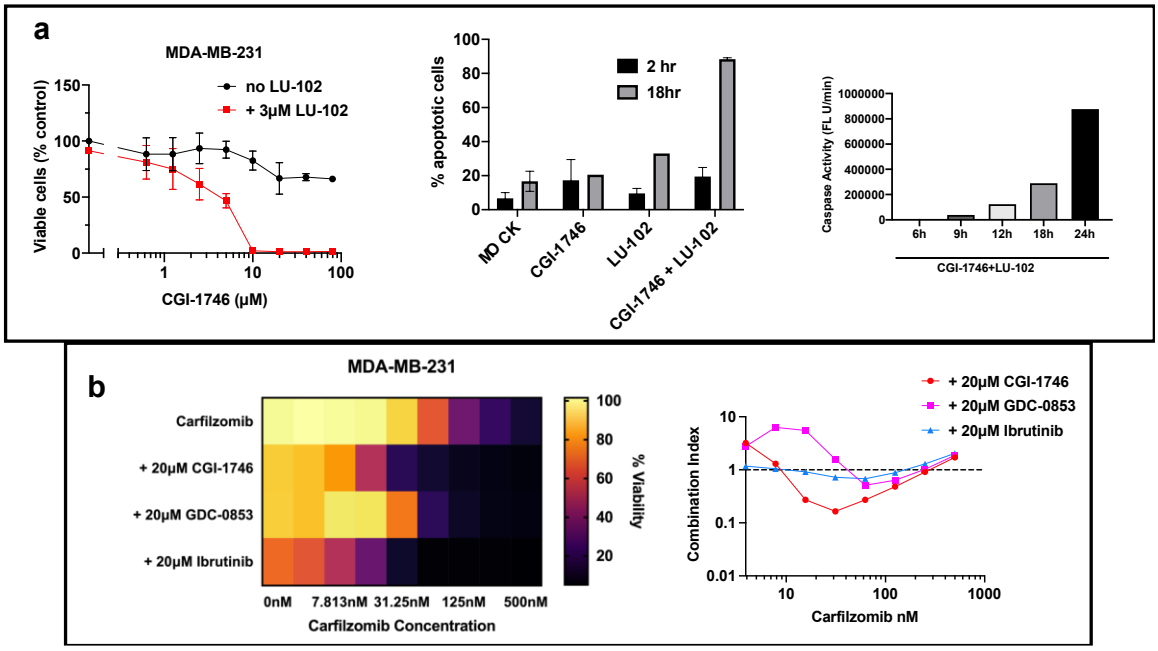

Figure 3. 4 Loss of viability in TNBC treated with the CGI-1746 and LU-102 combination is due to apoptotic cell death.

(A) Detailed analysis of effects of CGI-1746/LU-102 combination on MDA-MB-231 cells. Data on the left graph was used to generate the heat map in A (left) and is also presented in Fig. S3.3. Apoptosis of cells treated with 10 μM CGI-1746, and 3 μM LU-102 was determined by flow-cytometry using Caspase 3/7 probe (middle) and my measuring by caspase 3/7 in extracts using Ac-DEVD-AMC (right, n=3).

(B) MDA-MB-231 cells were pulse-treated with carfilzomib for one hour, after which carfilzomib-containing media was replaced with drug-free media or media containing sub-toxic concentrations of CGI-1746, GDC-0853, and ibrutinib. 48 hours after treatment, viability was determined by Alamar Blue (n>3).

The combination of BTK and proteasome inhibitors shows hallmarks of proteasome inhibition in cells. To identify the secondary target of BTK inhibitors that is responsible for the synergy with LU-102, we decided to focus on TNBC cells so that any effects related to direct inhibition of BTK are excluded and to focus on CGI-1746 because it was most synergistic and less toxic when used as a single agent. We performed next-generation RNA sequencing of MDA-MB-231 cells treated with CGI-1746 at 20 μM, LU-102 at 3 μM, the combination of the two drugs, a vehicle control, and 25 nM bortezomib as a proteasome inhibitor control. The cells were treated for four hours and then collected, and RNA was isolated and sequenced in order to identify early changes in the cell that precede the onset of apoptosis. Upon RNA sequencing analysis, two top-upregulated mRNA in cells treated with the drug combination encoded molecular chaperons of Hsp70 family pathways (Fig. 3.5). These genes are usually upregulated by proteasome inhibitors[283,284]. This was unsurprising as LU-102 is a proteasome inhibitor, however, what was surprising is that CGI-1746 up-regulated these genes more than LU-102 as a single agent.

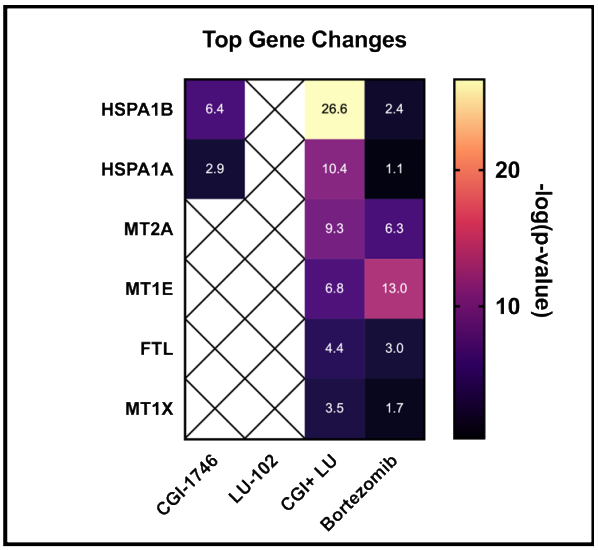

Figure 3. 5 Top Gene Changes in TNBC upon treatment with CGI-1746 and proteasome inhibitors.
MDA-MB-231 cells were treated with 10 μM CGI-1746, 3 μM LU-102, and 20 nM Btz for 4 hours, RNA expression was determined by RNA sequencing. Fold-increase over mock-treated samples in the expression of protein-encoding genes most up-regulated by CGI-1746/LU-102 combination is presented**.**

The results of RNA sequencing suggest that CGI-1746 exerts its effects in the ubiquitin proteasome pathway (UPS).

Proteasome inhibition by FDA-approved inhibitors has been shown to upregulate protein chaperones and aggresome formation which precedes induction of the autophagic pathway[285–290]. It has been reported that upon proteasome inhibition, BiP (ER-resident protein chaperone) expression increases and it becomes arginylated at the N-terminal. At the same time, p62 (also known as sequestome 1/SQSMT1, an autophagy receptor) is upregulated and becomes phosphorylated at serines 405 and 409[291]. The interaction of BiP and phosphorylated p62 leads to the formation of aggresomes which sequester ubiquitinated proteins, delaying their delivery to the proteasome, and also upregulating autophagy[291–293]. We probed for evidence of BiP-p62-

induced aggresome formation. In Figure 3.6, we found that with CGI-1746 alone, BiP upregulation was seen at 12 hours of treatment, and a slight increase in phosphorylation of p62 was seen at 2 hours of treatment. However, LU-102 on its own did not cause any change in the expression of either protein when compared to the control treatment. With the combination treatment, rapid BiP upregulation was seen at 2 hours of treatment with a peak at 6 hours of treatment. An increase in p62 phosphorylation was similarly seen starting at 2 hours, with peak expression at 6 hours of treatment. At 6 hours of treatment with a low concentration of bortezomib (25nM), BiP upregulation was seen, although, at this concentration, no change in p62 phosphorylation was seen, though it has been reported to occur as a pro-survival mechanism before apoptosis induction[292,294–298]. Other signs of compromised UPS function were also observed with the combination treatment. c-Myc, a short-lived protein that accumulates when the proteasome is inhibited, is seen here to accumulate with the CGI-1746 – LU-102 combination treatment, and HSP70, a protein chaperone known to be upregulated by proteasome inhibition and ER stress was also induced by the CGI-1746 – LU-102 combination treatment to levels comparable with bortezomib (Fig. S3.5).

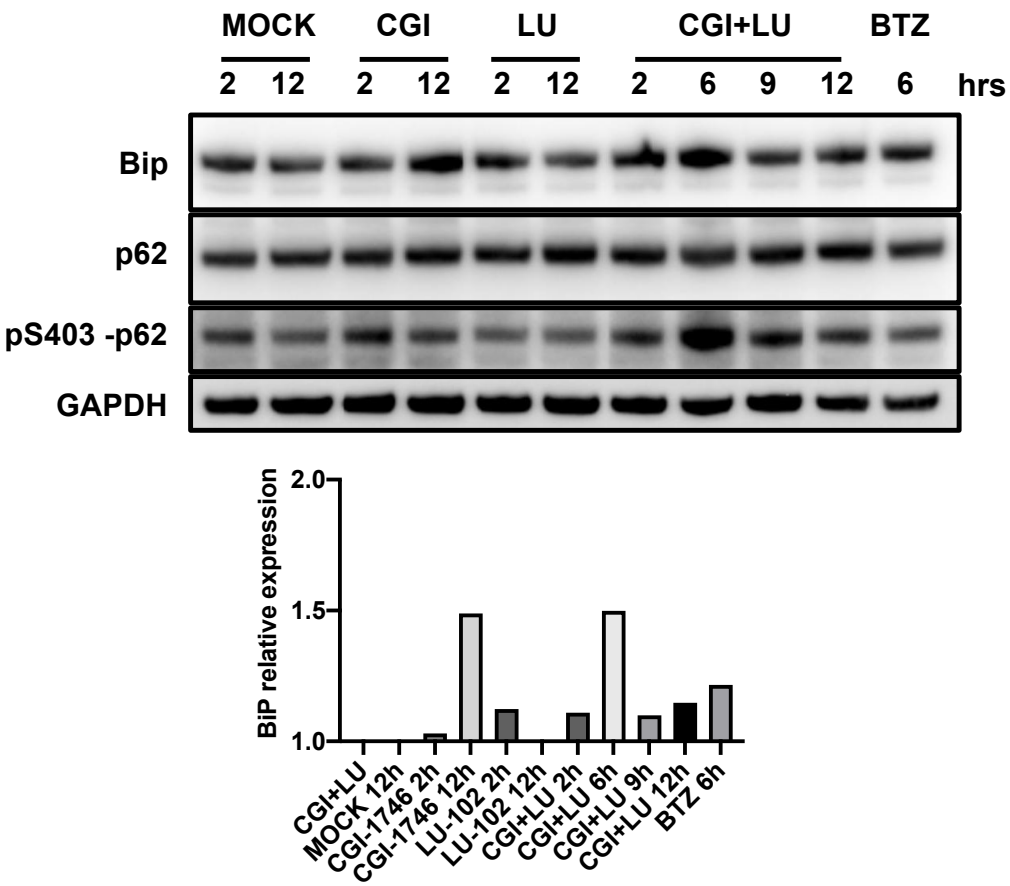

Figure 3. 6 TNBC cells treated with the CGI-1746 and LU-102 combination show markers of aggresome formation.

MDA-MB-231 cells were treated with 10 μM CGI-1746, 3μM LU-102, a combination of CGI-1746 and LU-102, or bortezomib for the indicated times, after which the cells were collected, lysed and protein expression was determined by western blot (top). BiP expression relative to GAPDH for each sample is shown on the bottom graph.

Accumulation of ubiquitin conjugates is the hallmark of intracellular proteasome inhibition. Indeed, we found that the combination of LU-102 with CGI-1746, GDC-0853, and ibrutinib caused the accumulation of conjugates. In contrast, a combination with acalabrutinib did not cause accumulation (Fig. 3.7).

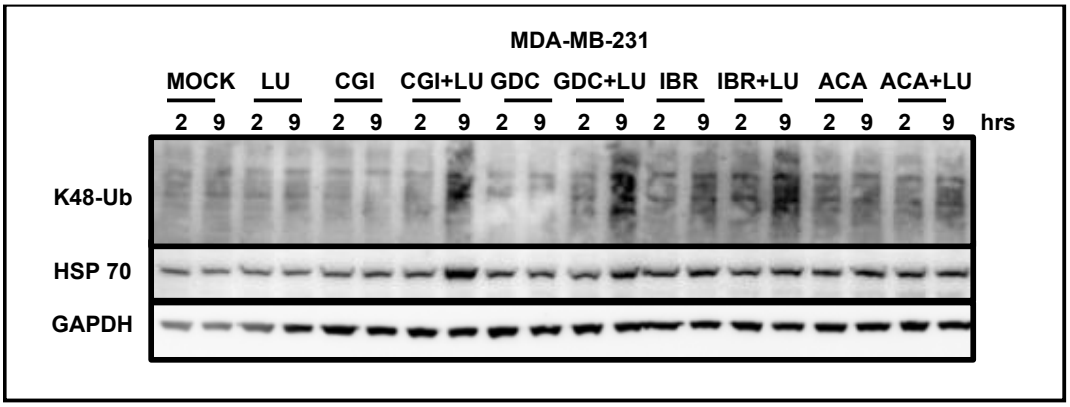

Figure 3. 7 BTK inhibitors that synergize with LU-102 in reducing TNBC viability also synergize with LU-102 in causing ubiquitin conjugate accumulation.
MDA-MB-231 cells were treated for the indicated length of time with BTK inhibitors (20 μM) alone, or in combination with LU-102 (3 μM), and protein expression was determined by western blots.

In fact, a combination of CGI-1746 and LU-102 caused a more robust accumulation of conjugates in MDA-MB-231 cells than bortezomib (Fig. 3.8a). However, they caused little or no accumulation when used as a single agent (Fig. 3.8a). CGI-1746 also enhanced carfilzomib-induced conjugate accumulation (Fig. 3.8b). These results confirm the compromised UPS pathway upregulation reported by RNA sequencing.

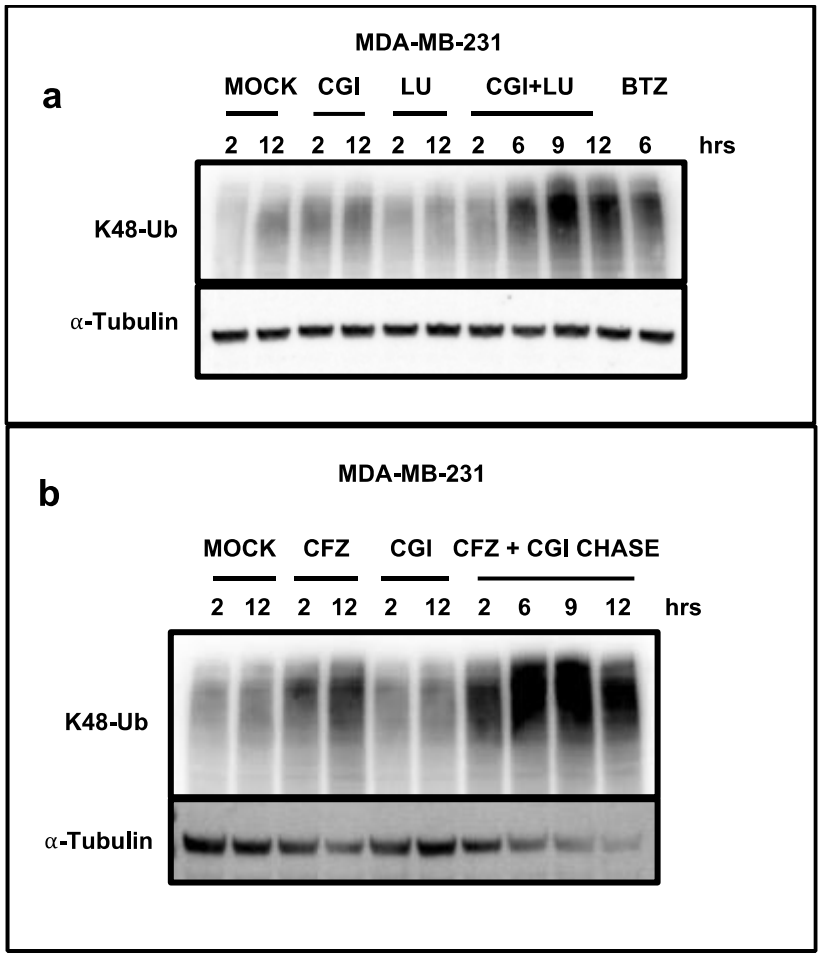

Figure 3. 8 CGI-1746 causes synergistic ubiquitin conjugate accumulation in combination with proteasome inhibitors.

(A) MDA-MB-231 cells were treated for the indicated length of time with CGI-1746 (20 μM) alone, or in combination with LU-102 (3 μM), and protein expression was determined by western blots. Btz (25 nM, 4hrs) was used as a positive control.

(B) MDA-MB-231 cells were pulse-treated with carfilzomib (CFZ) for one hour, after which carfilzomib-containing media was replaced with drug-free media or media containing 20 μM of CGI-1746.

The CGI-1746 and LU-102 combination induces cell death via proteasome inhibitor related death mechanisms. To determine whether cell death with the combination of CGI-1746 with LU-102 is due to a compromised ubiquitin-proteasome system (UPS), we considered if the changes that are known to occur upon proteasome inhibition with FDA-approved inhibitors of the β5 site of the proteasome also occur with the combination treatment.

Though catastrophic protein load is the main mechanism by which proteasome inhibitors cause cell death in multiple myeloma, the generation of reactive oxygen species (ROS) by proteasome inhibitors is thought to be the main mechanism of death in mantle cell lymphoma (MCL) for which proteasome inhibitors are also approved. ROS generation by proteasome inhibitors in other cancers and other cytotoxic agents cause ROS generation[299–302]. Furthermore, ROS generation by proteasome inhibitors in MCL causes death in a p53-independent manner[303]. Since p53 is mutated in MDA-MB-231 cells, it is possible that ROS generation upon treatment with proteasome inhibitors contributes to apoptosis in these cells. Glutathione is the main non-protein thiol in cells and serves as a cofactor for antioxidant enzymes. Upon reaction with ROS, glutathione becomes oxidized to form GSSG, detoxifying ROS in the process. We found that both bortezomib and the combination treatment caused a rapid increase in the ratio of oxidized glutathione (GSSG) to reduced glutathione (GSH) at 8 hours of treatment, using Promega GSH/GSSG-GLO™ Assay, while the individual treatments of CGI-1746 and LU-102 remained consistent with the MOCK treatment (Fig. 3.9). These results indicate that the combination treatment causes as much ROS generation as bortezomib which may contribute to apoptosis in TNBC.

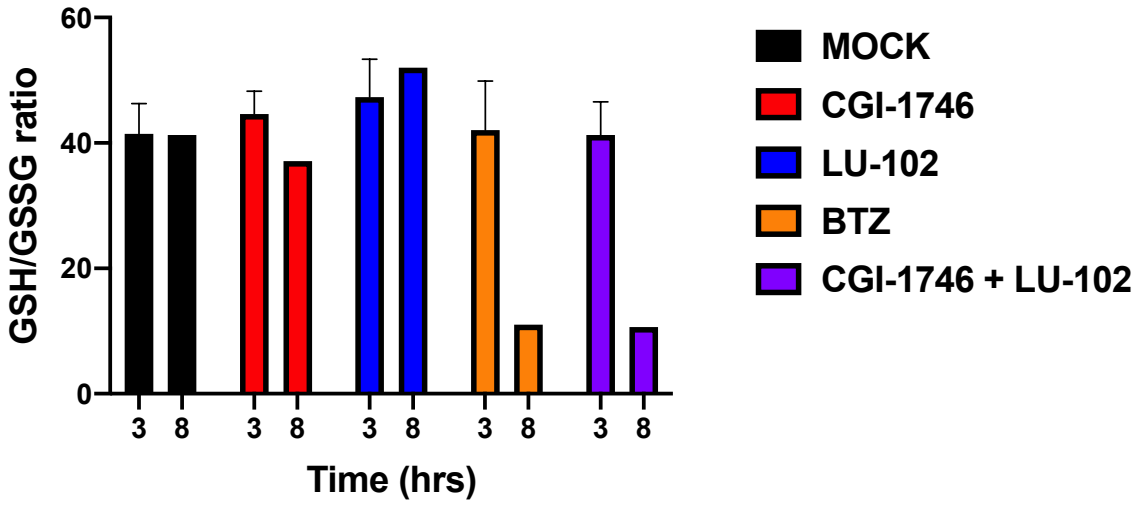

Figure 3. 9 The CGI-1746 and LU-102 combination treatment induces ROS generation in TNBC.
MDA-MB-231 cells were treated with CGI-1746 (10 μM), LU-102 (3 μM), a combination of the two, or bortezomib (25 nM) for the times indicated and the amount of oxidized glutathione and total glutathione were measured using a GSH/GSSG-Glo™ Assay. The amount of reduced glutathione was then calculated and expressed as a ratio to the amount of oxidized glutathione.

Another mechanism by which proteasome inhibitors have been shown to cause cell death is by accumulation of BH3-only proteins. Short-lived BH3-only protein, NOXA, builds up open proteasome inhibition. It has been reported that accumulation of NOXA upon proteasome inhibition is partly dependent upon c-Myc upregulation[304]. Apoptosis induction by proteasome inhibitors has been shown to be dependent on NOXA in several cancers[303,305–307]. Our lab has found that knocking down NOXA completely rescues triple-negative breast cancer cells from proteasome inhibitor-induced cell death (unpublished data). We found using immunoblotting, in MDA-MB-231 cells that had been treated with CGI-1746, LU-102, and a combination of the two drugs, that although CGI-1746 and LU-102 individually caused the accumulation of NOXA, the combination treatment caused substantially more accumulation of NOXA, staring at 9 hours of treatment, possibly contributing to apoptosis in these cells (Fig. 3.10).

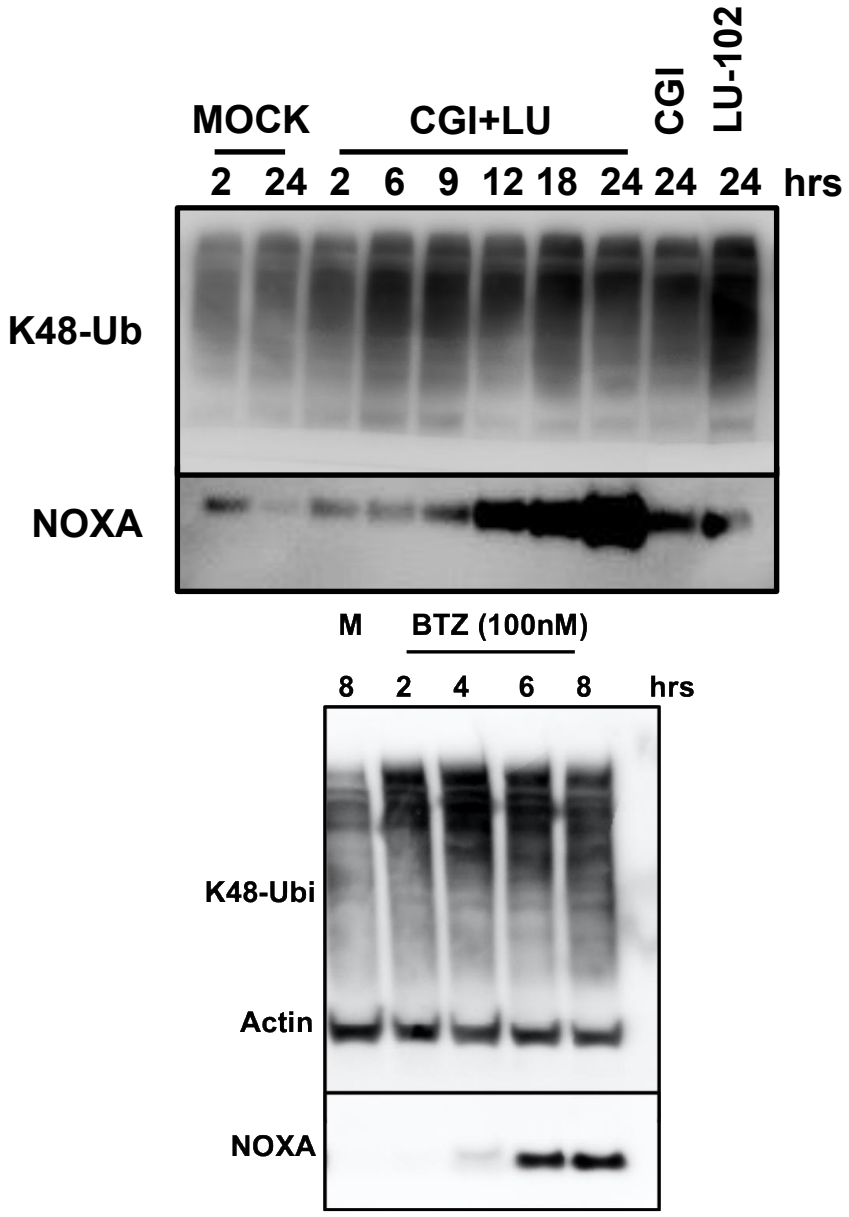

Figure 3. 10 NOXA accumulation is preceded by ubiquitin conjugate accumulation during treatment of TNBC with the CGI-1746 and LU-102 combination, or bortezomib.
MDA-MB-231 cells were treated with 10 μM CGI-1746, 3μM LU-102, or a combination of CGI-1746 and LU-102 (top), or 100 nM bortezomib (BTZ) (bottom), for the indicated times, after which the cells were collected, lysed and protein expression was determined by western blot.

CGI-1746 directly inhibits the 26S proteasome. We have confirmed (Fig. 3.11a) that BTK inhibitors and proteasome inhibitors did not inhibit deubiquitylating enzymes, which could also account for conjugate accumulation. Inhibition of valosin-containing protein (VCP/p97) has also been shown to cause ubiquitin conjugate accumulation[308,309]. Because BTK inhibitors are kinase inhibitors, there is a possibility that these inhibitors interfered with VCP ATPase function[310,311]. We performed an ATPase assay and found that CGI-1746 did not inhibit VCP ATPase activity (Fig. 3.11b). These data strongly suggest that CGI-1746 reduces proteasome activity and that this inhibition is responsible for synergistic cytotoxicity.

Proteasome activity is regulated by phosphorylation on different sites by various kinases[312–316]. Since CGI-1746 is a kinase inhibitor, we first tested whether treatment with CGI-1746 changes the pattern of phosphorylation of proteasome subunits. We isolated proteasomes from CGI-1746-treated MDA-MB-231 cells and used a phosphorylation-specific stain to identify phosphorylated subunits. We did not find any changes (Fig. 3.11c). Thus, CGI-1746 does not inhibit proteasome by reducing its phosphorylation.

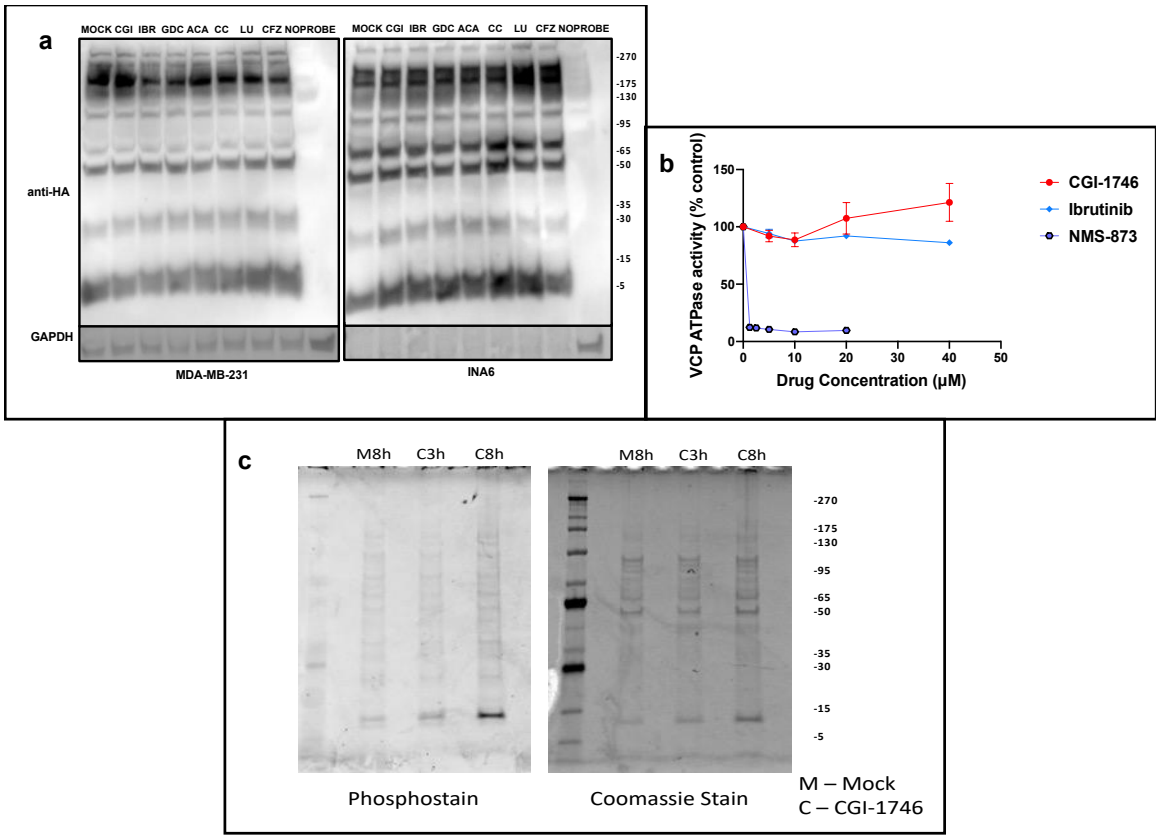

Figure 3. 11 CGI-1746 does not inhibit deubiquitinases, VCP, or proteasome subunit kinases.

(A) To investigate whether BTK inhibitors inhibit deubiquitinating enzymes (DUBs), Hemagglutinin (HA) tagged Ubiquitin-vinyl sulfone was incubated with MDA-MB-231 and INA-6 lysates, previously treated with BTK inhibitors and proteasome inhibitors, for 30 minutes at 37°C. Western blot was then performed on the lysates, probing the membrane for HA.

(B) To determine whether CGI-1746 or ibrutinib inhibits VCP ATPase activity, an ADP Glo ATPase activity assay was performed with purified VCP according to the manufacturer's protocol, using NMS-873 as a positive control for VCP inhibition.

(C) MDA-MB-231 cells were treated with CGI-1746 or mock-treated for the indicated times, after which cells were collected, lysed (by sonication in affinity purification buffer, in the presence of PhoSTOP) and proteasomes were isolated. Isolated proteasomes were separated by SDS-PAGE, and phosphorylated subunits were imaged after staining with Pro-Q Diamond Phosphoprotein Gel Stain according to the manufacturer's protocol.

To determine whether CGI-1746 directly inhibits proteasome, we examined degradation by, isolated 26S proteasome, of a ubiquitinated proteasome substrate, Ub-Sic1^{PY}, first described by Saeki et al[246]. We modified the substrate with N-terminal tetramethyl-rhodamine to increase the sensitivity and selectivity of detection. We found that CGI-1746 inhibited the degradation of Ub-Sic1^{PY} by the 26S proteasome by about 50% (Fig. 3.12).

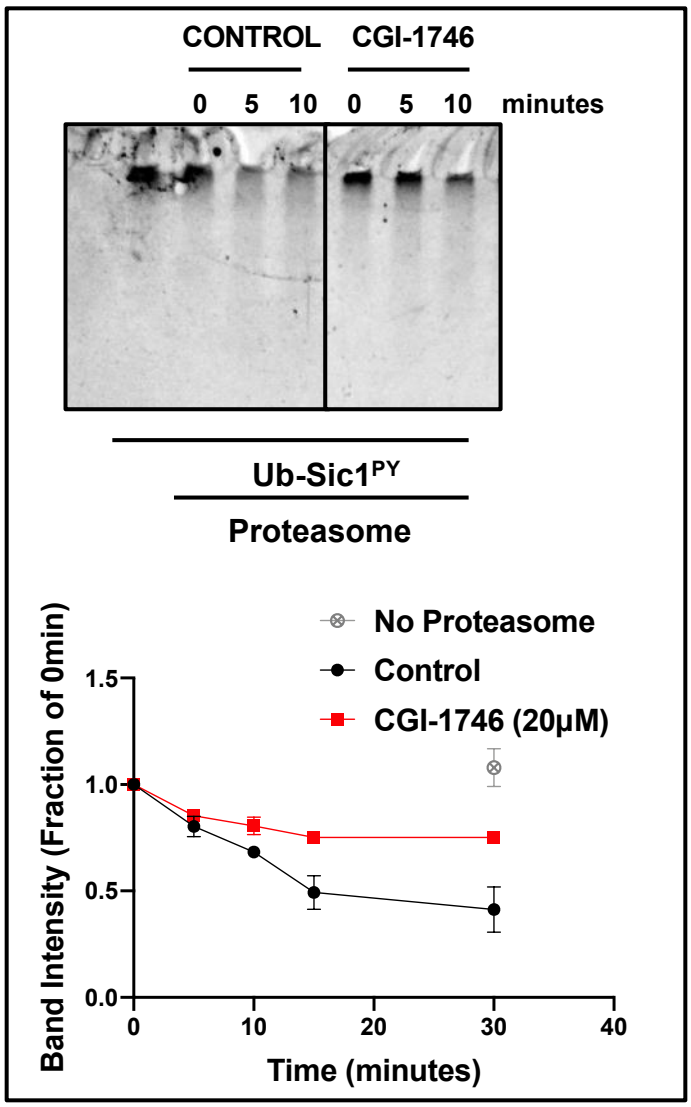

Figure 3. 12 CGI-1746 inhibits the degradation of a model proteasome substrate. Isolated human 26S proteasomes were pre-incubated with CGI-1746 for one hour, after which Rhodamine labeled Ub_n-$Sic1^{PY}$ substrate was added. Aliquots were withdrawn at indicated times and the reaction was terminated by the addition of LDS sample buffer. The reactions were then run on an SDS-PAGE, substrate was detected by fluorescent imaging, and quantified (n=5).

CGI-1746 inhibits peptidase and ATPase activities of the 26S proteasome. CGI-1746 inhibited all three peptidase (Fig. 3.13a) and partially inhibited ATPase (Fig. 3.13b) activities of the 26S particle. Except for weaker inhibition of β1 sites, ibrutinib, and GDC-0853 did not inhibit these activities. CGI-1746 also inhibited all three peptidase activities of the 20S core (Fig. 3.13c) and the ATPase activity of isolated 19S particles (Fig. 3.13d), suggesting that it has binding sites on both particles. However, inhibition of 19S ATPases and 20S core was weaker than in 26S proteasomes. ATPases were inhibited by ~30% by 5 μM CGI-1746 in 26S and 19S. Inhibition of 19S particles plateaued at this level but increased further in the 26S proteasomes. Peptidase activities in 26S proteasome were inhibited with lower IC_{50} than in 20S particles.

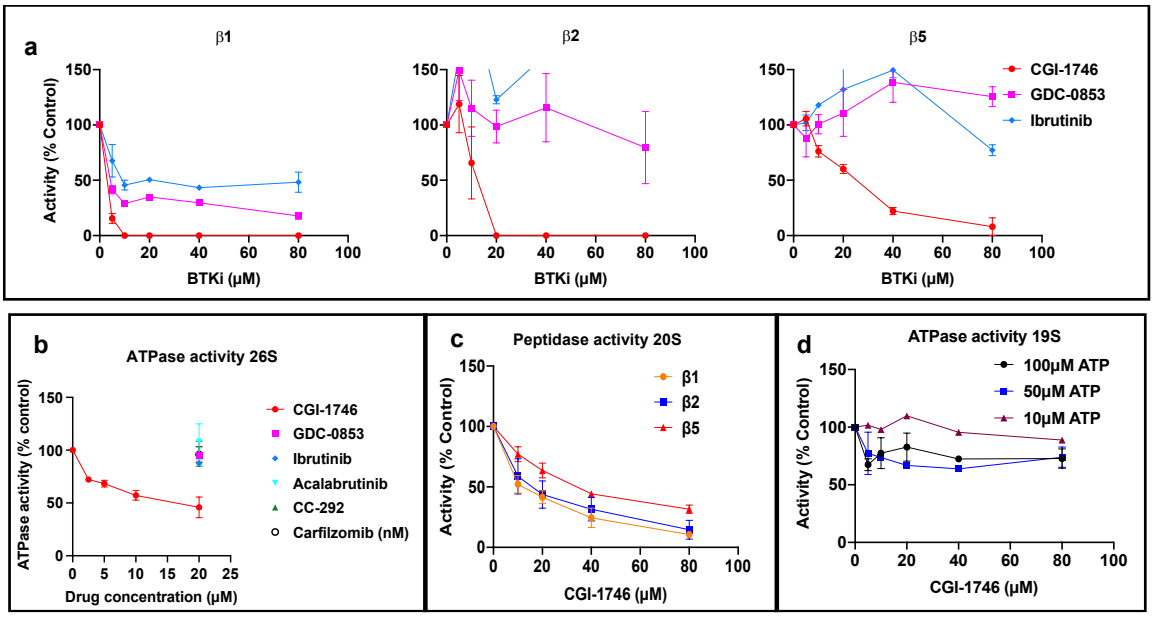

Figure 3. 13 CGI-1746 inhibits peptidase and ATPase activities of the 26S proteasome.

(A) Activities of the human 26S proteasomes were measured in the presence of BTK inhibitors using Suc-LLVY-AMC (β5), Ac-RLR-AMC (β2), and Ac-nLPnLD-AMC (β1).

(B) The ATPase activity of human 26S proteasomes was measured using ADP Glo (100 μM ATP) in the presence or absence of the indicated drugs according to the manufacturer's protocol.

(C) Activities of the 20S proteasomes in the presence of CGI-1746 were measured using peptidase substrates of individual active sites.

(D) The effect of CGI-1746 on the ATPase activity of isolated 19S (PA700) particles was measured with ADP-Glo at the indicated ATP concentrations.

These differences can be potentially explained if CGI-1746 binds at the interface between the 20S and 19S, and that binding to both increases the potency of each inhibition. Such binding should result in allosteric inhibition, and indeed inhibition of 19S ATPase activities not only did not increase with decreasing ATP concentrations but was lost at 10 μM ATP. CGI-1746 reduced V_{max} for three peptidase activities in 26S and 20S proteasomes (Fig. 3.14 a-b), clearly indicating allosteric inhibition. However, CGI-1746 appeared to induce cooperativity and slightly enhance Km, raising the possibility of two binding sites on the 20S core. Finally, we noticed that the IC_{50} for inhibition of 26S peptidase activities is higher when the assay is conducted in the absence of magnesium, which renders ATP nonhydrolyzable. This observation suggests that inhibition of ATPase activities translates to inhibition of peptidase activities at lower concentrations of CGI-1746 (Fig. 3.14c).

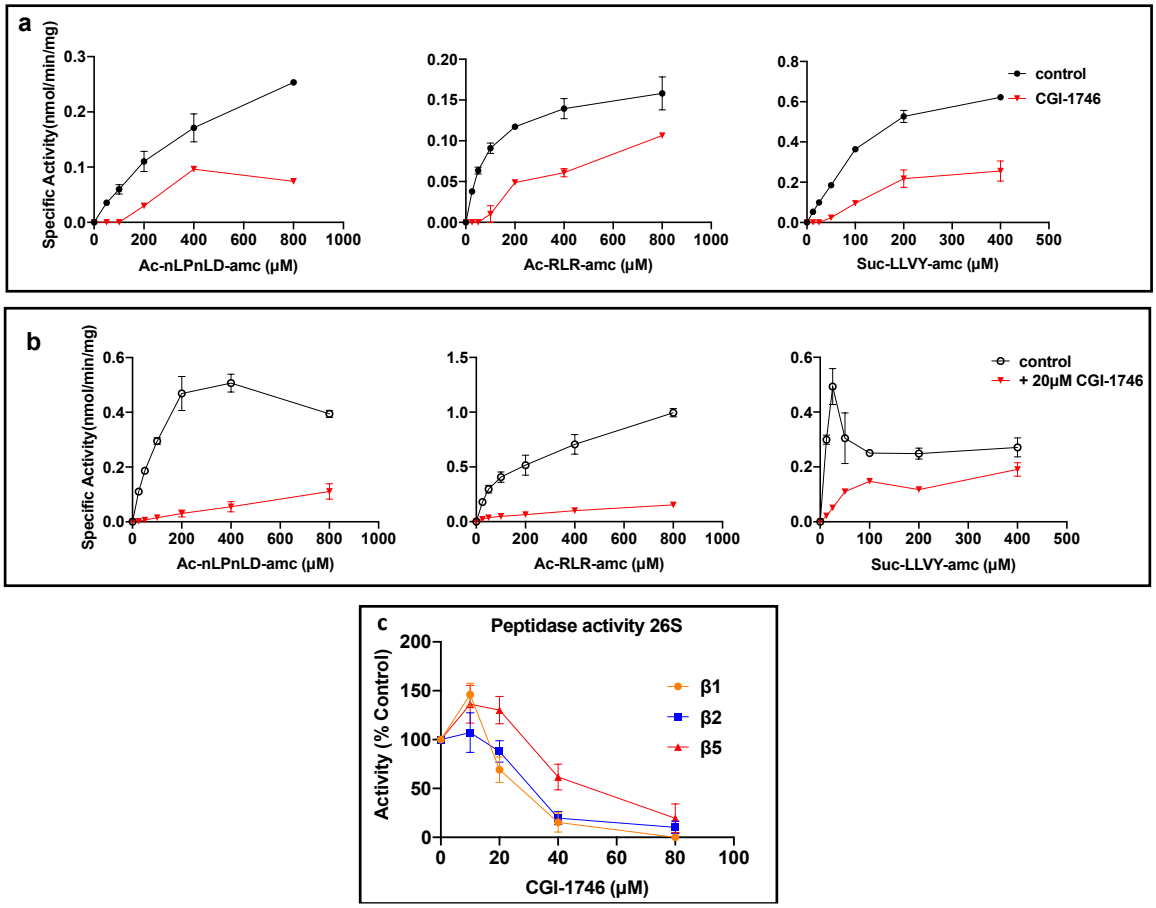

Figure 3. 14 The inhibition of the proteasome by CGI-1746 is allosteric.

(A) Peptidase activities of rabbit 26S proteasomes were measured in the presence or absence of CGI-1746 (20 μM for β1 and β5 sites, 40 μM for β2) using the indicated concentrations of site-specific substrates.

(B) 20S peptidase activities were measured in the presence or absence of 20 μM CGI-1746 at indicated concentrations of site-specific substrates for each site.

(C) Proteolytic activities of human 26S proteasomes were measured as in Fig 3.13a, except that $MgCl_2$ was omitted from the assay buffer.

We conclude that CGI-1746 has at least two binding sites on the 26S proteasome. Binding to the higher affinity binding site on the 19S particle, or perhaps at the 19S-20S interface, inhibits ATPase and peptidase sites while binding to the lower affinity site inhibits peptidase activities further and perhaps contributes to the inhibition of ATPase activities and explains the slight increase in ATPase inhibition in 26S proteasomes at higher concentrations of CGI-1746 that is not observed in the 19S particles.

CGI-1746 reduces the proportion of 26S proteasomes in cells. While CGI-1746 was able to partially inhibit proteasome proteolytic and ATPase activities at the concentrations at which it causes synergistic toxicity with LU-102, it does not cause accumulation of ubiquitin conjugates on its own in cells. Though this is expected of weaker proteasome inhibitors such as LU-102 which also does not cause accumulation of ubiquitin conjugates at concentrations at which it is specific for inhibition of the β2 site of the proteasome, it is possible that CGI-1746 binding to the proteasome on both subunits has an effect on proteasome composition within the cells.

In addition to the 26S proteasome which is responsible for the majority of protein degradation within the cell, 20S and 19S subunits of the proteasome also exist separately. These subunits spontaneously assemble to form functioning 26S proteasomes in the presence of ATP. A recent study from our lab has shown that the recovery of proteasome activity after pulse treatment of cells with proteasome inhibitors is dependent on the formation of new proteasomes but is independent of the translation of new proteasome subunits[317]. Therefore, proteasome recovery is likely due to the assembly of new 26S proteasomes from already existing individual subunits. If CGI-1746 binds to the individual subunits, it might prevent the assembly of new proteasomes

and thus, recovery of activity. We tested for interference of 26S assembly by CGI-1746 and show, in Figure 3.15, that CGI-1746 is unable to prevent the assembly of isolated proteasome subunits. However, in cells, after treatment with CGI-1746, the ratio of 26S proteasome to 20S proteasome within the cells reduced (Fig. 3.16). We are unsure about the reason for the discrepancy in the results between isolated proteins and proteins within cells. It could indicate that CGI-1746 is indirectly able to prevent proteasome assembly in a cellular context. We have not been able to test for proteasome recovery after treatment with FDA-approved proteasome inhibitors in the presence of CGI-1746 due to the inhibition of proteasome activity by CGI-1746 on its own.

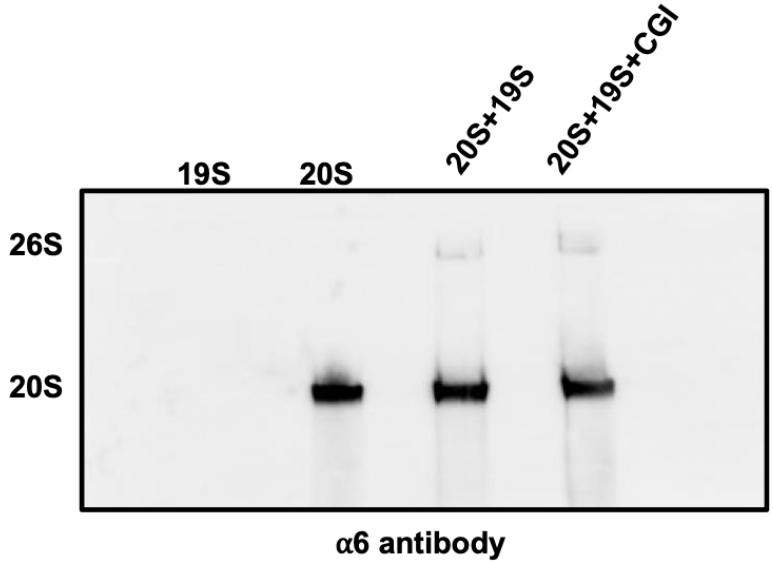

Figure 3. 15 CGI-1746 does not directly prevent 26S proteasome assembly.
Bovine 19S and 20S proteasome subunits were allowed to assemble in the presence and absence of CGI-1746. 19S, 20S, and the assembly reactions were separated by NATIVE-PAGE followed by western blot. Protein expression was determined by probing for proteasome α6 subunit.

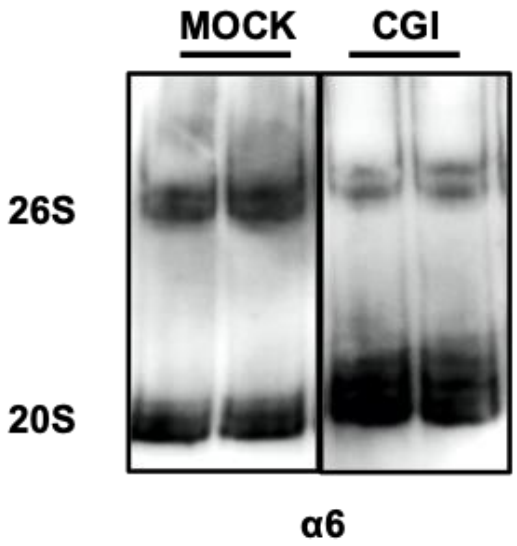

Figure 3. 16 CGI-1746 treatment results in a reduction in the proportion of 26S proteasomes in TNBC cells.
MDA-MB-231 cells were treated for 24 hours with DMSO (MOCK) or 20 μM CGI-1746. Cells were harvested and NATIVE-PAGE, western blotting was performed. Protein expression was determined by probing for proteasome α6 subunit.

Triple-negative cancer cells resistant to the CGI-1746 + LU-102 combination are also resistant to FDA-approved β5 site proteasome inhibitors. If the effectiveness of the LU-102 and CGI-1746 combination in TNBC is due to inhibition of multiple sites of the proteasome, including the β5 site and proteasomal ATPases, then TNBC cells which are made resistant to treatment by the combination therapy should also be resistant to FDA-approved inhibitors of the β5 site of the proteasome. MDA-MB-231 cells were made resistant to the combination of CGI-1746 and LU-102 (231CL.R) by repeated exposure to the combination over the period of one year, and then compared for differences in drug sensitivity. There was no significant difference in cell growth between normal MDA-MB-231 cells and resistant 231CL.R cells (Fig. 3.17).

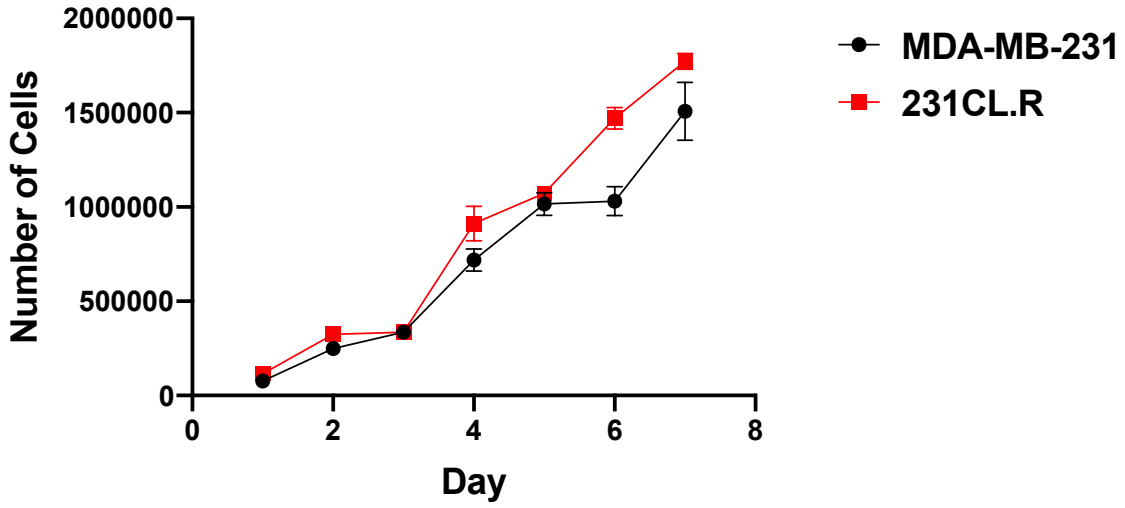

Figure 3. 17 MDA-MB-231 and 231CL.R cell growth curves.
100,000 MDA-MB-231 or 231CL.R cells were seeded on Day 0 and counted on days 1 through 7.

231CL.R and naïve MDA-MB-231 cells were treated with bortezomib and carfilzomib (Fig. 3.18). 231CL.R cells were magnitudes more resistant to treatment by bortezomib and carfilzomib than normal MDA-MB-231 cells. This indicates that 231CL.R cells have adapted to become more resistant to inhibition of the β5 site of the proteasome.

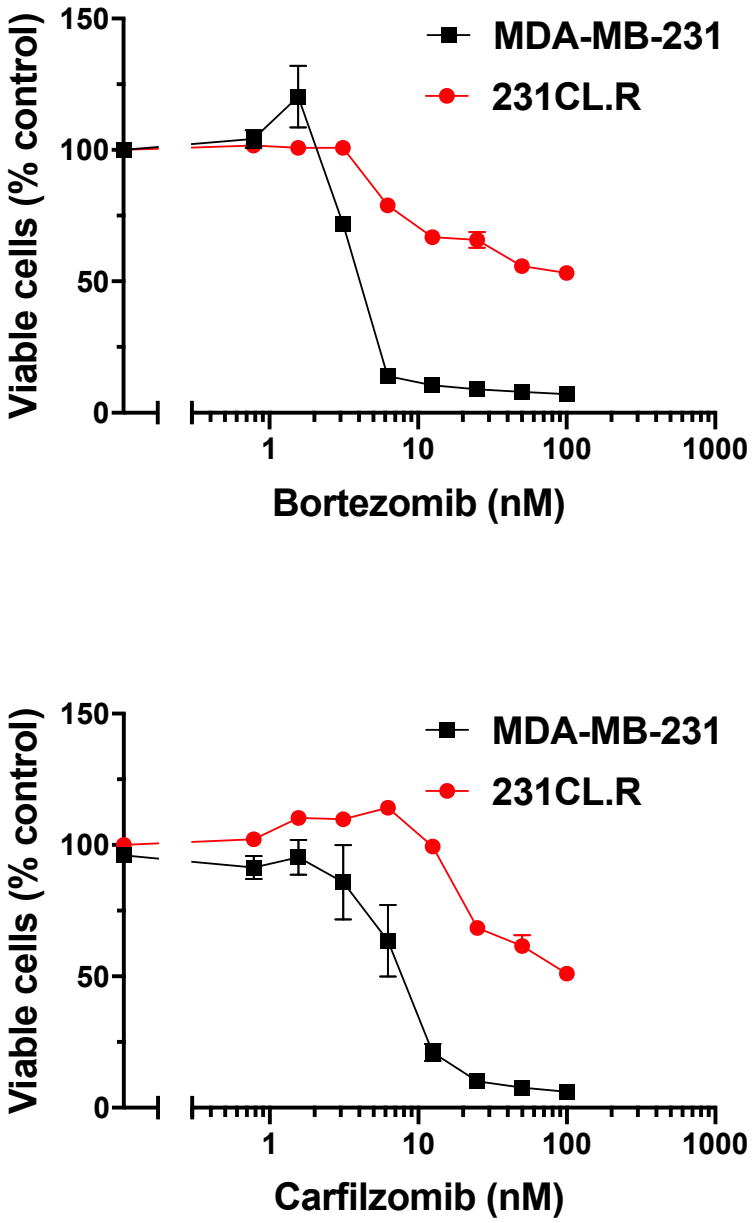

Figure 3. 18 231CL.R cells are resistant to inhibitors of the β5 site of the proteasome. MDA-MB-231 or 231CL.R cells were treated with the indicated concentrations of bortezomib (top) or carfilzomib (bottom). Viability was determined, using the Alamar Blue assay, 48 hours after treatment.

Discussion

The major goals of this chapter were to prove that ibrutinib synergy with proteasome inhibitors, with a focus on our β2 specific inhibitor LU-102, is not caused by the BTK inhibition and to identify a novel ibrutinib target responsible for this synergy. We used five different BTK inhibitors and found, that while CGI-1746 and GDC-0853 behaved similarly to Btz, two, acalabrutinib and CC-292 (spebrutinib) showed little or no synergy. For inhibitors that were synergistic, we confirmed the previous finding that synergy occurs at a much higher concentration than the concentration that completely inhibits BTK. Finally, synergy was observed in cell lines that do not express BTK. Thus, synergistic cytotoxicity between BTK and proteasome inhibitors is caused by binding to a novel target.

We switched our target identification efforts from ibrutinib to CGI-1746 because the latter showed the strongest synergy, and because CG-1746's off-target effect was the most surprising as this is the most specific BTK inhibitor among those tested in this study[278]. The compound surprised us again when we found that CGI-1746 is a dual inhibitor of 19S proteasome ATPases and of proteolytic sites of the 20S core particle. To the best of our knowledge, this is the first example of such a dual inhibitor, and the ability of CGI-1746 to inhibit free 20S and 19S suggests binding sites on both particles, although a binding site on their interface cannot be ruled out. Decrease in the V_{max} for inhibition of peptidase sites, and lack of inhibition at lower ATP concentration are consistent with non-competitive, allosteric inhibition of both activities.

Several ATPase binders were described in the literature but their ability to inhibit their ATPase activity was not reported[271–273]. As such, CGI-1746 is the first small molecule inhibitor of 19S

ATPase activity, which is not a non-hydrolyzable ATP analog. Inhibition of ATPases was detectable at lower concentrations than inhibition of peptidases but it plateaued at ~2/3 of activity in the free 19S, raising a question of whether it completely inhibits two of its six ATPases, or partially inhibits all of them. Interestingly, the activity of ATPases of the 26S, which also appeared to plateau at ~2/3 of the control at ~5 μM CGI-1746 as in the 19S, declined further at higher concentrations. This decline which coincided with the inhibition of peptidase activities of free 20S, suggests that CGI-1746 binding to the 20S core also causes mild allosteric inhibition of 19S ATPases. Conversely, IC_{50} for inhibition of 20S peptidase active sites, and for 26S measured in the absence of Mg^{2+} were higher than for 26S in the presence of Mg^{2+} suggesting that inhibition of peptidase activities of 26S at lower concentrations of CGI-1746 may be by inhibition of 19S functions. High-resolution structural studies of the 26S are needed to determine whether such allosteric interactions between 19S and 20S exist.

Allosteric inhibition of 20S peptidase activities is not as novel as inhibition of ATPases because several allosteric inhibitors have been reported[318–321]. The increasing number of allosteric inhibitors of the proteasome is raising the question of whether allosteric effects play any role in the regulation of 26S activity in the cells. If allosteric inhibitors bind inside the particles, can these sites be used by incoming proteins or degradation intermediates to fine-tune the activity of proteolytic sites[319]? If allosteric regulators bind outside, could intracellular peptides, metabolic intermediates, or other small molecules bind to them to regulate proteasome activity as suggested recently by the Sharon group[320]? If they bind at the 20S/26S interface, could they regulate gating and/or dynamic interactions between 19S and 20S? In any case, the time is ripe for rigorous structural studies of allosteric inhibitors.

Ibrutinib and GDC-0853, which synergize with LU-102 in causing cell death, also synergized in causing ubiquitin conjugate accumulation. However, they did not inhibit ATPase activities of 19S and p97/VCP and inhibited only the β1 sites, plateauing at 50%. It remains to be determined whether this inhibition of β1 sites is sufficient to cause synergy, or if other mechanisms are involved.

The micromolar concentration at which synergy is observed is too high for the observed effect to have any therapeutic value, especially for CGI-1746, which had to be used at 100 mg/kg to achieve BTK inhibition in mice[278]. While analysis of proteasome inhibition by other kinase inhibitors is underway, the possibility that some of them will be more potent inhibitors of the proteasome cannot be ruled out. In fact, mTOR inhibitor rapamycin allosterically inhibits 20S and interferes with 26S assembly at a lower concentration than CGI-1746[322]. Therefore, we believe that all new kinase inhibitors should be counter-screened for proteasome inhibition.

Another goal of this chapter was to show that the combination of CGI-1746 and LU-102 in cells promotes the same proteasome inhibitor-related cell death mechanisms as those elicited by FDA-approved inhibitors of the β5 site of the proteasome and whether this multi-modal inhibition of the proteasome is responsible for synergistic cytotoxicity with the combination treatment. There are several reasons to believe that the observed inhibition of proteasome ATPase (and perhaps proteolytic activities) is responsible for CGI-1746 synergistic cytotoxicity with LU-102 and β5-specific inhibitors. ATPase inhibition was observed at the same concentration as synergy. CGI-1746 inhibited the degradation of a model protein at the concentrations that caused synergy. Gene expression profiling was consistent with a combination of CGI-1746 and LU-102 acting as

proteasome inhibitors. The combination also synergized in causing the accumulation of ubiquitylated proteins in cells. β2 inhibitors are much weaker inhibitors of protein degradation[323], and as such LU-102 may benefit more from additional inhibition of ATPase activities than carfilzomib or bortezomib, thus explaining stronger synergy of the LU-102/CGI-1746 combination.

We found that hallmark mechanisms of antineoplastic activity of proteasome inhibitors – aggresome formation, unfolded protein response, heat shock response, c-Myc upregulation, and generation of reactive oxygen species – are induced by the combination treatment. These signs all point to proteasome inhibition being the reason for apoptosis in triple-negative breast cancer cells treated with the combination of CGI-1746 and LU-102.

Part of developing a novel treatment modality is understanding the possible resistance mechanisms that might emerge as a result of the treatment. We developed 231CL.R cells from MDA-MB-231 cells which were made resistant to the combination of CGI-1746 and LU-102. These cells are also resistant to FDA-approved inhibitors of the β5 site of the proteasome. Mutations in the β5 catalytic site are common with cells made resistant to FDA-approved inhibitors of the β5 site in vitro[324–327]. Due to the inhibition of the β2 site by LU-102 and resistance to β5 site inhibitors, 231CL.R cells will need to be assessed for mutations in both the β2 and β5 sites. Furthermore, 231CL.R cells should be evaluated for the efficiency of ATP hydrolysis in the future. Finally, RNA sequencing of 231CL.R cells should be performed and compared to MDA-MB-231 cells to find overall pathways changed in resistance that may better mimic changes that may arise in vivo.

In Summary, we have identified a dual inhibitor of 20S proteolytic core and 19S regulatory particles. While it is not yet clear whether this discovery has therapeutic implications, this inhibitor should at least serve as a novel tool to dissect proteasome mechanisms and serve as a starting point for the development of specific inhibitors of proteasomal ATPases.

Significance

This chapter unequivocally demonstrates that the previously described synergy between BTK inhibitor ibrutinib and proteasome inhibitors in inducing the death of cells derived from B-cell malignancies is due to an off-target effect of ibrutinib. We also found that another BTK inhibitor, CGI-1746, is a dual inhibitor of proteasome proteolytic and ATPase activity. To the best of our knowledge, CGI-1746 is the first inhibitor of the proteasomal ATPases.

Chapter 4: Sustained inhibition of the β2 and β5 sites of the 26S proteasome is necessary to cause synergistic cell death in combination with inhibition of the proteasome ATPases in triple-negative breast cancer

Abstract

Specific inhibitors of the β5 site of the proteasome are approved for the treatment of multiple myeloma. Specific inhibitors of the other two sites of the proteasome have also been developed to further sensitize multiple myeloma and other cancer cells to FDA-approved proteasome inhibitors. It is known that at high concentrations, site-specific proteasome inhibitors inhibit other proteasome active sites. Here we show that at concentrations thought to be specific, given time, site-specific inhibitors lose their specificity and inhibit other proteolytic sites. We demonstrate that this loss of specificity contributes to their efficacy in reducing neoplasm viability. We further show that a combination of site-specific inhibitors at site-specific concentrations and site-specific length of treatment allows for a significant dose reduction of the inhibitors used. The results of this chapter provide a proof-of-concept for creating a treatment regimen comprising multiple site-specific proteasome inhibitors for the treatment of cancer.

Introduction

In Chapter Three of this dissertation, we showed that the synergy between CGI-1746 and LU-102 is due, in part, to the inhibition of both proteolytic and ATPase activities of the 26S proteasome by CGI-1746. Our lab has previously demonstrated that inhibition of the proteasome at multiple sites allows clinically achievable inhibition of the proteasome – enough to cause significant cell death in solid tumors – which FDA-approved inhibitors of the β5 site of the

proteasome are unable to achieve when used alone[112]. For this reason, our lab developed specific inhibitors of the two other catalytic sites of the proteasome, β1 and β2.

The reason for stronger synergy with LU-102 rather than FDA-approved inhibitors of the β5 site of the proteasome was speculated in the previous chapter. In this chapter, we show that inhibition of the β2 site of the proteasome, alone, in combination with inhibition of the proteasome's ATPases is insufficient to cause synergistic cell death in TNBC, and that inhibition of the β5 site is also required.

Results

The synergy between LU-102 and CGI-1746 is not entirely due to the inhibition of the proteasome's β2 site by LU-102. Since we have determined CGI-1746's contribution to synergy with LU-102 to be at least partly due to the inhibition of proteasomal ATPases, we wanted to find out if LU-102's contribution to synergy is strictly due to the inhibition of the proteasome's β2 site. This was due to the fact that the inhibition of the proteasome's β2 site by LU-102 was more synergistic in combination with BTK inhibitors than FDA-approved inhibitors of the β5 site. Though we speculated, in Chapter 3, that the synergy was due to dual inhibition of the proteasome's ATPase and proteolytic activities by CGI-1746 eliciting a synergistic inhibitory effect on the proteasome as β2 site inhibition alone is not as detrimental to proteasome function as β5 site inhibition, it could also be that LU-102 has an additional target that enhances synergy with BTK inhibitors.

Our lab has generated MDA-MB-231 cell lines that have the proteasome's β2 site mutated by CRISPR[112]. The proteasomes in these cells lack β2 activity, though β1 and β5 activities are unaffected, and the proteasomes remain intact. Treatment of these cell lines with CGI-1746 did not cause the reduction in viability that was expected given the high synergy between CGI-1746 and LU-102 treatments in wild-type MDA-MB-231 cells (Fig. 4.1). Not much difference was seen when the mutant cells (β2ΔI3 and β2T1A) were treated with LU-102 when compared to the wild-type cells though there was a slight reduction in the EC_{50}s for the mutant cells compared to the wild-type cells.

On the other hand, loss of viability was seen upon treatment with bortezomib as would be expected with both β2 and β5 site inhibition.

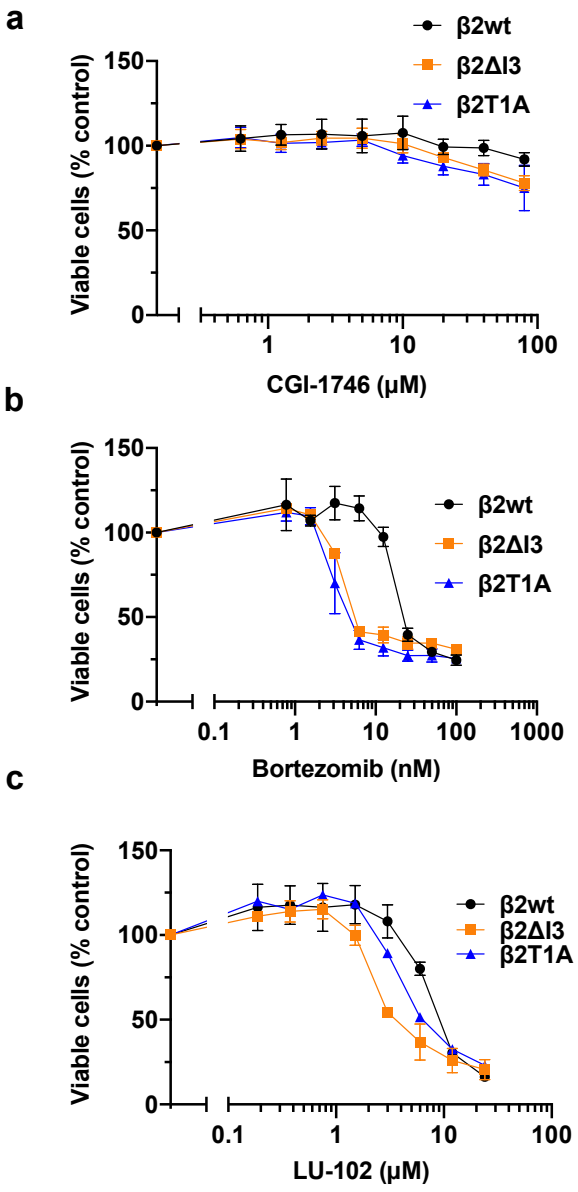

Figure 4. 1 Response to CGI-1746 and proteasome inhibitors in CRISPR wild-type and proteasome β2 site mutated MDA-MB-231 cells.

CRISPR wild-type and proteasome β2 site mutated cells were treated with CGI-1746 (A), LU-102 (B), and bortezomib (C) at the indicated concentrations for 48 hours after which viability was measured using Alamar Blue dye. Absorbance was measured on a plate reader.

Treatment with a combination of CGI-1746 and LU-102 in the mutant cells was highly synergistic at low concentrations of CGI-1746, even more so than in the wild-type cells (Fig 4.2) though this synergism was muted at higher concentrations of CGI-1746, possibly due to the toxicity of LU-102 in these cells. This could indicate a secondary target for LU-102 in these cells.

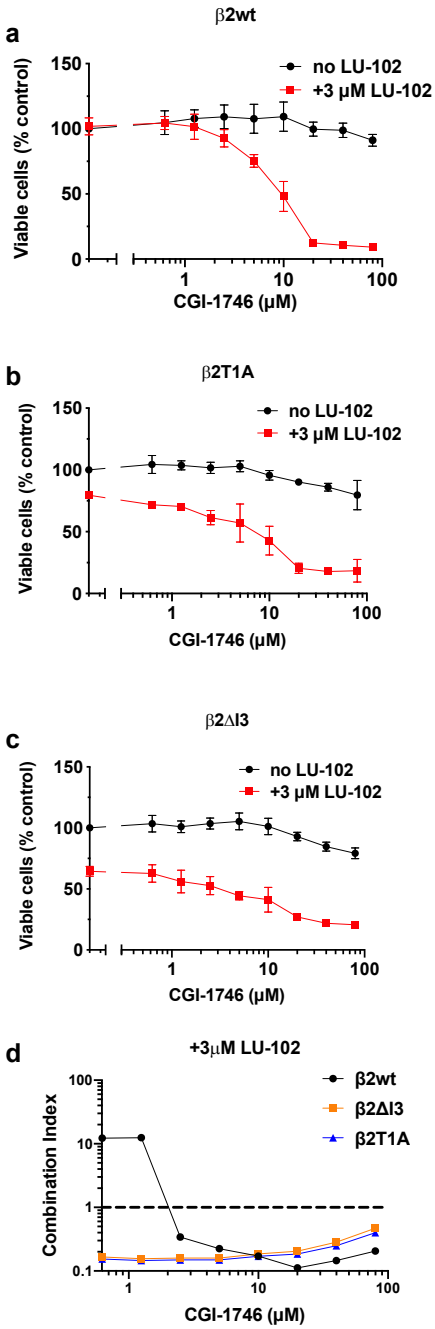

Figure 4. 2 CGI-1746 and LU-102 synergize in the reduction of viability of MDA-MB-231 cells with CRISPR mutated β2 sites of the proteasome and wild-type cells.
Wild-type MDA-MB-231 (A) and MDA-MB-231 cells with CRISPR mutated β2 sites of the proteasome, (B) and (C), were treated with the indicated concentrations of CGI-1746 without, or in combination with, 3 μM of LU-102 for 48 hours after which viability was determined. (D) – The combination indices of the experiments performed in (A-C)

We were aware that LU-102, at high concentrations, inhibits cathepsins and the β5 site of the proteasome[328]. These effects have not been observed at the concentration of LU-102 (3 μM) used in these experiments. Given the length of time of our treatments for viability studies, however, we thought it possible that low concentrations of LU-102 could inhibit these two targets.

We considered the possibility that a low concentration of LU-102, a vinyl sulfone, could inhibit cathepsins. Cathepsins are a group of (mostly cysteine) proteases, several cathepsins are responsible for protein digestion in lysosomes. Vinyl sulfones were developed to inhibit this class of proteases[329–332] which also play a role in malignancy; therefore, it was not out of the realm of possibility that synergy with CGI-1746 could be due to the inhibition of cathepsins. We treated both wild-type and mutant cells with a combination of CGI-1746 and cell-permeable pan cathepsin inhibitor, E64d (Fig. 4.3), and β5 inhibitors with E64d (Fig. 4.4) There was no synergy with these treatments which indicated that synergy between LU-102 and CGI-1746 is not due to off-target inhibition of cathepsins by LU-102.

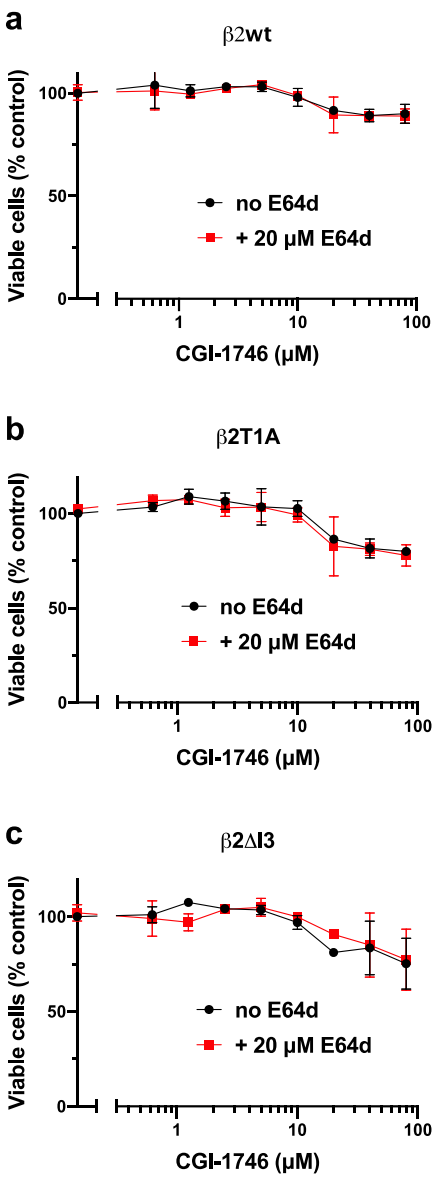

Figure 4. 3 The synergy between LU-102 and CGI-1746 is not due to inhibition of cathepsins.

Wild-type MDA-MB-231 (A) and MDA-MB-231 cells with CRISPR mutated β2 sites of the proteasome, (B) and (C), were treated with the indicated concentrations of CGI-1746 without, or in combination with, 20 μM of E64d for 48 hours after which viability was determined.

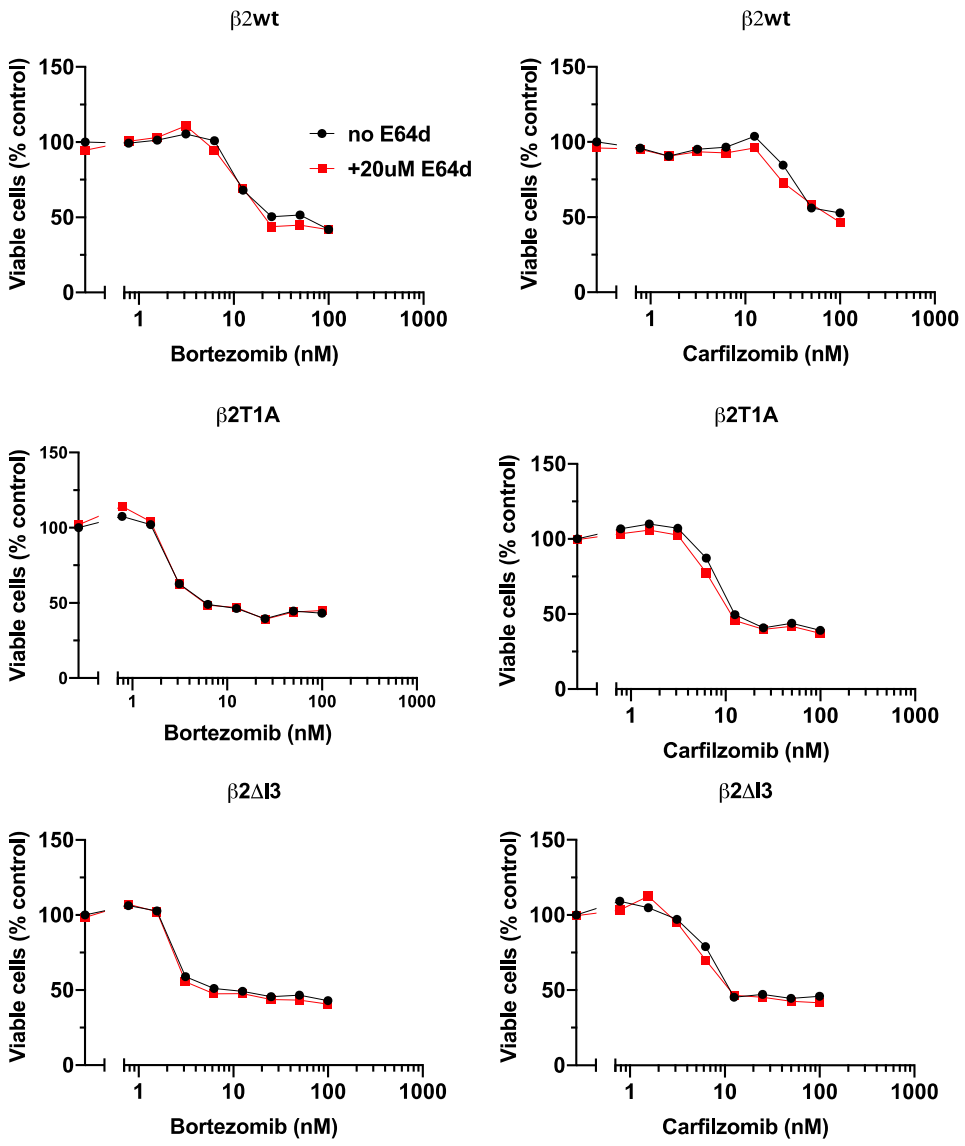

Figure 4. 4 Inhibitors of the proteasome's β5 site do not synergize with cathepsin inhibitor, E64D.

Wild-type (top) and mutant (middle and bottom) cells were treated with bortezomib (left), carfilzomib (right), at indicated concentrations, or a combination of either drug with E64D. Viability was determined 48 hours after treatment using Alamar Blue assay.

The synergy between LU-102 and CGI-1746 is partly due to the inhibition of the proteasome's β2 site by LU-102. To see if synergy is at least partly due to the pharmacologic inhibition of β2 activity, we treated MDA-MB-231 cells with a combination of CGI-1746 and an inactive analog of LU-102 which lacks the vinyl sulfone (VS-less) so that it does not inhibit proteasome β2 activity. We found that neutered LU-102 does not improve the toxicity of CGI-1746 and has no effect on the viability of MDA-MB-231 cells (Fig. 4.5)

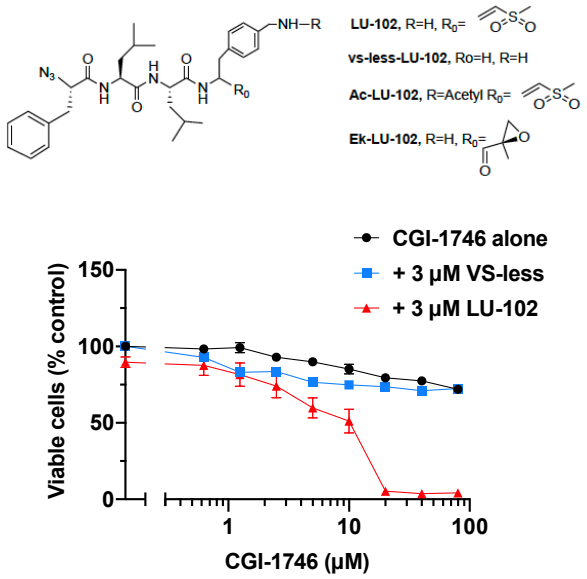

Figure 4. 5 Inhibition of the β2 site of the proteasome ins necessary for synergy with CGI-1746.
The structure of β2 site inhibitor with R representing the side chain, and R_0 representing the warhead for each inhibitor (top). MDA-MB-231 cells were treated with the indicated concentrations of CGI-1746 alone (black), in combination with 3 µM of VS-less (blue), and 3 µM of LU-102 (red) for 48 hours, after which viability was determined (bottom).

Furthermore, analogs of LU-102, an epoxyketone instead of a vinyl sulfone moiety, and acetylated LU-102, that inhibit β2 activity also synergize with CGI-1746 (Fig. 4.6a). Both inhibitors were more synergistic with CGI-1746 than LU-102. We know that both these compounds are less specific for β2-site inhibition than LU-102 and also inhibit the β5 site of the proteasome even at low (1 μM) concentrations (Fig. 4.6b). Therefore co-inhibition of the β2 and β5 sites of the proteasome sensitizes TNBC cells to inhibition of proteasomal ATPases by CGI-1746.

While LU-102 is considered specific for the β2 site of the proteasome at the 3 μM concentration we used in these experiments[328], we considered whether it could also inhibit other sites of the proteasome in cells given time. While our mechanistic investigation into cell death with the combination treatment, in Chapter 3, looked into a short window of treatment time (12 hours), viability measurements that show synergy were determined 48 hours after treatment. Also, in Chapter 3, Figure 3. 10, treatment with LU-102, at 3 μM, alone causes significant ubiquitin conjugate accumulation in MDA-MB-231 cells after 24 hours of treatment. Because inhibition of the β2 site of the proteasome alone is not able to cause critical ubiquitin conjugate accumulation, other sites of the proteasome might also be inhibited. To consider whether LU-102 inhibits other sites of the proteasome during the 48-hour treatment time, we treated MDA-MB-231 cells with 3 μM of LU-102 and determined whether the β5 site of the proteasome is inhibited using affinity-based probe MV-151. We found that while, at first, LU-102 selectively inhibits proteasome β2 activity, over time, it begins to inhibit β5 activity in cells as well (Fig. 4.6c).
Over the same period, we treated MDA-MB-231 cells with LU-102 and identified hallmarks of proteasome inhibition by western blotting. We found that ubiquitin conjugate accumulation

continued to increase over the 24-hour period (Fig. 4.6d) when maximum ubiquitin conjugate accumulation would be expected during the 2–6-hour window at which maximum inhibition of the β2 would have been achieved. The inhibition of the β5 site of the proteasome seen using affinity-based probes corresponded with the increase in ubiquitin conjugate accumulation in cells.

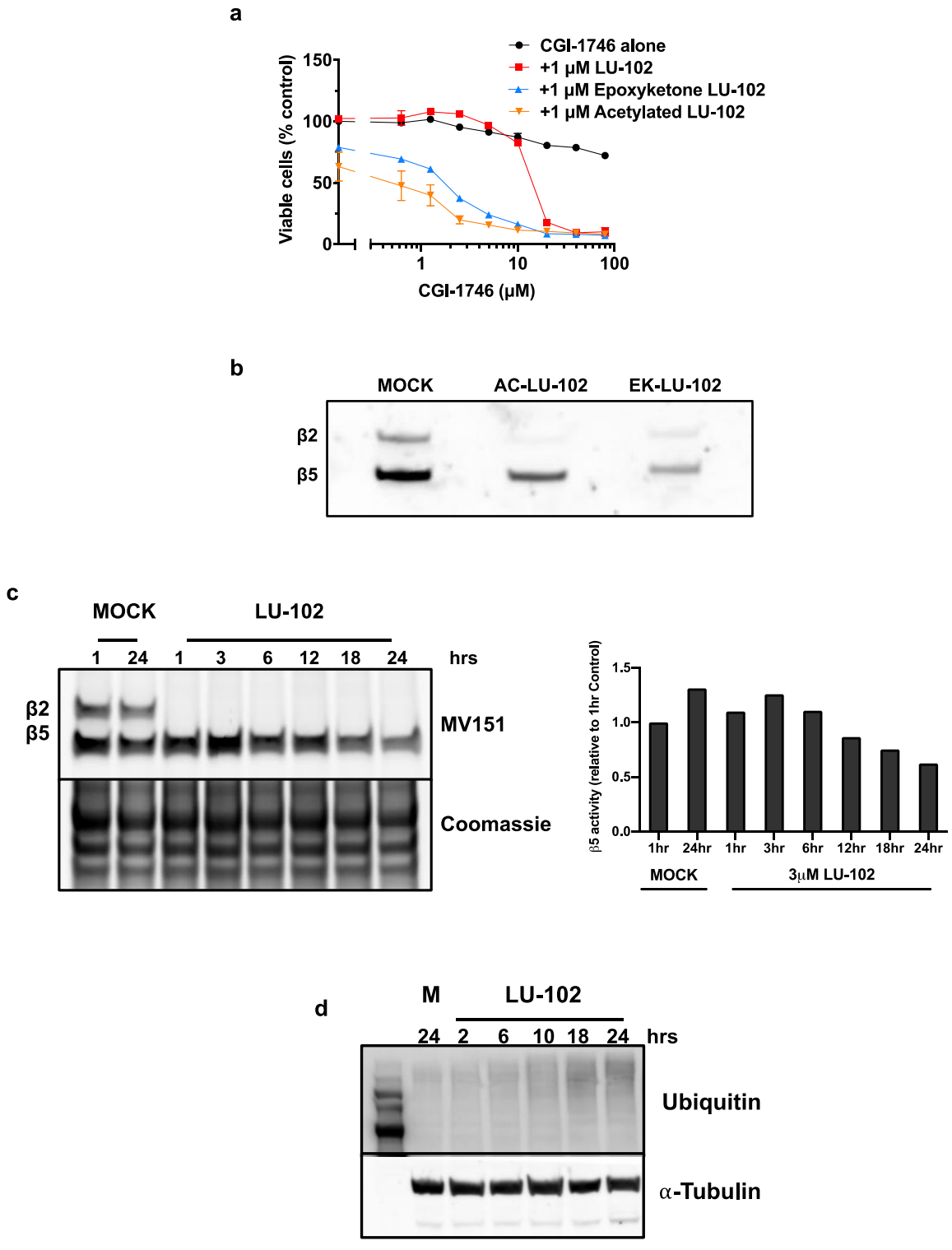

Figure 4. 6 Inhibition of the β5 site of the proteasome by β2 site inhibitors increases the sensitivity of cells to combined inhibition of the proteasome's β2 site and ATPases.

A) MDA-MB-231 cells were treated with the indicated concentrations of CGI-1746 alone (black), in combination with LU-102 (red), an epoxyketone analog of LU-102

(blue), or acetylated LU-102 (orange) for 48 hours, after which viability was determined.

B) Lysates of MDA-MB-231 cells were treated with 1 μM of acetylated LU-102 (AC-LU-102), the epoxyketone analog of LU-102 (EK-LU-102), or DMSO (MOCK) for 30 minutes. The treated lysates were then incubated with 1 μM of affinity-based probe, MV-151, for 30 minutes at 37°C after which the lysates were run on SDS-PAGE, and MV-151 fluorescence was captured on an imager (left). Activities of the proteasome β5 subunit are shown on the right.

C) MDA-MB-231 cells were treated with DMSO (MOCK), or 3 μM LU-102. Cells were harvested at the time points indicated. Cell pellets were lysed and 20 μg of protein was incubated with 1 μM of MV-151 and fluorescence was captured as in (B).

D) MDA-MB-231 cells were treated, collected, and lysed as in (A). Protein expression was determined with a western blot.

Specific β5 inhibition aids specific β2 inhibition in the synergy between CGI-1746 and LU-102. Given that we discovered LU-102 also inhibits β5 activity in cells over the period viability is monitored, we wanted to see if we could attain specific inhibition of the β2 site of the proteasome in cells over the same period, and if attaining specific inhibition of the β2 site would result in the synergy seen with continuous incubation of LU-102, or if results would be more akin to CGI-1746 treatment in MDA-MB-231 cells in which the proteasome β2 site had been mutated. The former would suggest that the synergy between CGI-1746 and LU-102 is due to the inhibition of the β2 site of the proteasome by LU-102 while the latter would suggest that synergy is more due to the inhibition of the β5 site of the proteasome by LU-102. We identified the concentration at which LU-102 is specific for the inhibition of the β2 site of the proteasome. This was achieved by pulse-treating the cells for one hour with 3 μM LU-102 at which point the media was replaced with drug-free media for the rest of the 47 hours. FDA-approved inhibitors of the β5 site of the proteasome are also known to inhibit other sites. Bortezomib can inhibit the β1 site at high concentrations, carfilzomib can inhibit the β2 site at high concentrations, and we

have also found it to inhibit the β2 site of the proteasome in cells at low concentrations with a prolonged period of treatment. We discovered, using the same method of pulse treatment as was used for LU-102, that carfilzomib is specific for β5 inhibition in cells at a 25 nM one-hour pulse treatment (Fig. S4.1).

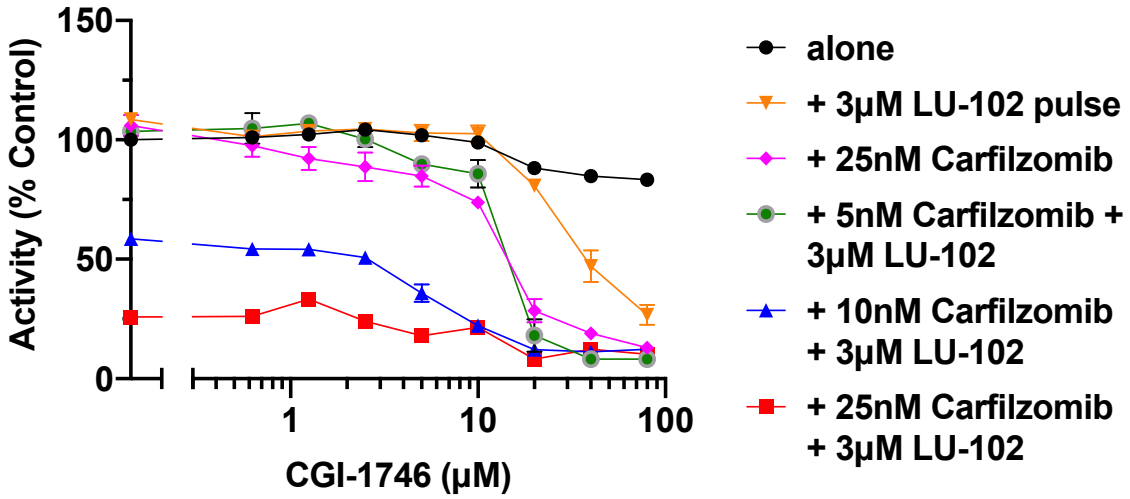

Figure 4. 7 Specific β5 inhibition aids specific β2 inhibition in the synergy between CGI-1746 and LU-102.
MDA-MB-231 cells were treated with the indicated concentrations of CGI-1746 alone (black), pulse-treated for one hour with 3 μM LU-102 (orange), 25 nM carfilzomib (pink), a combination of 5 nM carfilzomib and 3 μM LU-102 (green), a combination of 10 nM carfilzomib and 3 μM LU-102 (blue), or a combination of 25 nM carfilzomib and 3 μM LU-102 (red), and chased with the indicated concentrations of CGI-1746. Alamar blue viability assay was carried out 48 hours after the initial treatment.

We found that specific inhibition of β2 enhanced CGI-1746 toxicity in MDA-MB-231 cells at high concentrations of CGI-1746 (Fig. 4.7). Specific inhibition of the β5 site (pink) enhanced toxicity more than specific inhibition of the β2 site (orange). Specific inhibition of the β5 site and the β2 site together at 25 nM of carfilzomib and 3 μM of LU-102 respectively was highly toxic to cells with the addition of CGI-1746 providing little additional toxicity (red). The addition of CGI-1746 allowed for lower concentrations of carfilzomib to be just as effective in reducing viability in these cells (blue). These results confirm that β2 inhibition alone is insufficient to cause synergy with CGI-1746 and that β5 inhibition is also required. Therefore, the synergy we see between LU-102 and CGI-1746 is due to dual inhibition of the β2 and β5 sites of the proteasome by LU-102 during continuous treatment over the 48-hour period.

Discussion

Out of concern that strong synergy with specific β2 site inhibitor, LU-102, was stronger than synergy with β5 site inhibitors due to off-target effects of LU-102, we investigated the possible off-target effects of LU-102. We found that though LU-102 was specific for the β2 site of the proteasome, this specificity was only to an extent; given time, LU-102 will also inhibit the β5 site of the proteasome in cells, and this secondary inhibition of the β5 site contributes to the synergy with CGI-1746. Specific inhibition of the β2 site of the proteasome in combination with inhibition of the proteasomal ATPases is not sufficient to cause synergistic cell death in triple-negative breast cancer cells.

Results from this chapter provide the rationale for multi-point inhibition of the proteasome in solid tumors including triple-negative breast cancer. Specific inhibition of the β2 and β5 sites of the proteasome in combination with inhibition of the proteasome's ATPases may effectively 'cripple' cellular proteasomes at very low concentrations of each inhibitor. As such, we may be able to achieve effective proteasome inhibition, sufficient for antineoplastic activity, in solid tumors in vivo with more specific inhibition of the proteasome sites, and low concentrations of the compounds used theoretically eliciting fewer side effects. It has been shown that inhibition of two catalytic sites of the proteasome is more effective than inhibition of only the β5 site of the proteasome[265,333–335]; here, we show that additional inhibition of the proteasome's ATPases is even more effective.

Future directions of this work will involve in vivo experiments with mice models of triple-negative breast cancer. Drug combinations of carfilzomib and LU-102 have been performed in

multiple myeloma-bearing mice at up to 2mg/kg and 30mg/kg respectively[333]. In vivo experiments involving CGI-1746, on the other hand, used the compound at 100mg/kg and 200mg/kg to see the effects of the drug[336,337]. Treatment of mice bearing triple-negative breast cancer tumors should be effective with much lower doses of all three compounds used in combination based on the results seen in Figure 4.7.

In Summary, the synergy described between CGI-174 and LU-102 in Chapter Three, and in this chapter, is likely due to a 'crippling' effect on the proteasome in triple-negative breast cancer as a result of the combined inhibition of the proteasome's ATPases as well as the β2 and β5 sites. The inhibition of these sites in vivo should be effective in reducing triple-negative breast cancer tumor burden at very low concentrations due to the high synergy of this modality.

Chapter 5: Small Nucleolar RNA, SNORA71D, regulates proteostasis and apoptosis in response to proteasome inhibition

Abstract

Elucidation of the mechanisms that govern cellular response to proteasome inhibition has mainly focused on protein effectors in response to stress. Here we show through RNA sequencing, confirmed using quantitative PCR, that upon proteasome inhibition, a class of non-coding RNAs is upregulated far above any protein-coding transcript. These are small nucleolar RNAs. Focusing on one small nucleolar RNA, SNORA71D, we show, using an apoptosis-inducing drug, doxorubicin, that SNORA71D upregulation is not dependent on apoptosis. Through the use of potent endoplasmic reticulum stress-inducing compounds, we show that SNORA71D upregulation is dependent on endoplasmic reticulum stress. We further demonstrate using siRNA mediated knockdown of a SNORA71D and proteomic analysis, that SNORA71D mediates proteostasis through regulation of proteins that respond to endoplasmic reticulum stress.

Introduction

Proteasome inhibitors prevent the breakdown of unneeded and misfolded proteins by the ubiquitin-proteasome system (UPS), the primary quality control mechanism in mammalian cells. Proteasome inhibitors are approved for the treatment of multiple myeloma. Multiple myeloma is a cancer of plasma cells and is immunoglobulin-producing. Due to immunoglobulin production, there is a high protein load within the endoplasmic reticulum (ER) of these cells which is exacerbated by proteasome inhibitors and leads to cell death. Thus, proteasome inhibitors are

initially effective in the treatment of multiple myeloma in the majority of cases. However, there is an almost inevitable recurrence of multiple myeloma in patients, and this relapse is associated with resistance to proteasome inhibitors. In addition, due to the pleiotropic nature of the effect of proteasome inhibition, there remains debate about the most crucial mechanisms that lead to the death of cancer cells.

As stated in Chapter 1, one of the main mechanisms is the unfolded protein response (UPR). Misfolded proteins accumulating in the ER result in a scarcity of the ER molecular chaperone, Binding immunoglobulin protein (BiP). BiP is typically bound to ER-stress-sensing receptors in the lumen face of the ER membrane. When the buildup of misfolded protein within the ER occurs, BiP binds to the misfolded proteins within the ER, leaving the stress-sensing receptors, IRE1α, ATF6, and PERK, unbound and active[142–144]. These receptors activate downstream pathways that act to combat ER stress, typically a pro-survival response. However, the inability of these mechanisms to resolve ER stress leads to the initiation of apoptosis through the UPR. Protein regulators and initiators of apoptosis are mostly known[141,143,152], however, there remains some debate about the details of apoptosis initiation through this pathway.

Non-coding regions of DNA were previously thought of as 'junk DNA[338]', 98.5% of human genetic material which do not encode proteins and once thought unimportant, unlikely to confer any evolutionary advantage. However, we now know that this so-called 'junk DNA' is a treasure trove of information that governs cellular function and is transcribed along with exons and is processed post-splicing. The transcripts from this DNA include long non-coding RNAs (lncRNAs), microRNAs (miRNAs) and small nucleolar RNAs (snoRNAs). MicroRNAs and long

non-coding RNAs have been shown to govern a multitude of cellular processes, including the response of cancer cells to anti-neoplastic agents[339].

Small nucleolar RNAs, a class of non-coding RNAs that guide chemical modification of cellular RNAs are the least studied group of small RNA, whose regulatory functions beyond rRNA biogenesis were discovered recently[340]. They are just beginning to be studied in relation to oncology. A few have been found to be oncogenic, with their expression resulting in sustained proliferative signaling; some participate in the activation of invasion and metastasis, others in angiogenesis; others still function as tumor suppressors, and some have been found to modulate the response of cancer cells to therapy [341,342]. There are two main classifications of snoRNAs: H/ACA box snoRNAs which classically guide the psuedouridylation of ribosomal RNAs, and C/D box snoRNAs guide methylation of ribosomal RNAs. It has recently been shown that snoRNAs are also capable of guiding the modifications of non-ribosomal RNAs[343–346]. Recent studies have observed correlations between some snoRNAs and multiple myeloma[347], though no studies have been done that show snoRNA induction by proteasome inhibitor treatment or other treatment in multiple myeloma, or that fully characterize the mechanisms by which snoRNAs function in multiple myeloma in response to proteasome inhibitors and only one snoRNA, ACA11, has been found to modulate the response of multiple myeloma cells to proteasome inhibitor therapy[348].

In this Chapter, we elucidate the relationship with one relatively understudied snoRNA, box H/ACA SNORA71D, and ER stress. We relate this relationship to the response to proteasome

inhibitors in cancer cells and demonstrate how knocking down this snoRNA is cytoprotective in cancer.

Results

Small nucleolar RNAs are positively upregulated following proteasome inhibitor treatment. In Chapter Three, we performed RNA sequencing on triple-negative (TNBC) breast cancer cells, MDA-MB-231, treated with bortezomib; we found that a subset of non-coding RNAs, small nucleolar RNAs (snoRNAs), were positively upregulated, more so than any mRNA or other non-coding RNA (Fig. 5.1). To confirm the RNA sequencing results, we used qPCR to determine whether the most upregulated SNORA71D, a snoRNA in the SNHG17 group of genes that have also been implicated in cancer, was truly upregulated. Tellingly, SNORA71D was also the transcript most upregulated by both CGI-1746 and LU-102 alone, and in combination according to the RNA sequencing experiments (Table S1). We found that SNORA71D was indeed upregulated upon bortezomib treatment (Fig. 5.2a). Proteasome inhibitors, though effective in vitro, are not approved for the treatment of TNBC clinically. They are, however, approved for the treatment of multiple myeloma. We performed the same experiment in INA-6 multiple myeloma cells. We found that SNORA71D is positively upregulated in multiple myeloma upon bortezomib treatment, even to a greater degree than seen in TNBC (Fig. 5.2a). Pulse treatment of cancer cells with proteasome inhibitors better mimics the clinical scenario wherein proteasome inhibitors are administered in a bolus dose and reach peak plasma concentration within one hour, after which they are eliminated. Pulse treatment of INA-6 cells with bortezomib reveals that SNORA71D upregulation is concentration-dependent (Fig. 5.2b). Results from Figure 5.2 indicate that SNORA71D upregulation is a delayed response to proteasome inhibition.

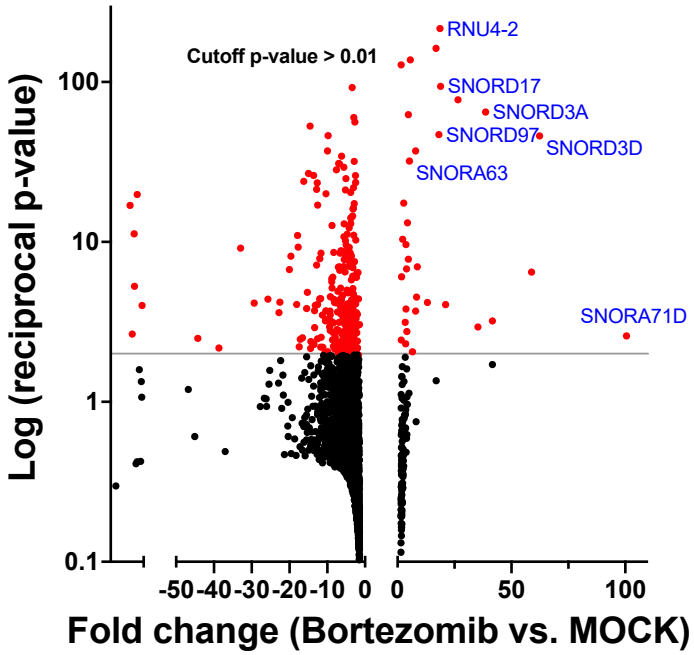

Figure 5. 1 Transcript changes upon bortezomib treatment.
MDA-MB-231 cells were treated with 25 nM of bortezomib for 4 hours, after which RNA was isolated and sequenced as in Chapter 3.

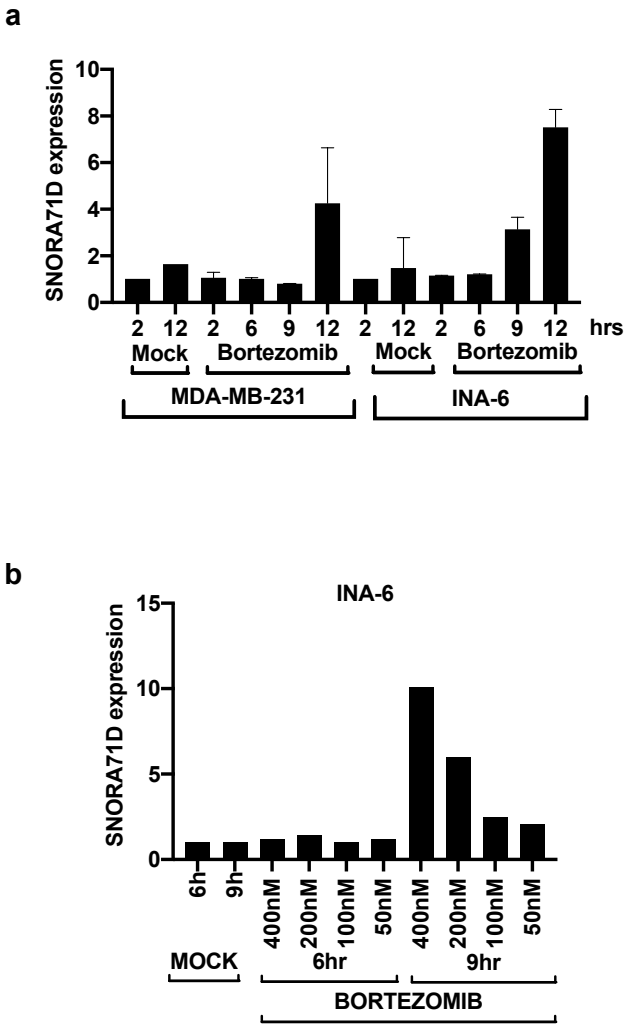

Figure 5. 2 SNORA71D is upregulated by bortezomib treatment.

A) MDA-MB-231 cells and INA-6 cells were treated with 25 nM bortezomib or DMSO (Mock) for the times indicated. qPCR was performed and SNORA71D expression was normalized to the control treatment for each cell line.

B) INA-6 cells were pulse-treated with DMSO (MOCK) or the indicated concentrations of bortezomib for one hour, and the time from the onset of treatment was 6 or 9 hours. qPCR was performed and SNORA71D expression was determined for each sample (n=1).

Treatment with another proteasome inhibitor, carfilzomib, showed a similar increase in SNORA71D expression in INA-6 cells (Fig. 5.3a). In vitro, sensitivity to proteasome inhibitors has been shown to vary in multiple myeloma cell lines[235]. MM1.S, a multiple myeloma cell line sensitive to proteasome inhibitors, showed an increased expression of SNORA71D upon bortezomib treatment compared to the control. Bortezomib caused a massive increase in SNORA71D in NCI H929 cells which are extremely sensitive to proteasome inhibitors (Fig. 5.3b). These results indicate that snoRNA upregulation may indicate sensitivity to proteasome inhibitors and may serve as a biomarker to predict patient response.

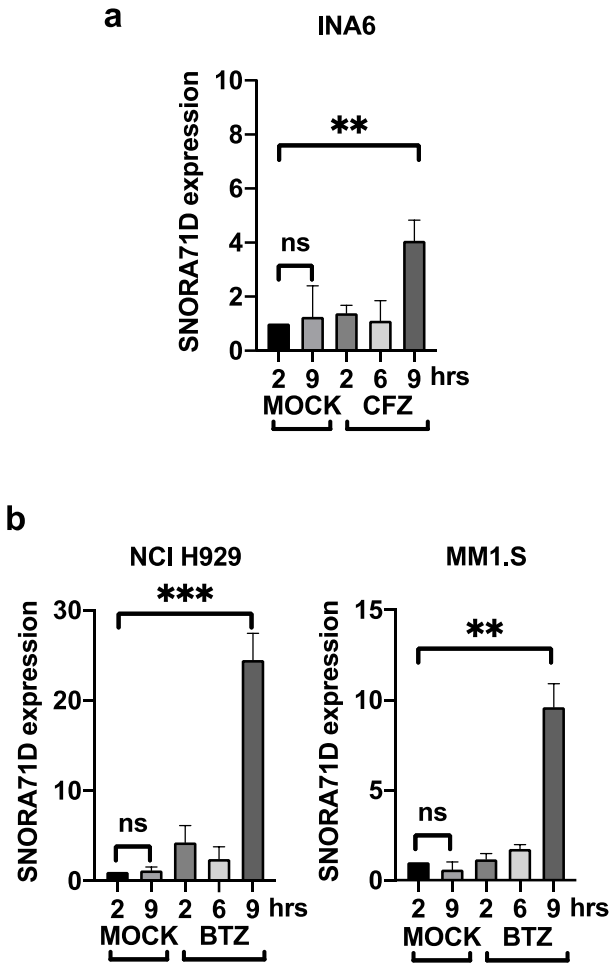

Figure 5. 3 SNORA71D is upregulated by proteasome inhibition.

A) INA-6 cells were pulse-treated with DMSO (MOCK) or 400 nM of carfilzomib for one hour, and the time from the onset of treatment was as indicated. qPCR was performed and SNORA71D expression was determined for each sample.

B) NCI H929 (left) and MM1.S (right) cells were pulse-treated with DMSO (MOCK) or 400 nM of bortezomib for one hour. Time from the onset of treatment was as indicated. qPCR was performed as in (A).

SNORA71D upregulation is dependent on endoplasmic reticulum stress. snoRNA upregulation above appears at later time points, around the time of apoptosis onset (Fig. S5.1). To determine whether other apoptosis inducers cause a similar increase in SNORA71D expression, we treated INA-6 cells with doxorubicin. Doxorubicin is a drug currently used in multiple myeloma therapeutic regimens and exerts its effects via a distinct mechanism from proteasome inhibitors, by inducing DNA damage. We found that treatment with doxorubicin at a concentration and within a time frame that results in apoptosis in INA-6 cells did not result in a corresponding increase in SNORA71D (Fig. 5.4). This indicates that SNORA71D upregulation is specific to a pathway induced by, and unique to, proteasome inhibitors.

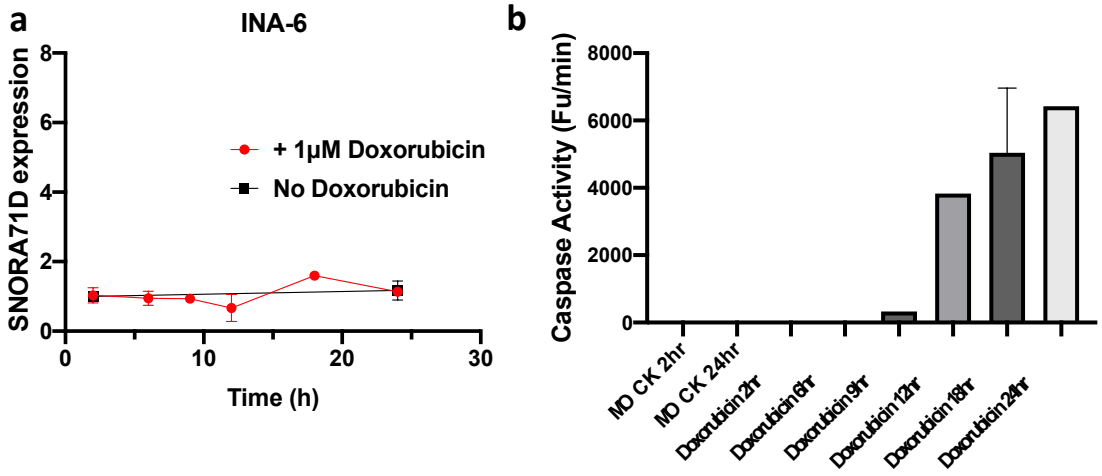

Figure 5. 4 SNORA71D upregulation is not apoptosis dependent.
INA-6 cells were treated with DMSO or 1 μM Doxorubicin continuously. At the time points indicated, cells were collected and qPCR was performed to determine SNORA71D expression (A). Caspase activity was determined by cleavage of fluorescent substrate (B).

Proteasome inhibitors cause the accumulation of misfolded proteins within the endoplasmic reticulum (ER) and the cytosol, which results in ER stress. ER stress is combated within cells by multiple pro-survival mechanisms, including the unfolded protein response, or UPR. One of the indicators of UPR activation is the phosphorylation of eukaryotic initiation factor 2α (eIF2α). Phosphorylation of eIF2α results in the inhibition of protein synthesis to mitigate ER stress. To determine whether ER stress causes the upregulation of SNORA71D, we treated INA-6 cells with two known ER stressors, tunicamycin, and thapsigargin. Both ER stressors caused an increase in the expression of SNORA71D (Fig. 5.5). These results show that ER stress upregulates SNORA71D expression.

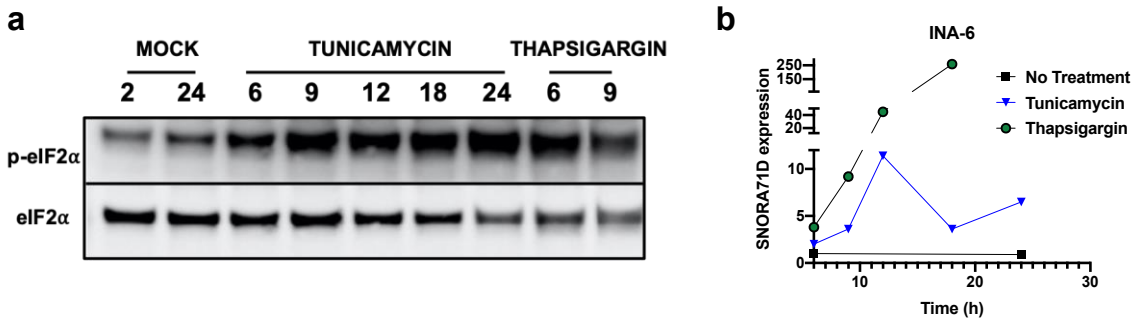

Figure 5. 5 SNORA71D is upregulated by ER stress.
INA-6 cells were treated with classic ER stressors, signified by eIF2 phosphorylation (A), tunicamycin (500 ng/ml), and thapsigargin (500 nM) for the length of time indicated. The same experiment was performed in (B), RNA was isolated and qPCR was performed to determine SNORA71D expression.

SNORA71D upregulation by proteasome inhibitors is cytosolic. Because we found that snoRNAs are upregulated strictly in response to ER stress which occurs outside of the nucleus, we wondered if upregulated snoRNAs might translocate out of the nucleolus and the nucleus to exert effects in the cytosol, perhaps in an attempt to combat ER stress. We treated INA-6 cells

with bortezomib and then fractionated the samples into nuclear and cytosolic fractions. We found that for SNORA71D, while there was a slight, but significant increase in expression in the nucleus following bortezomib treatment, there was a significant 40-fold increase in cytosolic expression. However, the increase in SNORA71D expression in the whole cell is more modest but significant (Fig. 5.6).

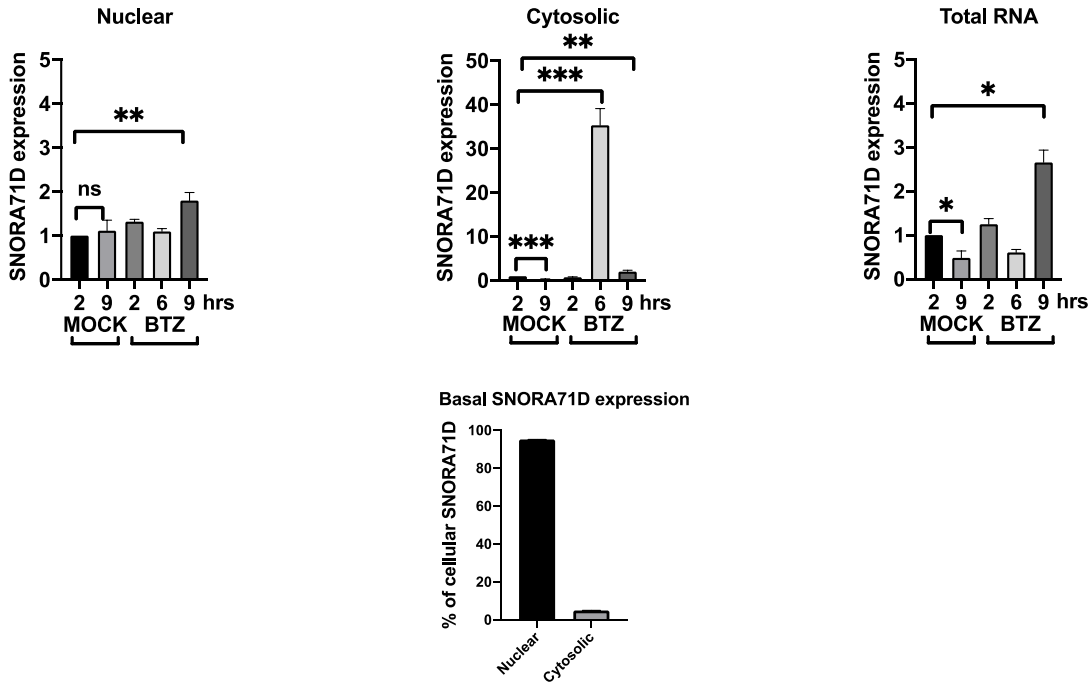

Figure 5. 6 SNORA71D upregulation by proteasome inhibitors is cytosolic.
INA-6 cells were treated with 400 nM of bortezomib for the length of time indicated. Cells were collected and fractionated into total, nuclear, and cytosolic fractions. RNA was isolated and qPCR was performed to determine SNORA71D expression (top). Basal expression of SNORA71D in cytoplasmic and nuclear fractions (bottom).

Knockdown of SNORA71D is cytoprotective. To investigate how SNORA71D might be involved in the response of cancer cells to proteasome inhibition and ER stress, we knocked it down in MDA-MB-231 cells. We used siRNAs for the knockdown because we were more interested in the cytosolic effects of the snoRNA. We found that siRNAs only marginally reduced the expression of SNORA71D at the basal level but prevented the increase in its expression upon proteasome inhibitor treatment (Fig.5.7).

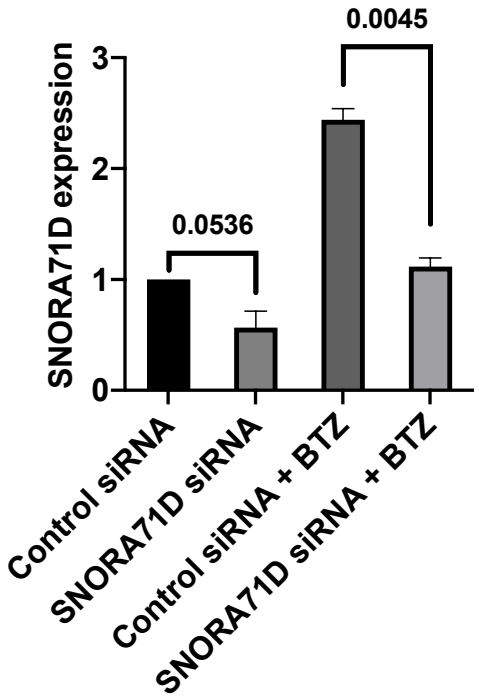

Figure 5. 7 Knockdown of SNORA71D prevents proteasome inhibitor-induced upregulation.
MDA-MB-231 cells were transfected with Control siRNA or SNORA71D siRNA for 48 hours. After the transfection period, media containing siRNAs was withdrawn and cells were pulse-treated with 400 nM bortezomib (BTZ) or DMSO for 1 hour. 9 hours after start of treatment, cells were harvested and qPCR was used to determine SNORA71D expression.

We pulse-treated MDA-MB-231 cells (previously transfected with control siRNA and SNORA71D siRNA) with 400 nM bortezomib and determined if the knockdown (KD) of SNORA71D had any effect on the sensitivity of the cells to proteasome inhibition. Using caspase-3 activity assay in cell extracts and detection of apoptotic cells with a caspase-activity-based probe by flow cytometry, we found that cells with reduced SNORA71D expression were less sensitive to bortezomib – lower levels of caspase activity and a lower proportion of apoptotic cells (Fig. 5.8).

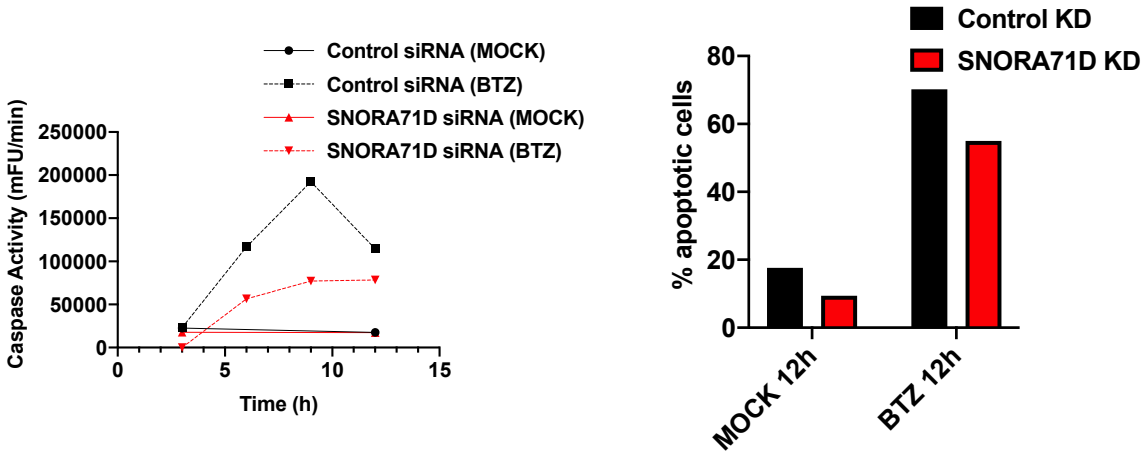

Figure 5. 8 Knockdown of SNORA71D is cytoprotective.
Control KD and SNORA71D KD cells were treated with bortezomib or DMSO (MOCK) for the length of time indicated. Caspase activity in treated cells (left) was determined by cleavage of fluorescent caspase substrates (DEVD-AMC). Flow cytometry was performed on treated cells incubated with caspase activity-based probe to determine the percentage of cells undergoing apoptosis (right).

SNORA71D is one of several orthologs of the SNORA71 gene (SNORA71 A-D) and is found on the host gene, small nucleolar RNA host gene 17 (SNHG17) (Fig. 5.9). SNHG17 itself exists as a long non-coding RNA that has been shown to promote malignancy in several cancers[349–354]. It is reported to promote proliferation, invasion, and epithelial-to-mesenchymal transition (EMT) by targeting multiple microRNA (miRNA) axes including the microRNA (miRNA/miR)-193a-5p and neuropilin and tolloid-like 2 (NETO2) (miR-193a-5p/NETO2) axis and the miR-338-3p and SRY-box transcription factor 4 (SOX4) (miR-338-3p/SOX4) axis. SNHG17 expression is inversely correlated with survival in patients[355]. Though the effects of SNHG17 have been extensively studied in cancer, the effects of the snoRNAs it hosts are relatively unknown.

- **SNORA71** – TCTTGTATCCAAAAGTGATCATGGGTTGCCTGTGTCCCGATCATTAACAGTGCAGGGGTAGGAGTGCTGA
  AAGACATCTTCCCTGCGTTGGTCCAGCCTTCCCTTTCAAACCCTGGAGCTTTCCCACG
- **SNORA71A** – CTCCTGCATCCGAAAGTGATCATAGGCTGCCTGTGCCTAGGTCATTGATAGTGCAGGGAGAGGAACGCTG
  AAAGAGGTTGTCCCCGTGTTTGGAGGGGTCCACCCTATCCCATCCGAACCCTGAAGCTTTCACACAACT
- **SNORA71B** – CCTGTATTCGAAAGTGATCGTGGGCTGCCTTTGCCCTGGTCATTGATAGTGCAGGGAGAGGAATCAATGA
  AAGCGCTTCCCCGTGTTTGAAGGGTCCACTCCTATCCCTTCCAAACTCTGGAGCTTTCGTACATGC
- **SNORA71C** – CCCCTGCATTCGAAAGTGATCATGAGCTGCCCGTGCCCTGGTCATTGGTAGTGCAGGGAGAGGAACTGCC
  GAGAGCACTTCCCCGTGTTTGGAGGGGTCCACTCCTGTCTCTTCCAAACCCTGGAGCTTTCCCACACCT
- **SNORA71D** – CACCTGTATTCGAAAGTGATCGTGGGCTGCCTGTGCCCTGGTCATTGATAGTGCAGGGAGAGAAATCGCG
  GAAAGTGCTTCCCCGTGTTTGGAGGGTCCGCTCCTGTCCCTTTCAAACTCTGGAGCTTTCTCACACCT

Map of the SNHG17 gene obtained from the University of California, Santa Cruz Genome Browser. Below, the sequences of the SNORA71 RNAs resident on SNHG17 (Source: NCBI).

Figure 5. 9 SNHG17 gene and snoRNA sequences.

We have found using the gene expression profiling interactive analysis (GEPIA) database that like SNHG17, SNORA71D expression inversely correlates with survival in patients (Fig. 5.10). On the other hand, though SNORA71D expression was highly upregulated by bortezomib in our RNA-sequencing experiment, SNHG17 was not. It has been reported that SNORA71D and SNORA71D ortholog, SNORA71B, are positively correlated with cyclin B1 expression, which leads to cell proliferation[356,357]. SNORA71B and SNORA71D expression has also been reported to negatively correlate with forkhead box O3 (FOXO3) expression and therefore negatively correlate with apoptosis[357]. Furthermore, metastatic colorectal carcinoma is associated with high expression of SNORA71D while low expression is associated with non-metastatic disease[358]. Additionally, SNORA71D expression is high in tumors compared to normal tissues for all tumors in The Cancer Genome Atlas (TCGA) Signatures of Differentially Expressed Genes for Tumors dataset[359].

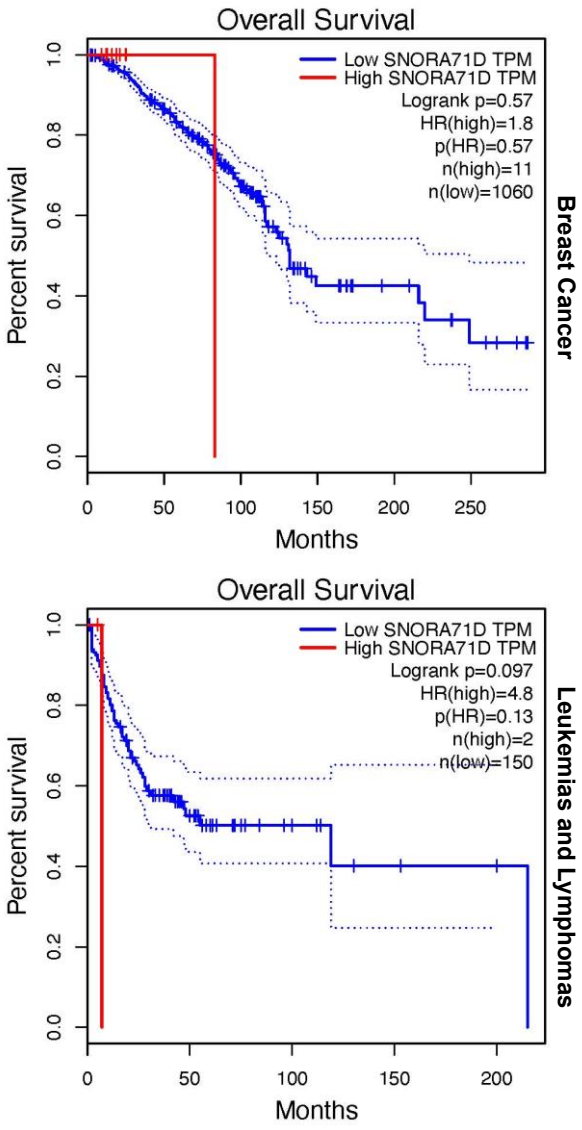

Figure 5. 10 High SNORA71D expression correlates with poorer outcomes in patients. GEPIA-derived patient data in breast cancer (top) and leukemias and lymphomas (bottom). Survival of patients with low SNORA71D expression is depicted in blue, high SNORA71D expression is depicted in red. HR – Hazard Ratio. HR > 1 indicates high expression of the gene results in lower expectation of survival. p(HR) – p-value of HR.

As mentioned earlier, SNORA71D is a member of the box H/ACA class of snoRNAs. Therefore, it is involved in the pseudouridylation of RNAs through interactions with DKC1 (dyskerin), GAR1 (nucleolar protein family A, member 1), NHP2 (nucleolar protein family A, member 2), and NOP10 (nucleolar protein family A, member 3), members of the H/ACA snoRNP (small nucleolar ribonucleoprotein) complex[360]. The only known RNA interactors of SNORA71D, DEAF1, a transcription factor, and 18S ribosomal RNA (rRNA) were reported in a study mapping global RNA-RNA interactions[361]. Not much else is known. DEAF1 has been reported to exist in multiple isoforms generated by alternative splicing, and transcriptionally activates and represses various genes. Loss of DEAF1 function results in developmental disorders. DEAF1 activation or inactivation affects several cellular pathways, including cellular transport, regulation of secretion, and cell-to-cell signaling[362]. One of its isoforms, suppressin (SPN), inhibits cell proliferation by arresting cells in the G0 or G1 phase upon secretion[363]. 18S rRNA is a small subunit rRNA, a component of the eukaryotic ribosome small subunit (the 40S subunit). The 18S rRNA is the active center of protein synthesis in the 40S subunit and base pairs with mRNA during translation initiation[364]. Therefore, 18S expression in cells is an indicator of protein synthesis. SNORA71D could be involved in the pseudouridylation of DEAF1 mRNA and 18S rRNA, affecting their processing and therefore response to proteasome inhibition.

Knockdown of SNORA71D results in the reduction of protein synthesis upon bortezomib treatment. Based on the known interaction of SNORA71D with 18S rRNA, we considered whether the knockdown of SNORA71D might affect protein translation. We used a puromycin incorporation assay in which puromycin – an aminoacyl tRNA mimic which upon insertion into a polypeptide undergoing synthesis, causes chain termination – is added to cells in culture.

Puromycin incorporation can be determined by western blotting and relative incorporation is a readout of the rate of protein synthesis. In this experiment, we also knocked down an additional snoRNA upregulated by bortezomib treatment in the RNA sequencing experiment, SNORD3D, also known as U3. SNORD3D, a box C/D snoRNA, is a part of the small ribosome subunit processome, and so we hypothesized that it might affect cellular function in a similar manner as SNORA71D. We show in Figure 5.11 that upon knockdown of SNORA71D and SNORD3D, in the absence of bortezomib treatment, puromycin incorporation was higher in the snoRNA knockdown cells, compared to the control, indicating higher basal protein synthesis at 3 hours though there was no difference in protein synthesis 12 hours after treatment onset. However, upon bortezomib treatment, the reduction of both snoRNAs resulted in reduced puromycin incorporation, indicating a reduction in protein synthesis when the snoRNAs are knocked down. A reduction in protein synthesis upon treatment with proteasome inhibitors would indicate a reduced protein load within cells which could explain how knockdown of SNORA71D protects cells from bortezomib-induced cytotoxicity.

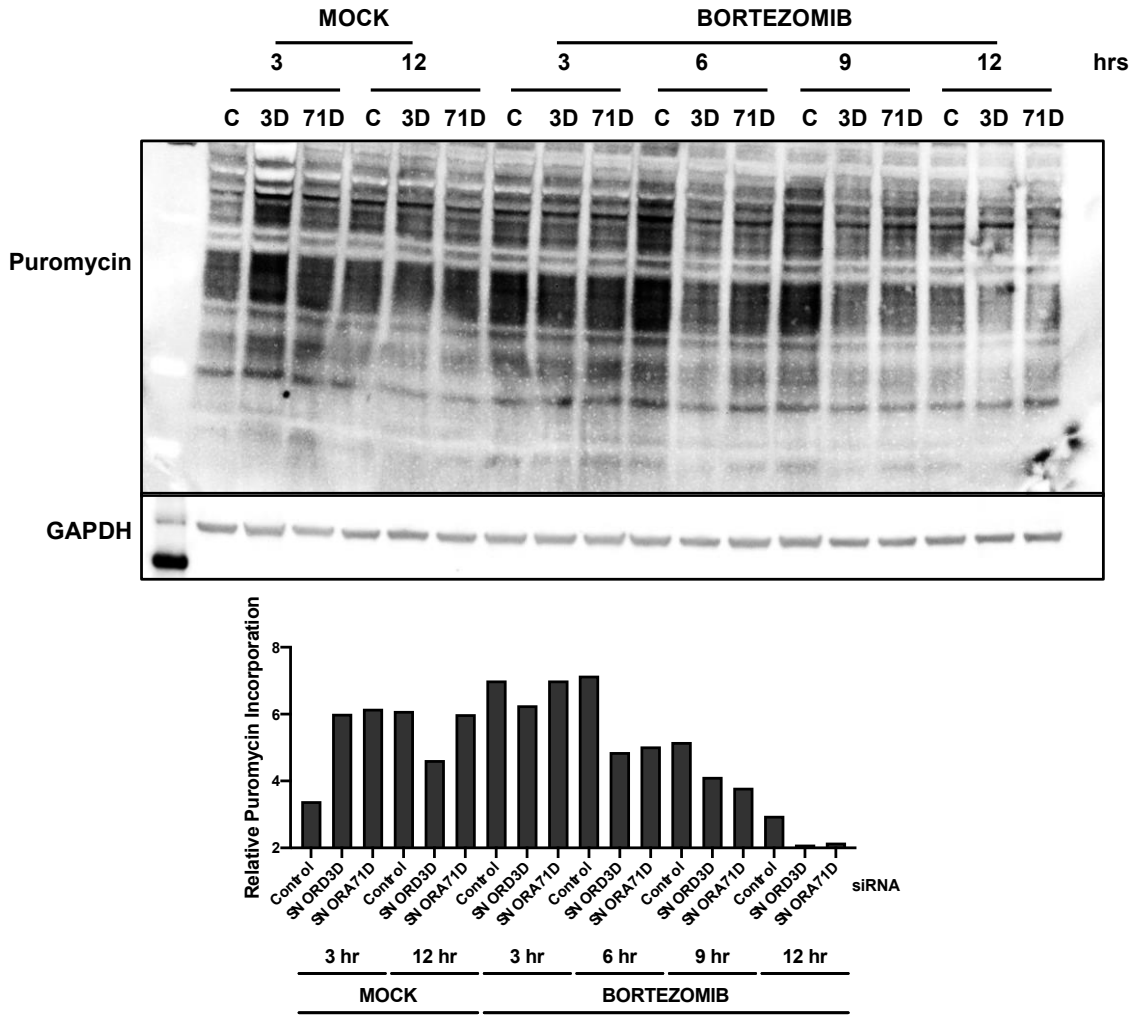

Figure 5. 11 Knockdown of snoRNAs prevents proteasome inhibitor-induced upregulation of protein synthesis.
Control KD (C), SNORD3D (3D), and SNORA71D KD (71D) cells were pulse-treated with DMSO (MOCK) or 400 nM bortezomib for one hour and harvested at the time points after treatment onset as indicated. 25 minutes before each time point was reached, 25 μM of puromycin was added. At the end of each time point cells were collected, and western blotting was performed to determine the levels of puromycin incorporation. Relative puromycin incorporation is shown on the bottom graph.

Knockdown of SNORA71D results in increased ubiquitin conjugate accumulation upon proteasome inhibitor treatment. It has been reported that nascent proteins/polypeptides constitute the majority of the proteasome's substrates, and therefore constitute the majority of ubiquitin conjugates that accumulate upon proteasome inhibition. Given that we found that knocking down SNORA71D results in reduced nascent protein synthesis upon bortezomib treatment, we considered whether reduced SNORA71D expression would also result in reduced ubiquitin conjugate accumulation. Contrary to our expectation, we found that the knockdown of SNORA71D resulted in increased ubiquitin conjugate accumulation upon treatment with bortezomib (Fig. 5.12). However, the increase in ubiquitin conjugate accumulation was not evident at 3 hours after treatment, indicating that the increase is not a direct result of proteasome inhibition. A substantial increase in ubiquitin conjugate accumulation is seen in cells in which SNORA71D was knocked down beginning around the nine-hour mark, which is when the increase in SNORA71D expression upon bortezomib treatment and its translocation to the cytosol occurs (Fig. 5.6). This was unexpected as increased ubiquitin conjugate accumulation would indicate more proteasome dysfunction and, therefore, more cell death. However, this could be explained by the cells undergoing apoptosis and therefore reducing protein synthesis which we see at the 12-hour time point (Fig. 5.11).

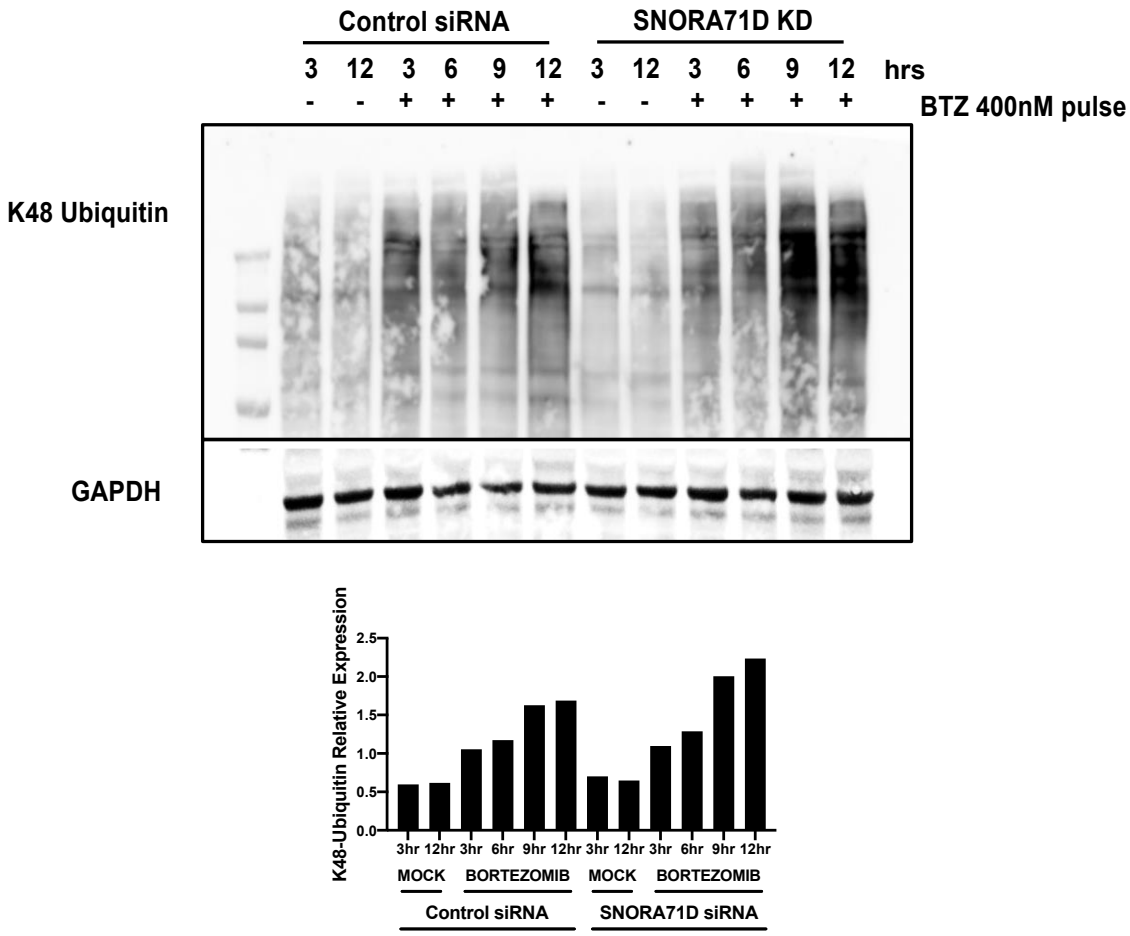

Figure 5. 12 Knockdown of SNORA71D results in increased ubiquitin conjugate accumulation upon proteasome inhibitor treatment.
Control KD and SNORA71D KD cells were 1hr-pulse-treated with bortezomib as indicated. Cells were harvested at the indicated time points after the onset of bortezomib treatment and western blotting was performed to determine ubiquitin conjugate accumulation (top). Relative expression of K-48 ubiquitin (bottom).

Proteomics analysis of TNBC cells with reduced SNORA71D expression reveals impaired ER stress response.

Table 2. Ingenuity Pathway Analysis of low SNORA71D expressing cells versus control cells.

Ingenuity Canonical Pathways	-log(p-value)	Ratio	z-score	Molecules
Insulin Secretion Signaling Pathway	1.46	0.0181	-2.2	EIF4A3,PLCG1,SEC61A1,SRP68,SRP72
Processing of Capped Intron-Containing Pre-mRNA	3.23	0.0279	-2.1	EIF4A3,HNRNPA3,LSM7,NUP155,NUP93,POLR2B,SF3B2,SRSF3
ISG15 antiviral mechanism	2.93	0.0563	-2.0	EIF4A3,NUP155,NUP93,PLCG1
NER (Nucleotide Excision Repair, Enhanced Pathway)	2.55	0.0444	-2.0	COPS3,GPS1,POLR2B,RAD23B
Mitotic Prophase	2.34	0.0388	-2.0	GOLGA2,NUMA1,NUP155,NUP93
Nonsense-Mediated Decay (NMD)	2.14	0.0342	-2.0	EIF4A3,RPL5,RPLP0,RPS14
RNA Polymerase II Transcription	1.79	0.0268	-2.0	EIF4A3,POLR2B,SRSF3,SUPT5H
Major pathway of rRNA processing in the nucleolus and cytosol	1.48	0.0215	-2.0	NOP58,RPL5,RPLP0,RPS14
Mitotic Prometaphase	1.36	0.0197	-2.0	CLIP1,DCTN3,NUMA1,SMC3
Mitotic G2-G2/M phases	1.39	0.0201	0.0	DCTN3,PSMD10,PSMD11,TP53
Neddylation	1.65	0.0203	0.4	COPS3,GPS1,PSMD10,PSMD11,UBE2M
CLEAR Signaling Pathway	1.96	0.0211	0.8	ATP6V1C1,ATP6V1G1,CTSB,PLCG1,PRKAA1,TP53
Ferroptosis Signaling Pathway	1.97	0.0305	1.0	CTSB,PRKAA1,TFRC,TP53
Neutrophil degranulation	2.94	0.021	1.3	AGL,CTSB,DDOST,HLA-B,HMGB1,MVP,PGM2,PSMD11,SERPINB1,UNC13D
Microautophagy Signaling Pathway	2.4	0.0312	1.3	CHMP3,PRKAA1,PSMD10,PSMD11,TP53
Intra-Golgi and retrograde Golgi-to-ER traffic	1.97	0.0246	1.3	COPE,DCTN3,RAB3GAP1,TMED9,TRIP11
NAFLD Signaling Pathway	1.79	0.0221	1.3	APOB,ATP2A2,CTSB,MBOAT7,PRKAA1

The results of proteomic analysis of SNORA71D KD cells versus Control KD cells. Downregulated pathways in the cells with reduced SNORA71D expression are indicated by a negative z-score (green), and upregulated pathways are indicated by a positive z-score (red).

Table 3. Most changed proteins in low SNORA71D expressing cells versus control cells.

Upregulated Proteins	Fold Change	Downregulated Proteins	Fold Change
UNC13D (unc-13 homolog D)	6.2	SEC61A1 (SEC61 translocon subunit alpha 1)	-5.5
RAB3GAP1 (RAB3 GTPase activating protein catalytic subunit 1)	4.4	RAD23A (RAD23 homolog A, nucleotide excision repair protein)	-4.2
CCN1 (cellular communication network factor 1)	4	AGL (amylo-alpha-1, 6-glucosidase, 4-alpha-glucanotransferase)	-3.9
ENG (endoglin)	3.1	NOLC1 (nucleolar and coiled-body phosphoprotein 1)	-3.3
IPO9 (importin 9)	3	SRP68 (signal recognition particle 68)	-3.2
AHNAK2 (AHNAK nucleoprotein 2)	2.8	SGTA (small glutamine rich tetratricopeptide repeat co-chaperone alpha)	-3.2
IPO4 (importin 4)	2.6	NASP (nuclear autoantigenic sperm protein)	-3.1
TRIO (trio Rho guanine nucleotide exchange factor)	2.6	ATP2B1 (ATPase plasma membrane Ca2+ transporting 1)	-3
NIT1 (nitrilase 1)	2.5	HSDL2 (hydroxysteroid dehydrogenase like 2)	-2.8
TMED5	2.5	EIF3J (eukaryotic translation initiation factor 3 subunit J)	-2.8

The top upregulated and downregulated genes in the SNORA71KD cells compared to the Control KD cells.

To better understand SNORA71D function at the basal level and the changes that might lead to a differential response upon treatment with proteasome inhibitors, we performed proteomics on MDA-MB-231 cells in which SNORA71D was knocked down and compared pathway changes to MDA-MB-231 cells transfected with control siRNA (Table 2). We found that the pathways most downregulated in cells with reduced SNORA71D expression were the insulin secretion signaling pathway and pre-mRNA processing (splicing). A decrease in protein synthesis – which we see in Figure 5.11 – and in the secretory pathway is expected to be cytoprotective in cells undergoing proteasome inhibition, particularly in the case of multiple myeloma cells which

secrete immunoglobulins. Therefore, high expression of SNORA71D, which corresponds with an increase in protein synthesis and protein secretion, will result in more cell death upon proteasome inhibition. rRNA processing pathway was also downregulated, however, the most downregulated molecule in cells with reduced SNORA71D expression was Sec61 (Table 3).

Sec61 is a protein complex that is a core component of the translocon (channels within membranes that allow the transport of proteins). Sec61 is closely associated with ribosomes and facilitates the entry of proteins into the ER co-translationally. This ER translocation is BiP dependent[365]. Loss of function of Sec61 has been reported to result in dysregulated response to ER stress[366] and compromised ER-associated degradation (ERAD)[367]. A reduction in the expression of Sec61 and compromised ERAD could explain the increase in ubiquitin conjugate accumulation upon bortezomib treatment with reduced SNORA71D expression in Figure 5.12. A dysregulated response to ER stress could explain the reduced levels of apoptosis upon bortezomib treatment in the same cells.

Critically, one arm of the UPR, the IRE1α arm, is linked to Sec61 activity. In fact, Sec61 forms a hetero-oligomeric complex with IRE1α that is activated upon ER stress leading to the recruitment and splicing of Xbp1u mRNA into Xbp1s mRNA. Xbp1s is synthesized from this mRNA and translocates into the nucleus to promote the expression of UPR target genes such as protein chaperones. Loss of Sec61 leads to the continuous activation of the IRE1α arm upon ER stress and sustained activity of Xbp1[368].

We considered the possibility that cells with reduced SNORA71D expression have sustained Xbp1s activity, and therefore, more chaperone production and a greater capacity of cells to better cope with misfolded proteins and ER stress. We performed western blotting on MDA-MB-231 cells transfected with control siRNA or SNORA71D siRNA and found that there is a slight increase in the expression of protein chaperones BiP and HSP70 in the SNORA71D KD cells compared to the control, upon treatment with bortezomib (Fig. 5.13 a-b). Analysis of the proteomics data obtained from SNORA71D KD cells treated with bortezomib for 6 hours confirms this observation though the increase at this time point is slight and not statistically significant (Fig. 5.13c). These results indicate that SNORA71D is involved in regulating proteotoxic stress.

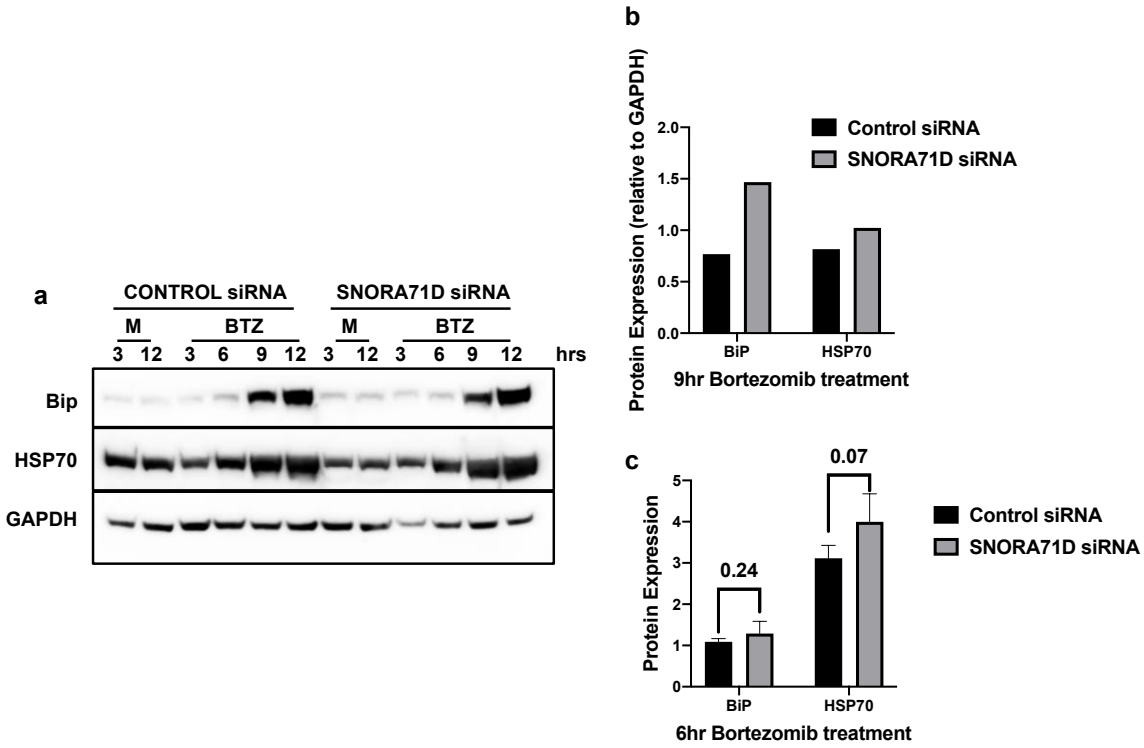

Figure 5. 13 Knockdown of SNORA71D leads to increased chaperone expression after proteasome inhibition.
Control KD and SNORA71D KD cells were pulse-treated with DMSO (M) or 400 nM of bortezomib (BTZ). Cells were harvested and western blotting was performed (A) to determine protein expression quantified in (B). Proteomic analysis of cells harvested 6 hours after pulse treatment also shows protein expression (C).

Discussion

An unexpected finding with RNA-sequencing experiments performed in TNBC in Chapter 3 is the upregulation of snoRNAs by proteasome inhibitors. In this chapter, we confirm, using qPCR, that the most upregulated snoRNA in the RNA-sequencing experiment, SNORA71D, is upregulated in TNBC and multiple myeloma cell lines in an ER stress-related manner. While it is known that failure of the adaptive stress response in cells to retain cellular homeostasis leads to the initiation of apoptosis, the exact sequence of cellular changes that begins apoptosis is often debated[124,369], yet non-protein regulators of these systems are seldom considered. Our discovery that SNORA71D upregulation is specific to ER stress suggests that it, and possibly other non-coding RNAs, are involved in regulating cellular response to proteotoxic stress.

SnoRNAs are largely considered to be strictly nucleolar-resident. Here we show that upon proteasome inhibition, SNORA71D translocates into the cytoplasm where it may regulate ER stress responses. It has been reported that box C/D snoRNAs migrate to the cytoplasm upon oxidative stress including treatment with doxorubicin[370]. We know that proteasome inhibitors also cause oxidative stress, however, the snoRNA studied here is a box H/ACA snoRNA whose levels do not change in response to doxorubicin, indicating that it responds specifically to ER stress. In the study referenced above, NOX4 (NADPH oxidase 4), regulates the translocation of box C/D snoRNAs to the cytoplasm. We expect a different regulator for SNORA71D translocation to the cytosol upon ER stress.

Importantly, the absence of SNORA71D appears to be cytoprotective in cells treated with bortezomib, indicating that SNORA71D may play a heretofore unknown role in effecting

apoptosis in response to proteasome inhibition. Since we found that the knockdown of SNORA71D leads to reduced expression of Sec61 and thus, aberrant response to ER stress, increased protein chaperone expression while global protein synthesis appears to be reduced, SNORA71D in cells may regulate response to stress selectively modifying RNAs involved in ER stress responses. Since SNORA71D is a H/ACA box snoRNA, it is necessary to perform pseudouridine RNA-sequencing (Pseudo-Seq) to identify specific modifications of pseudouridine on ribosomal RNAs, mRNAs, or other RNAs that may affect the translation of proteins involved in ER stress response starting with pseudouridylation of 18S rRNA or Sec61 mRNA. Knockdown of SNORA71D also affects splicing of pre-mRNA according to proteomics analysis, therefore we will perform RNA-sequencing with a focus on alternative splicing of mRNAs.

This study does have a number of limitations. Though we confirmed the upregulation of SNORA71D in different multiple myeloma cell lines, we used only one TNBC cell line for knockdown studies. To confirm the results seen in MDA-MB-231 cells, we will need to use other cancer cell lines. We also need lentiviral knockdown and overexpression studies in multiple myeloma and other cancer cell lines to confirm the role that SNORA71D plays in the modulation of response to proteasome inhibition.

We understand that the upregulated snoRNAs we observed by RNA sequencing may exert their effects in concert. The effects exerted by SNORA71D may be potentiated by other snoRNAs upregulated by bortezomib treatment. Future knockdown and overexpression studies must be performed in snoRNA pairs (or more) to provide a more holistic view of their effects at a basal level and in response to proteasome inhibition.

In summary, in this work, we provide preliminary evidence that small nucleolar RNAs are non-protein regulators of ER stress and that they modulate the response of cancer cells to proteasome inhibitors. We show that the upregulation of SNORA71D upon treatment of cells with proteasome inhibitors corresponds to sensitivity to proteasome inhibitors in multiple myeloma cell lines. It remains to be determined if the expression of SNORA71D in patients upon treatment with bortezomib also corresponds with proteasome inhibitor therapy response rates. However, the results from this work implicate SNORA71D in effecting apoptosis since knocking it down attenuates apoptosis possibly through the interaction of Sec61 and IRE1α. Finally, this work, though debate of the exact mechanisms that lead to cell death upon proteasome inhibition has been raging since they began to be used for the treatment of cancer, suggests that the fate of the cancer cell may hinge on the expression of a small-non-coding RNA.

Chapter 6: Concluding Remarks and Future Directions

Efficacious combination therapies in the treatment of cancer are often necessary to achieve complete remission in patients. For rational combinations to be effective, drugs should interact with their targets with minimal off-target interactions which could elicit adverse drug events. Furthermore, the physiological effects of inhibiting targets should be well-elucidated in order to understand the pathways involved in response and to find other potential targets to induce an even more potent response.

Proteasome inhibitors are effective in the treatment of some hematologic malignancies. They are, however, not a cure. Several therapies are used in combination with proteasome inhibitors currently, and more still are being developed. In addition, proteasome inhibitors have the potential to be effective in solid tumors that have proteasome dependencies such as triple-negative breast cancer. In these cancers, the level of inhibition achievable by FDA-approved proteasome inhibitors is not sufficient to cause an effective reduction in tumor burden. Therefore, combination therapies with proteasome inhibitors are essential.

Kraus et al., found in 2015, that the combination of BTK inhibitor, ibrutinib, with a specific inhibitor of the β2 site of the proteasome, LU-102, is highly synergistic in a variety of hematologic malignancies, ranging from those with very high BTK expression and activity to those with no BTK expression[108]. Owing to the fact that synergy was seen in cell lines with no BTK expression, we wondered if the synergy between ibrutinib and LU-102 is due to an off-target effect of ibrutinib. At the onset of this project, as stated in Chapter 1, we proposed to answer the following questions:

- Is the synergy between ibrutinib and LU-102 really due to an off-target effect of ibrutinib?
- If it is, what is the 'off-target' responsible for synergy?
- Do other BTK inhibitors synergize with LU-102 in the same way?
- If the 'off-target' is not specific to BTK-expressing hematologic cancer cells, will the BTK inhibitor + LU-102 combination be efficacious in other types of cancer?

We showed, in Chapter 3, that the synergy between LU-102 and ibrutinib is indeed due to an off-target effect of ibrutinib and other BTK inhibitors. Of the BTK inhibitors tested, CGI-1746 was the most synergistic with LU-102. We then showed that CGI-1746 inhibits all three proteolytic sites of the 20S proteasome in a gating-independent manner. In addition, it is a more potent inhibitor of the 26S proteasome due to additional inhibition of the proteasome's ATPases.

Though we were unable to identify the binding sites of CGI-1746 on the proteasome, we propose it to be on the interface between the 19S particle and the core particle, inhibiting the ATPases and causing a 'trickle-down' inhibition of the proteolytic sites in the 26S proteasome. High-resolution structural studies of the 26S and CGI-1746 interaction will aid in determining the binding site on the 26S proteasome. Pinpointing the exact binding sites of the proteasome will aid in understanding how CGI-1746 inhibits the proteasome and will aid in the development of more potent inhibitors of the 26S ATPases which can be used in combination with inhibitors of the core particle to improve 26S proteasome inhibition and, possibly, improve response in patients.

In Chapter 3, we also developed a cell line resistant to the combination of CGI-174 and LU-102 – 231CL.R. We have found that this cell line is also resistant to FDA-approved inhibitors of the β5 site of the proteasome, and thus represents an excellent tool to investigate acquired resistance. Analysis of the mechanisms of resistance is currently ongoing. So far, we have found that 231CL.R has a reduced expression of proteasomes at the basal level, which is unexpected (Fig. 6.1).

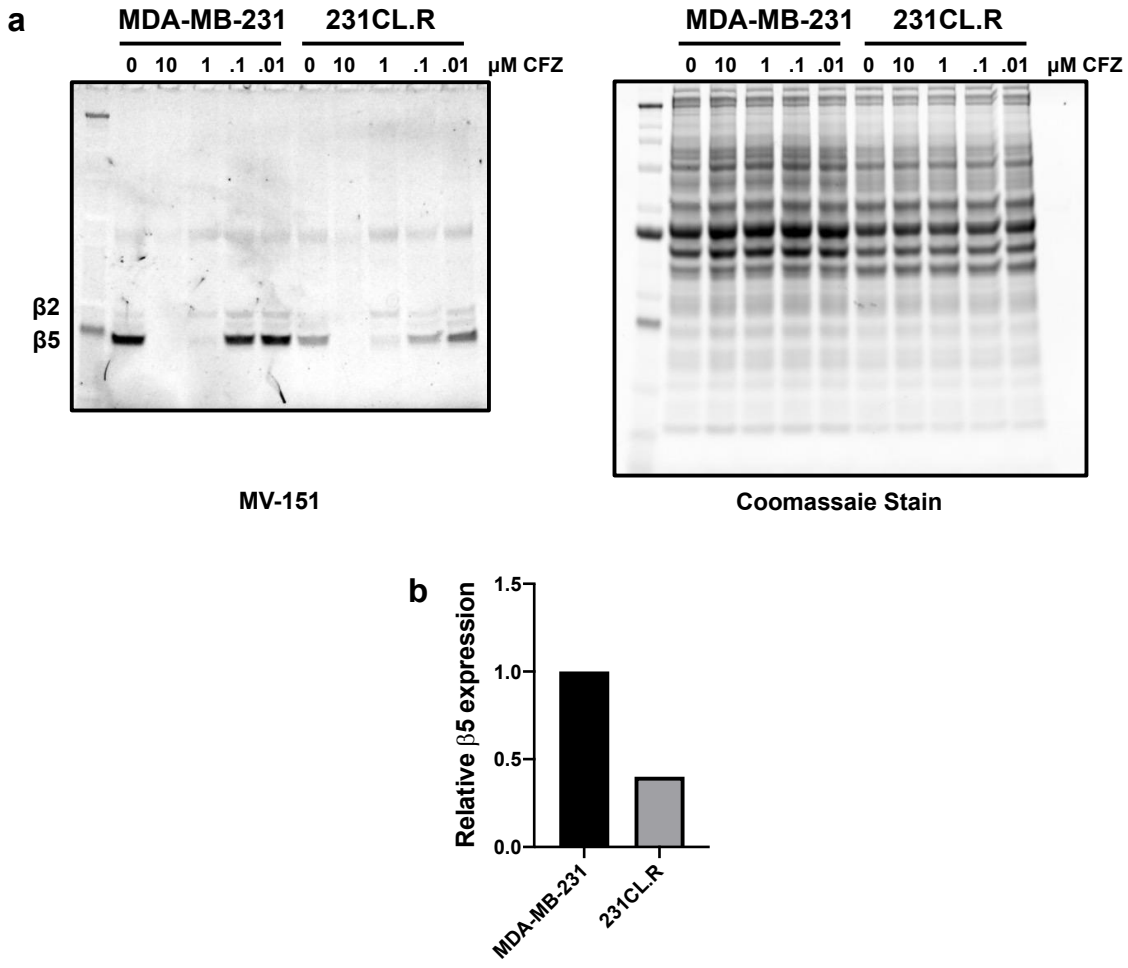

Figure 6. 1 Cells resistant to the CGI-1746 an LU-102 combination have reduced basal proteasome expression.

A) Lysates of MDA-MB-231 or 231CL.R cells were treated with the indicated concentrations of carfilzomib for 30 minutes. The treated lysates were then incubated with 1 μM of affinity-based probe, MV-151, for 30 minutes at 37°C after which the lysates were run on SDS-PAGE, and MV-151 fluorescence was captured on an imager (left). The same gel was stained with Coomassie dye and imaged to determine the relative amounts of protein loaded on the gel.

B) Quantification of the β5 bands of MDA-MB-231 and 231CL.R in (A) relative to the Coomassie loading control.

Rationale for the development of inhibitors of the proteasome's ATPases

It has been established that inhibition of multiple sites of the proteasome is superior to inhibition of the β5 site[108]. Marizomib, a proteasome inhibitor that inhibits all three of the proteasome's proteolytic sites, has been tested in several clinical trials, which have failed due to the drug crossing the blood-brain barrier and eliciting adverse events due to central nervous system toxicities. Marizomib is now in clinical development by Bristol-Myers Squibb for Glioblastoma Multiforme (GBM). Patients in the phase III clinical trial are reported to have had serious adverse events while experiencing no improvement in progression-free survival or overall survival[371]. It is also under development for other gliomas[372]. More recently, the mechanism of known endogenous proteasome inhibitor, PI31, has been elucidated in yeast and mammalian cells. The protein, PI31, is inserted into the proteasome's catalytic core and directly interacts irreversibly with all the proteasome's catalytic sites, preventing any further degradation of substrates[373,374].

Synthesis of a protein with the capabilities of PI31 to function as a drug is improbable, and due to the toxicities elicited by marizomib, it is unlikely to be effectively used in combination therapies in patients. The development of CGI-1746 as a proteasome ATPase inhibitor and achieving multi-site proteasome through ATPase inhibition may be more practicable. Though CGI-1746 is strictly a research tool, GDC-0853 (fenebrutinib) was developed based on CGI-1746 and is in clinical trials for multiple sclerosis by Genentech. GDC-0853 does not inhibit the proteasome's ATPases, but intermediate compounds may be more potent inhibitors of the ATPases than CGI-1746 and may be available for testing in combination with inhibitors of the β2 and β5 sites of the proteasome.

To the best of our knowledge, only one inhibitor of the proteasome's ATPases has been reported in the literature, a nucleoside-capped peptoid, Regulatory Particle Inhibitor Peptoid-1 (RIP-1), which binds to Rpt4[375,376]. Unlike CGI-1746, however, RIP-1 did not inhibit the peptidase activity of the 20S core particle, though it inhibited the peptidase activity of the 26S proteasome, which would indicate that CGI-1746 binds to a different (or secondary) target on the proteasome. Though RIP-1 was discovered in 2007, there is no other information in the literature about its biological effects or other possible interactions with cellular ATPases. Personal communication from our collaborator, Dr. George DeMartino, revealed that the inhibition of the 19S regulatory particle ATPases by RIP-1 could not be replicated.

Other questions remain unanswered. We showed in Chapter 3 that three BTK inhibitors – ibrutinib, CGI-1746, and GDC-0853 – synergize with LU-102 in killing cancer cells, and that CGI-1746 demonstrated the strongest synergy. Therefore, we chose to focus on CGI-1746 for our subsequent experiments, erroneously anticipating that the other synergistic compounds – ibrutinib and GDC-0853 – exert their effects via the same mechanisms as we found that both compounds also cause synergistic accumulation of ubiquitin conjugates in combination with LU-102 (Chapter 3, Fig. 3.7). However, though both compounds inhibit all active sites in the 20S proteolytic core, they do not inhibit proteolysis of the 26S proteasome except for slight inhibition of the β1 site, and they also do not inhibit the proteasome's ATPases. It is unclear whether the inhibition of β1 by these compounds explains the synergy with LU-102. Future directions with these inhibitors include ascertaining whether β1 site inhibition is sufficient to cause synergistic cell death with LU-102 over the period in which LU-102 inhibits both β2 and β5 sites of the

proteasome. If this inhibition is insufficient to achieve the levels of synergy seen in Chapter 3, other targets in the ubiquitin-proteasome pathway that might cause synergistic ubiquitin conjugate accumulation and synergistic cell death will be considered. We have already ruled out the possibility of inhibition of deubiquitinases and VCP in Chapter 3. We ruled out the possibility of CGI-1746 inhibiting activating phosphorylation of proteasome subunits in cells but have not done the same for ibrutinib or GDC-0853; this would be the next logical step in identifying any additional targets. We are yet to rule out the possibility of ibrutinib and GDC-0853 blocking the 20S proteasome gating mechanism as a mode of 20S inhibition, however, this mechanism would not explain the synergistic accumulation of ubiquitin conjugates that occurs when either compound is used in combination with LU-102 in cells.

The allosteric inhibition of all three proteolytic sites of the 20S core particle by multiple BTK inhibitors (Fig. 6.2) prompted us to investigate if other kinase inhibitors inhibit the proteasome in the same manner. We found that though several kinase inhibitors inhibit the 20S proteasome at one or multiple sites, they did not inhibit the 26S proteasome, except for MK-2206, a Protein Kinase B (PKB/Akt) inhibitor, which inhibited the isolated 26S proteasome proteolysis though it did not inhibit the proteasome in cell lysates. Though LU-102 did sensitize MDA-MB-231 cells to MK-2206 treatment, this was probably due to inhibition of Akt in these cells as inhibition of the PI3K/Akt signaling pathway has been shown to sensitize cancer cells to proteasome inhibitors[377] (Fig. 6.3). While testing other classes of drugs used in human diseases for cross-reactivity with the proteasome, we found that inhibitors of the hepatitis C (HepC) virus NS3 protease also inhibit the 26S proteasome (Fig. 6.4). Analysis of this inhibition is currently ongoing.

These results illustrate the need for screening of kinase inhibitors for cross-inhibition of the proteasome and cellular ATPases and also illuminate the proteasome's ATPases as a potential target for combination therapy with FDA-approved proteasome inhibitors.

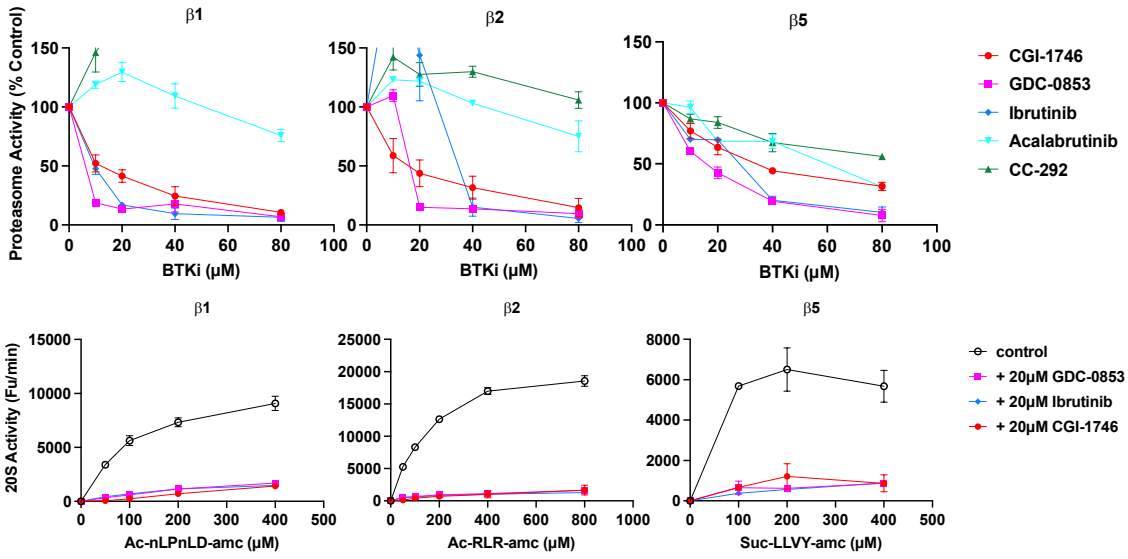

Figure 6. 2 BTK inhibitors that synergize with LU-102 inhibit the 20S proteasome allosterically.
20S mammalian proteasomes were incubated with the indicated concentrations of BTK inhibitors and proteasome activity was determined by proteolytic cleavage of 100 μM proteasome substrates (top). 20S mammalian proteasomes were incubated with 20 μM of BTK inhibitors and proteolytic cleavage of the indicated concentrations of proteasome substrates depict proteasome activity.

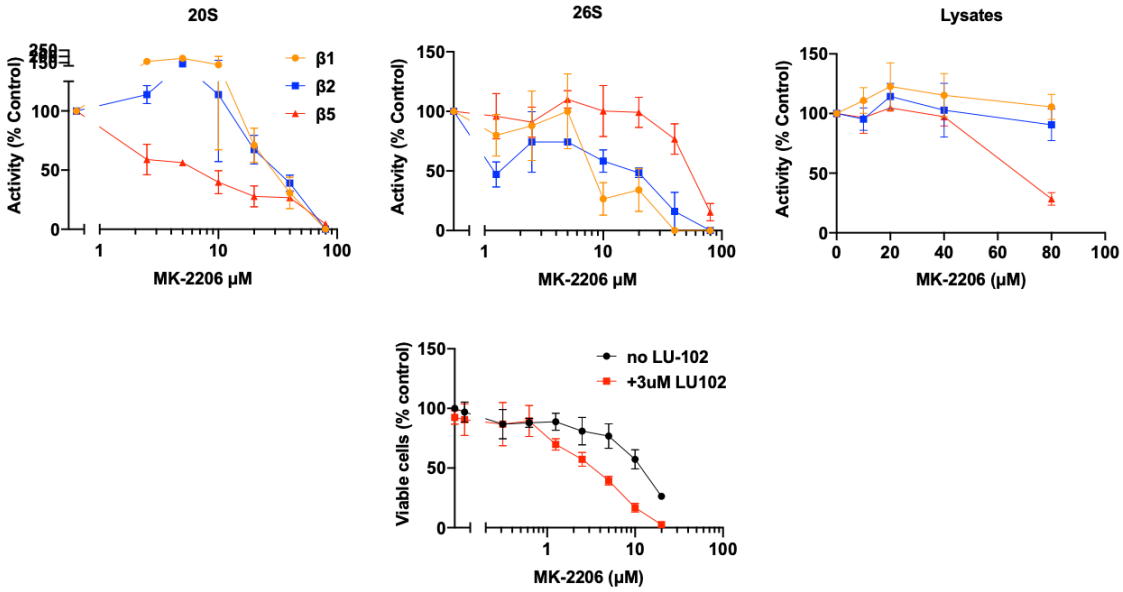

Figure 6. 3 MK-2206 inhibits isolated proteasomes, but not proteasomes in cells.
Indicated concentrations of MK-2206 were incubated with, top from the right: 20S proteasome, 26S proteasome, and cell lysates. proteasome activity was determined by proteolytic cleavage of 100 μM proteasome substrates. Bottom: MDA-MB-231 cells were treated with indicated concentrations of MK-2206 alone, or in combination with LU-102.

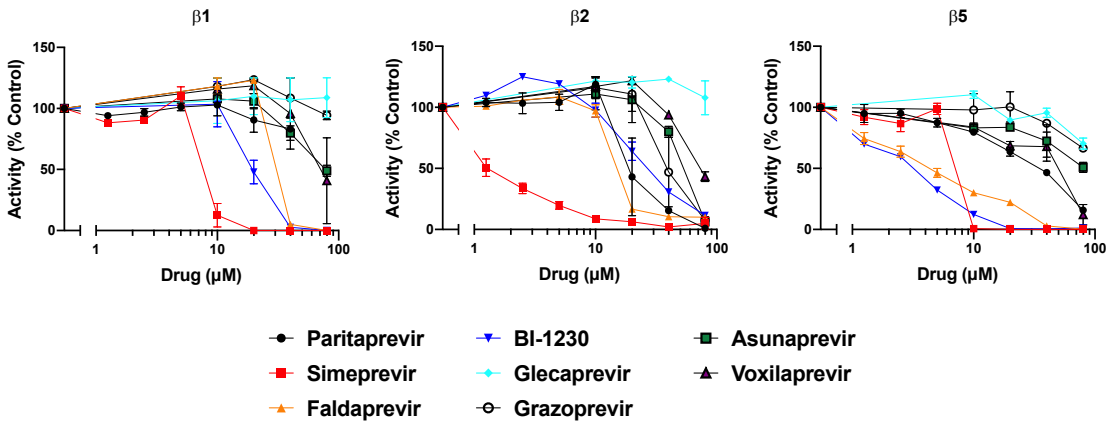

Figure 6. 4 Some HepC NS3 protease inhibitors inhibit the 26S proteasome.
26S mammalian proteasomes were incubated with the indicated concentrations of HepC NS3 protease inhibitors and proteasome activity was determined by proteolytic cleavage of 100 μM proteasome substrates.

The inhibition of multiple sites of the proteasome's core particle is essential to achieve cytotoxic proteasome inhibition in triple-negative breast cancer

In Chapter 4, we show that increasing exposure time leads to the decrease in specificity that is responsible for cell death by a single-site inhibitor in triple-negative breast cancer. Furthermore, specific inhibition of the β2 site of the proteasome is not enough to synergize with CGI-1746 to the extent we saw in Chapter 3. Additional specific inhibition of the β5 site is necessary to achieve synergy. Therefore, the synergy between CGI-1746 and LU-102 is due to the inhibition of the β5 and β2 sites of the proteasome as well as the proteasome's ATPases, effectively 'crippling' the proteasome and causing sufficient inhibition to lead to death in cells.

We propose using low concentrations of each inhibitor – CGI-1746, LU-102, and carfilzomib or bortezomib for solid tumors in future animal experiments. The idea has merit; we have shown that the triple combination of proteasome inhibitors is highly potent. It is also likely that by using low concentrations of each inhibitor, there would be fewer adverse events related to off-target interactions of each inhibitor. There is, however, the possibility of on-target toxicity with such potent crippling of the proteasome. Carfilzomib, for example, elicits on-target cardiotoxicity in patients[378]. Our lab is currently working on carfilzomib nanoparticle formulations that better target solid tumors and prevent on-target toxicity (unpublished data). With our proposed triple combination treatment regimen, there is a probable need for formulations that encapsulate low concentrations of the three compounds. There is likely a need for the formulations to only contain two compounds. Carfilzomib and LU-102 are irreversible inhibitors of the proteasome. Carfilzomib, in the clinic, is dosed in a bolus, twice weekly schedule per treatment cycle. LU-

102 may be dosed in the same manner. CGI-1746, an allosteric inhibitor of the proteasome may require daily dosing. Optimization of the molecules in formulations will be needed.

A non-coding RNA regulates cellular proteostasis in response to proteasome inhibition

Our RNA-sequencing experiment in Chapter 3 revealed snoRNA upregulation by bortezomib. In Chapter 5, we focused on the snoRNA most upregulated by bortezomib treatment as determined by RNA-sequencing, a box H/ACA snoRNA, SNORA71D. We demonstrate that SNORA71D is upregulated in TNBC and multiple myeloma cell lines upon proteasome inhibition. This upregulation upon bortezomib treatment correlates with cancer cell line sensitivity to bortezomib, therefore SNORA71D expression could serve as a biomarker for proteasome inhibitor response in patients.

We found, unexpectedly, that SNORA71D upregulation in cells is largely cytosolic. The translocation of SNORA71D out of the nucleus suggests possible interactions in the cytosol necessary to combat proteotoxic stress in the cells. Pulldown studies to identify SNORA71D interactors need to be performed in order to understand their effects upon translocation to the cytosol. It is known that some non-coding RNAs are involved in phase separation upon cellular stress[379]. It is possible that snoRNA translocation to the cytosol could result in the formation of ribonucleoprotein (RNP) stress granules within the cytosol[380]. Identification of SNORA71D interactors in combination with RNA-FISH (RNA fluorescence in situ hybridization) will provide a clearer picture of the effect of SNORA71D translocation.

We also demonstrate that SNORA71D upregulation is linked to endoplasmic reticulum stress; in response to proteasome inhibition, knockdown of SNORA71D is cytoprotective due to reduced protein synthesis and dysregulated response to ER stress, possibly due to reduced Sec61 expression as determined by proteomic analysis. Future directions will involve investigating Sec61 interactions with IRE1α (which knocking down SNORA71D may prevent) and downstream effects, including the expression of Xbp1 target genes.

Proteomic analysis of SNORA71D knockdown at the basal level also suggests SNORA71D is involved in pre-mRNA processing and splicing. It has been known that alternative splicing is a determinant of cell fate[381,382]. It is possible that at the basal level, SNORA71D governs alternative splicing of mRNA that results in increased proteotoxicity when the proteasome is inhibited. RNA-sequencing with a focus on alternative spliced transcripts will be performed in the future. Preliminary analysis of the proteomics data further revealed that the expression of the proteasome maturation protein (POMP), the 20S proteasome assembly factor, expression of which has been implicated in the recovery of proteasome activity upon treatment with proteasome inhibitors, is increased in cells with reduced expression of SNORA71D. Multiple myeloma patients who are refractory to bortezomib treatment have been shown to have increased POMP expression[383]. Preliminary experiments into proteasome activity recovery in cells with reduced expression of SNORA71D show an increase in proteasome activity recovery (Fig. 6.5). Increase in proteasome activity recovery may explain how knocking down SNORA71D is cytoprotective upon bortezomib treatment.

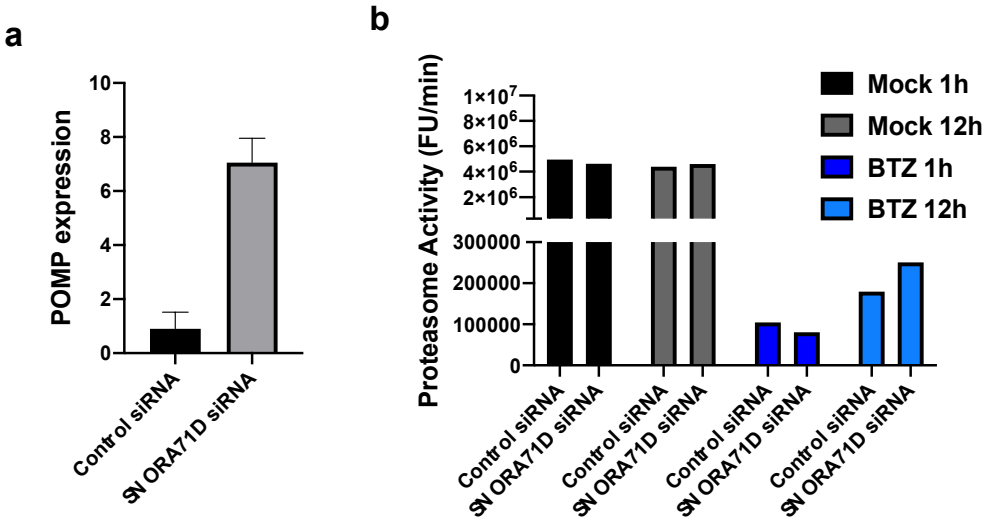

Figure 6. 5 Knockdown of SNORA71D results in increased expression of POMP and may lead to improved proteasome activity recovery.

A) POMP expression in control KD and SNORA71D KD cells as determined by proteomics.

B) Control KD and SNORA71D KD cells were pulse-treated with DMSO (Mock) or 400 nM of Bortezomib. One hour after treatment, the initial set of samples was collected. The other set of samples was allowed to recover in drug-free media and then collected 12 hours after the start of treatment. Proteasome activity assay by proteolytic cleavage of proteasome substrates was performed.

We need to further elucidate the mechanisms that govern the regulation of SNORA71D at the basal level and in response to proteasome inhibition, particularly the mechanisms that result in the upregulation of SNORA71D without co-upregulation of its orthologs or the host gene, SNHG17. This could lead to the discovery of a druggable target for combination therapies with proteasome inhibitors.

Finally, we will perform analysis of other snoRNAs that are upregulated in response to proteasome inhibitors to determine what role, if any, they play in the response of cancer cells to proteasome inhibition.

Summary

The work presented in this dissertation shows that BTK inhibitor, CGI-1746, is a dual ATPase and proteolysis proteasome inhibitor, provides a proof-of-concept for the development of a proteasome ATPase inhibitor, and demonstrates that proteasome 'crippling' causes cell death in triple-negative breast cancer cells. Furthermore, this dissertation provided preliminary data that proves SNORA71D regulates proteostasis upon treatment with proteasome inhibitors.

References

1. Siegel Mph, R. L. *et al.* Cancer statistics, 2023. *CA Cancer J Clin* **73**, 17–48 (2023).
2. Yan, L., Rosen, N. & Arteaga, C. Targeted cancer therapies. *Chinese Journal of Cancer* vol. 30 1–4 Preprint at https://doi.org/10.5732/cjc.010.10553 (2011).
3. Pal Singh, S., Dammeijer, F. & Hendriks, R. W. Role of Bruton's tyrosine kinase in B cells and malignancies. *Molecular Cancer 2018 17:1* **17**, 1–23 (2018).
4. Weber, A. N. R. *et al.* Bruton's tyrosine kinase: An emerging key player in innate immunity. *Front Immunol* **8**, 1454 (2017).
5. Wen, T., Wang, J., Shi, Y., Qian, H. & Liu, P. Inhibitors targeting Bruton's tyrosine kinase in cancers: drug development advances. *Leukemia 2020 35:2* **35**, 312–332 (2020).
6. Hendriks, R. W., Yuvaraj, S. & Kil, L. P. Targeting Bruton's tyrosine kinase in B cell malignancies. *Nature Reviews Cancer 2014 14:4* **14**, 219–232 (2014).
7. Burger, J. A. Bruton Tyrosine Kinase Inhibitors: Present and Future. *Cancer J* **25**, 386–393 (2019).
8. Markham, A. & Dhillon, S. Acalabrutinib: First Global Approval. *Drugs 2017 78:1* **78**, 139–145 (2017).
9. Keam, S. J. Pirtobrutinib: First Approval. *Drugs* **83**, 547–553 (2023).
10. Song, Y. *et al.* Zanubrutinib in relapsed/refractory mantle cell lymphoma: long-term efficacy and safety results from a phase 2 study. *Blood* **139**, 3148 (2022).
11. Update on IMBRUVICA® (ibrutinib) U.S. Accelerated Approvals for Mantle Cell Lymphoma and Marginal Zone Lymphoma Indications | AbbVie News Center. https://news.abbvie.com/news/press-releases/update-on-imbruvica-ibrutinib-us-accelerated-approvals-for-mantle-cell-lymphoma-and-marginal-zone-lymphoma-indications.htm.
12. Wang, M. L. *et al.* Ibrutinib plus Bendamustine and Rituximab in Untreated Mantle-Cell Lymphoma. *New England Journal of Medicine* **386**, 2482–2494 (2022).
13. De Claro, R. A. *et al.* FDA Approval: Ibrutinib for Patients with Previously Treated Mantle Cell Lymphoma and Previously Treated Chronic Lymphocytic Leukemia. *Clin Cancer Res* **21**, 3586–3590 (2015).
14. Byrd, J. C. *et al.* Acalabrutinib in treatment-naive chronic lymphocytic leukemia. *Blood* **137**, 3327 (2021).
15. FDA approves zanubrutinib for chronic lymphocytic leukemia or small lymphocytic lymphoma | FDA. https://www.fda.gov/drugs/resources-information-approved-drugs/fda-approves-zanubrutinib-chronic-lymphocytic-leukemia-or-small-lymphocytic-lymphoma.
16. Alexander, D. D. *et al.* Multiple myeloma: A review of the epidemiologic literature. *Int J Cancer* **120**, 40–61 (2007).
17. Aronson, L. I. & Davies, F. E. DangER: protein ovERload. Targeting protein degradation to treat myeloma. *Haematologica* **97**, 1119 (2012).
18. Fairfield, H., Falank, C., Avery, L. & Reagan, M. R. Multiple myeloma in the marrow: pathogenesis and treatments. *Ann N Y Acad Sci* **1364**, 32 (2016).
19. Iurlaro, R. & Muñoz-Pinedo, C. Cell death induced by endoplasmic reticulum stress. *FEBS J* **283**, 2640–2652 (2016).

20. Kim, I., Xu, W. & Reed, J. C. Cell death and endoplasmic reticulum stress: disease relevance and therapeutic opportunities. *Nature Reviews Drug Discovery 2008 7:12* **7**, 1013–1030 (2008).
21. Logue, S. E., Cleary, P., Saveljeva, S. & Samali, A. New directions in ER stress-induced cell death. *Apoptosis* **18**, 537–546 (2013).
22. Sano, R. & Reed, J. C. ER stress-induced cell death mechanisms. *Biochim Biophys Acta* **1833**, 3460–3470 (2013).
23. Szegezdi, E., Logue, S. E., Gorman, A. M. & Samali, A. Mediators of endoplasmic reticulum stress-induced apoptosis. *EMBO Rep* **7**, 880 (2006).
24. Kane, R. C., Bross, P. F., Farrell, A. T. & Pazdur, R. Velcade: U.S. FDA approval for the treatment of multiple myeloma progressing on prior therapy. *Oncologist* **8**, 508–513 (2003).
25. Raedler, L. A. Kyprolis (Carfilzomib) Received New Indications as Combination Therapy for Use in Relapsed and/or Refractory Multiple Myeloma. *Am Health Drug Benefits* **9**, 93 (2016).
26. Raedler, L. A. Ninlaro (Ixazomib): First Oral Proteasome Inhibitor Approved for the Treatment of Patients with Relapsed or Refractory Multiple Myeloma. *Am Health Drug Benefits* **9**, 102 (2016).
27. Kale, A. J. & Moore, B. S. Molecular mechanisms of acquired proteasome inhibitor resistance. *J Med Chem* **55**, 10317–10327 (2012).
28. Wallington-Beddoe, C. T., Sobieraj-Teague, M., Kuss, B. J. & Pitson, S. M. Resistance to proteasome inhibitors and other targeted therapies in myeloma. *Br J Haematol* **182**, 11–28 (2018).
29. Moore, B. S., Eustáquio, A. S. & McGlinchey, R. P. Advances in and applications of proteasome inhibitors. *Curr Opin Chem Biol* **12**, 434 (2008).
30. Qiang, Y. W. *et al.* MAFb protein confers intrinsic resistance to proteasome inhibitors in multiple myeloma. *BMC Cancer* **18**, 1–13 (2018).
31. Lü, S. & Wang, J. The resistance mechanisms of proteasome inhibitor bortezomib. *Biomark Res* **1**, 1–9 (2013).
32. Mokhtari, R. B. *et al.* Combination therapy in combating cancer. *Oncotarget* **8**, 38022 (2017).
33. Jin, H., Wang, L. & Bernards, R. Rational combinations of targeted cancer therapies: background, advances and challenges. *Nature Reviews Drug Discovery 2022 22:3* **22**, 213–234 (2022).
34. Pomeroy, A. E., Schmidt, E. V., Sorger, P. K. & Palmer, A. C. Drug independence and the curability of cancer by combination chemotherapy. *Trends Cancer* **8**, 915–929 (2022).
35. Woyach, J. A., Johnson, A. J. & Byrd, J. C. The B-cell receptor signaling pathway as a therapeutic target in CLL. *Blood* **120**, 1175–1184 (2012).
36. Weber, A. N. R. *et al.* Bruton's tyrosine kinase: An emerging key player in innate immunity. *Front Immunol* **8**, 302144 (2017).
37. Pal Singh, S., Dammeijer, F. & Hendriks, R. W. Role of Bruton's tyrosine kinase in B cells and malignancies. *Molecular Cancer 2018 17:1* **17**, 1–23 (2018).
38. Tsukada, S. *et al.* Deficient expression of a B cell cytoplasmic tyrosine kinase in human X-linked agammaglobulinemia. *Cell* **72**, 279–290 (1993).
39. Vetrie, D. *et al.* The gene involved in X-linked agammaglobulinaemia is a member of the src family of protein-tyrosine kinases. *Nature 1993 361:6409* **361**, 226–233 (1993).

40. Alu, A., Lei, H., Han, X., Wei, Y. & Wei, X. BTK inhibitors in the treatment of hematological malignancies and inflammatory diseases: mechanisms and clinical studies. *J Hematol Oncol* **15**, 138 (2022).
41. Burger, J. A. & Wiestner, A. Targeting B cell receptor signalling in cancer: preclinical and clinical advances. *Nature Reviews Cancer 2018 18:3* **18**, 148–167 (2018).
42. Marcotte, D. J. *et al.* Structures of human Bruton's tyrosine kinase in active and inactive conformations suggest a mechanism of activation for TEC family kinases. *Protein Sci* **19**, 429 (2010).
43. Rawlings, D. J. & Witte, O. N. The Btk subfamily of cytoplasmic tyrosine kinases: structure, regulation and function. *Semin Immunol* **7**, 237–246 (1995).
44. Mohamed, A. J. *et al.* Nucleocytoplasmic shuttling of Bruton's tyrosine kinase. *J Biol Chem* **275**, 40614–40619 (2000).
45. Herman, S. E. M. *et al.* The Bruton Tyrosine Kinase (BTK) Inhibitor Acalabrutinib Demonstrates Potent On-Target Effects and Efficacy in Two Mouse Models of Chronic Lymphocytic Leukemia. *Clinical Cancer Research* **23**, 2831–2841 (2017).
46. Dhillon, S. Orelabrutinib: First Approval. *Drugs* **81**, 503–507 (2021).
47. Dhillon, S. Tirabrutinib: First Approval. *Drugs* **80**, 835–840 (2020).
48. Schafer, P. H. *et al.* Spebrutinib (CC-292) Affects Markers of B Cell Activation, Chemotaxis, and Osteoclasts in Patients with Rheumatoid Arthritis: Results from a Mechanistic Study. *Rheumatol Ther* **7**, 101 (2020).
49. Catlett, I. M. *et al.* Safety, pharmacokinetics and pharmacodynamics of branebrutinib (BMS-986195), a covalent, irreversible inhibitor of Bruton's tyrosine kinase: Randomised phase I, placebo-controlled trial in healthy participants. *Br J Clin Pharmacol* **86**, 1849 (2020).
50. Tolerance and Pharmacokinetics of SHR1459 in Patients With Recurrent Replased/Refractory Mature B Cell Neoplasmstumor - Full Text View - ClinicalTrials.gov. https://classic.clinicaltrials.gov/ct2/show/NCT03664297.
51. Reich, D. S. *et al.* Safety and efficacy of tolebrutinib, an oral brain-penetrant BTK inhibitor, in relapsing multiple sclerosis: a phase 2b, randomised, double-blind, placebo-controlled trial. *Lancet Neurol* **20**, 729 (2021).
52. Montalban, X. *et al.* Placebo-Controlled Trial of an Oral BTK Inhibitor in Multiple Sclerosis. *N Engl J Med* **380**, 2406–2417 (2019).
53. Fleischmann, R. *et al.* Safety and efficacy of elsubrutinib or upadacitinib alone or in combination (ABBV-599) in patients with rheumatoid arthritis and inadequate response or intolerance to biological therapies: a multicentre, double-blind, randomised, controlled, phase 2 trial. *Lancet Rheumatol* **4**, e395–e406 (2022).
54. Muhowski, E. M. *et al.* Preclinical evaluation of combination nemtabrutinib and venetoclax in chronic lymphocytic leukemia. *J Hematol Oncol* **15**, 166 (2022).
55. Isenberg, D. *et al.* Efficacy, Safety, and Pharmacodynamic Effects of the Bruton's Tyrosine Kinase Inhibitor Fenebrutinib (GDC-0853) in Systemic Lupus Erythematosus: Results of a Phase II, Randomized, Double-Blind, Placebo-Controlled Trial. *Arthritis Rheumatol* **73**, 1835–1846 (2021).
56. Metz, M. *et al.* Fenebrutinib in H1 antihistamine-refractory chronic spontaneous urticaria: a randomized phase 2 trial. *Nature Medicine 2021 27:11* **27**, 1961–1969 (2021).

57. Allan, J. N. *et al.* Phase Ib dose-escalation study of the selective, non-covalent, reversible Bruton's tyrosine kinase inhibitor vecabrutinib in B-cell malignancies. *Haematologica* **107**, 984–987 (2022).
58. Kuter, D. J. *et al.* Rilzabrutinib, an Oral BTK Inhibitor, in Immune Thrombocytopenia. *New England Journal of Medicine* **386**, 1421–1431 (2022).
59. Phase 2a Study of the Safety, Tolerability, and Pharmacokinetics of Topically Administered PRN473 (SAR444727) in Patients With Mild to Moderate Atopic Dermatitis - Full Text View - ClinicalTrials.gov. https://classic.clinicaltrials.gov/ct2/show/NCT04992546.
60. Maurer, M. *et al.* Remibrutinib, a novel BTK inhibitor, demonstrates promising efficacy and safety in chronic spontaneous urticaria. *Journal of Allergy and Clinical Immunology* **150**, 1498-1506.e2 (2022).
61. Alu, A., Lei, H., Han, X., Wei, Y. & Wei, X. BTK inhibitors in the treatment of hematological malignancies and inflammatory diseases: mechanisms and clinical studies. *Journal of Hematology & Oncology 2022 15:1* **15**, 1–35 (2022).
62. Tasso, B., Spallarossa, A., Russo, E. & Brullo, C. The Development of BTK Inhibitors: A Five-Year Update. *Molecules* **26**, (2021).
63. Owens, T. D. *et al.* Discovery of Reversible Covalent Bruton's Tyrosine Kinase Inhibitors PRN473 and PRN1008 (Rilzabrutinib). *J Med Chem* **65**, 5300–5316 (2022).
64. Langrish, C. L. *et al.* PRN1008, a Reversible Covalent BTK Inhibitor in Clinical Development for Immune Thrombocytopenic Purpura. *Blood* **130**, 1052–1052 (2017).
65. Mato, A. R. *et al.* NX-2127-001, a First-in-Human Trial of NX-2127, a Bruton's Tyrosine Kinase-Targeted Protein Degrader, in Patients with Relapsed or Refractory Chronic Lymphocytic Leukemia and B-Cell Malignancies. *Blood* **140**, 2329–2332 (2022).
66. Lim, Y. S. *et al.* Orally bioavailable BTK PROTAC active against wild-type and C481 mutant BTKs in human lymphoma CDX mouse models. *Blood Adv* **7**, 92 (2023).
67. Arthur, R., Valle-Argos, B., Steele, A. J. & Packham, G. Development of PROTACs to address clinical limitations associated with BTK-targeted kinase inhibitors. *Explor Target Antitumor Ther* **1**, 131 (2020).
68. Chen, S. *et al.* Discovery of novel BTK PROTACs with improved metabolic stability via linker rigidification strategy. *Eur J Med Chem* **255**, 115403 (2023).
69. Zhao, Y. *et al.* Discovery of novel BTK PROTACs for B-Cell lymphomas. *Eur J Med Chem* **225**, 113820 (2021).
70. Buhimschi, A. D. *et al.* Targeting the C481S Ibrutinib-Resistance Mutation in Bruton's Tyrosine Kinase Using PROTAC-Mediated Degradation. *Biochemistry* **57**, 3564–3575 (2018).
71. Sun, Y. *et al.* Developing potent BTKC481S PROTACs for ibrutinib-resistant malignant lymphoma. *Chinese Chemical Letters* **34**, 107924 (2023).
72. Zain, R. & Vihinen, M. Structure-Function Relationships of Covalent and Non-Covalent BTK Inhibitors. *Front Immunol* **12**, (2021).
73. Gu, D., Tang, H., Wu, J., Li, J. & Miao, Y. Targeting Bruton tyrosine kinase using non-covalent inhibitors in B cell malignancies. *J Hematol Oncol* **14**, 1–15 (2021).
74. Gao, W. *et al.* Selective Antitumor Activity of Ibrutinib in EGFR-Mutant Non–Small Cell Lung Cancer Cells. *JNCI: Journal of the National Cancer Institute* **106**, (2014).

75. Wu, H. *et al.* Ibrutinib selectively and irreversibly targets EGFR (L858R, Del19) mutant but is moderately resistant to EGFR (T790M) mutant NSCLC Cells. *Oncotarget* **6**, 31313 (2015).
76. Di Paolo, J. A. *et al.* Specific Btk inhibition suppresses B cell– and myeloid cell–mediated arthritis. *Nature Chemical Biology 2010 7:1* **7**, 41–50 (2010).
77. Byrd, J. C. *et al.* First-in-human phase 1 study of the BTK inhibitor GDC-0853 in relapsed or refractory B-cell NHL and CLL. *Oncotarget* **9**, 13023 (2018).
78. Isenberg, D. *et al.* Efficacy, Safety, and Pharmacodynamic Effects of the Bruton's Tyrosine Kinase Inhibitor Fenebrutinib (GDC-0853) in Systemic Lupus Erythematosus: Results of a Phase II, Randomized, Double-Blind, Placebo-Controlled Trial. *Arthritis Rheumatol* **73**, 1835–1846 (2021).
79. Glickman, M. H. & Ciechanover, A. The ubiquitin-proteasome proteolytic pathway: Destruction for the sake of construction. *Physiol Rev* **82**, 373–428 (2002).
80. Thibaudeau, T. A. & Smith, D. M. A Practical Review of Proteasome Pharmacology. *Pharmacol Rev* **71**, 170 (2019).
81. Tanaka, K. The proteasome: Overview of structure and functions. *Proc Jpn Acad Ser B Phys Biol Sci* **85**, 12 (2009).
82. Schweitzer, A. *et al.* Structure of the human 26S proteasome at a resolution of 3.9 Å. *Proc Natl Acad Sci U S A* **113**, 7816–7821 (2016).
83. Bard, J. A. M. *et al.* Structure and Function of the 26S Proteasome. *https://doi.org/10.1146/annurev-biochem-062917-011931* **87**, 697–724 (2018).
84. Budenholzer, L., Cheng, C. L., Li, Y. & Hochstrasser, M. Proteasome Structure and Assembly. *J Mol Biol* **429**, 3500 (2017).
85. Wenzel, T. & Baumeister, W. Conformational constraints in protein degradation by the 20S proteasome. *Nature Structural Biology 1995 2:3* **2**, 199–204 (1995).
86. Liu, C. W., Corboy, M. J., DeMartino, G. N. & Thomas, P. J. Endoproteolytic activity of the proteasome. *Science (1979)* **299**, 408–411 (2003).
87. Majumder, P. & Baumeister, W. Proteasomes: Unfoldase-assisted protein degradation machines. *Biol Chem* **401**, 183–199 (2019).
88. Martinez-Fonts, K. *et al.* The proteasome 19S cap and its ubiquitin receptors provide a versatile recognition platform for substrates. *Nature Communications 2020 11:1* **11**, 1–16 (2020).
89. Sharon, M., Taverner, T., Ambroggio, X. I., Deshaies, R. J. & Robinson, C. V. Structural Organization of the 19S Proteasome Lid: Insights from MS of Intact Complexes. *PLoS Biol* **4**, 1314–1323 (2006).
90. Dambacher, C. M., Worden, E. J., Herzik, M. A., Martin, A. & Lander, G. C. Atomic structure of the 26S proteasome lid reveals the mechanism of deubiquitinase inhibition. *Elife* **5**, (2016).
91. Callis, J. The Ubiquitination Machinery of the Ubiquitin System. *The Arabidopsis Book / American Society of Plant Biologists* **12**, e0174 (2014).
92. Swatek, K. N. & Komander, D. Ubiquitin modifications. *Cell Research 2016 26:4* **26**, 399–422 (2016).
93. Ciechanover, A., Finley, D. & Varshavsky, A. Ubiquitin dependence of selective protein degradation demonstrated in the mammalian cell cycle mutant ts85. *Cell* **37**, 57–66 (1984).

94. Finley, D., Ciechanover, A. & Varshavsky, A. Thermolability of ubiquitin-activating enzyme from the mammalian cell cycle mutant ts85. *Cell* **37**, 43–55 (1984).
95. Pickart, C. M. Back to the Future with Ubiquitin. *Cell* **116**, 181–190 (2004).
96. Sun, L. & Chen, Z. J. The novel functions of ubiquitination in signaling. *Curr Opin Cell Biol* **16**, 119–126 (2004).
97. Ohtake, F., Tsuchiya, H., Saeki, Y. & Tanaka, K. K63 ubiquitylation triggers proteasomal degradation by seeding branched ubiquitin chains. *Proc Natl Acad Sci U S A* **115**, E1401–E1408 (2018).
98. Kliza, K. & Husnjak, K. Resolving the Complexity of Ubiquitin Networks. *Front Mol Biosci* **7**, 21 (2020).
99. Susanne, T., Judith, F., Christina, C. & Dmitri, P. Cancers adapt to their mutational load by buffering protein misfolding stress. *Elife* **12**, (2023).
100. Nagaraj, N. S., Singh, O. V. & Merchant, N. B. Proteomics: a strategy to understand the novel targets in protein misfolding and cancer therapy. *Expert Rev Proteomics* **7**, 613 (2010).
101. van Drie, J. H. Protein folding, protein homeostasis, and cancer. *Chin J Cancer* **30**, 124 (2011).
102. Chen, L. *et al.* Enhanced Degradation of Misfolded Proteins Promotes Tumorigenesis. *Cell Rep* **18**, 3143–3154 (2017).
103. Manasanch, E. E. & Orlowski, R. Z. Proteasome inhibitors in cancer therapy. *Nature Reviews Clinical Oncology 2017 14:7* **14**, 417–433 (2017).
104. Adams, J. The development of proteasome inhibitors as anticancer drugs. *Cancer Cell* **5**, 417–421 (2004).
105. DH, L. & AL, G. Proteasome inhibitors: valuable new tools for cell biologists. *Trends Cell Biol* **8**, 397–403 (1998).
106. Kisselev, A. F. & Goldberg, A. L. Proteasome inhibitors: from research tools to drug candidates. *Chem Biol* **8**, 739–758 (2001).
107. Kraus, M. *et al.* The novel β2-selective proteasome inhibitor LU-102 synergizes with bortezomib and carfilzomib to overcome proteasome inhibitor resistance of myeloma cells. *Haematologica* **100**, 1350–1360 (2015).
108. Kraus, J. *et al.* The novel β2-selective proteasome inhibitor LU-102 decreases phosphorylation of I kappa B and induces highly synergistic cytotoxicity in combination with ibrutinib in multiple myeloma cells. *Cancer Chemother Pharmacol* **76**, 383–396 (2015).
109. Downey-Kopyscinski, S. L., Srinivasa, S. & Kisselev, A. F. A clinically relevant pulse treatment generates a bortezomib-resistant myeloma cell line that lacks proteasome mutations and is sensitive to Bcl-2 inhibitor venetoclax. *Scientific Reports 2022 12:1* **12**, 1–11 (2022).
110. Besse, A. *et al.* Proteasome Inhibition in Multiple Myeloma: Head-to-Head Comparison of Currently Available Proteasome Inhibitors. *Cell Chem Biol* **26**, 340-351.e3 (2019).
111. Downey-Kopyscinski, S. *et al.* An inhibitor of proteasome β2 sites sensitizes myeloma cells to immunoproteasome inhibitors. *Blood Adv* **2**, 2443–2451 (2018).
112. Weyburne, E. S. *et al.* Inhibition of the Proteasome β2 Site Sensitizes Triple-Negative Breast Cancer Cells to β5 Inhibitors and Suppresses Nrf1 Activation. *Cell Chem Biol* **24**, 218–230 (2017).

113. Manasanch, E. E. & Orlowski, R. Z. Proteasome inhibitors in cancer therapy. *Nature Reviews Clinical Oncology 2017 14:7* **14**, 417–433 (2017).
114. Lazarus, D. D. *et al.* A new model of cancer cachexia: Contribution of the ubiquitin-proteasome pathway. *Am J Physiol Endocrinol Metab* **277**, (1999).
115. Penna, F. *et al.* Effect of the specific proteasome inhibitor bortezomib on cancer-related muscle wasting. *J Cachexia Sarcopenia Muscle* **7**, 345–354 (2016).
116. Sung, M. H. *et al.* Dynamic Effect of Bortezomib on NF-κB Activity and Gene Expression in Tumor Cells. *Mol Pharmacol* **74**, 1215 (2008).
117. Yang, D. T., Young, K. H., Kahl, B. S., Markovina, S. & Miyamoto, S. Prevalence of bortezomib-resistant constitutive NF-kappaB activity in mantle cell lymphoma. *Mol Cancer* **7**, 1–14 (2008).
118. Hideshima, T. *et al.* Bortezomib induces canonical nuclear factor-κB activation in multiple myeloma cells. *Blood* **114**, 1046 (2009).
119. Traenckner, E. B. M., Wilk, S. & Baeuerle, P. A. A proteasome inhibitor prevents activation of NF-kappa B and stabilizes a newly phosphorylated form of I kappa B-alpha that is still bound to NF-kappa B. *EMBO J* **13**, 5433 (1994).
120. Hideshima, T. *et al.* NF-κB as a therapeutic target in multiple myeloma. *Journal of Biological Chemistry* **277**, 16639–16647 (2002).
121. Liu, T., Zhang, L., Joo, D. & Sun, S. C. NF-κB signaling in inflammation. *Signal Transduction and Targeted Therapy 2017 2:1* **2**, 1–9 (2017).
122. Vodanovic-Jankovic, S., Hari, P., Jacobs, P., Komorowski, R. & Drobyski, W. R. NF-kappaB as a target for the prevention of graft-versus-host disease: comparative efficacy of bortezomib and PS-1145. *Blood* **107**, 827–834 (2006).
123. Hanna, J., Leggett, D. S. & Finley, D. Ubiquitin Depletion as a Key Mediator of Toxicity by Translational Inhibitors. *Mol Cell Biol* **23**, 9251 (2003).
124. Suraweera, A., Münch, C., Hanssum, A. & Bertolotti, A. Failure of Amino Acid Homeostasis Causes Cell Death following Proteasome Inhibition. *Mol Cell* **48**, 242 (2012).
125. Kale, J., Osterlund, E. J. & Andrews, D. W. BCL-2 family proteins: changing partners in the dance towards death. *Cell Death & Differentiation 2018 25:1* **25**, 65–80 (2017).
126. Marie Hardwick, J. & Soane, L. Multiple Functions of BCL-2 Family Proteins. *Cold Spring Harb Perspect Biol* **5**, (2013).
127. Huang, D. C. S. & Strasser, A. BH3-only proteins - Essential initiators of apoptotic cell death. *Cell* **103**, 839–842 (2000).
128. Giam, M., Huang, D. C. S. & Bouillet, P. BH3-only proteins and their roles in programmed cell death. *Oncogene 2009 27:1* **27**, S128–S136 (2009).
129. L.Omonosova, E. & C.Hinnadurai, G. BH3-only proteins in apoptosis and beyond: an overview. *Oncogene 2009 27:1* **27**, S2–S19 (2009).
130. Roufayel, R., Younes, K., Al-Sabi, A. & Murshid, N. BH3-Only Proteins Noxa and Puma Are Key Regulators of Induced Apoptosis. *Life 2022, Vol. 12, Page 256* **12**, 256 (2022).
131. Nikrad, M. *et al.* The proteasome inhibitor bortezomib sensitizes cells to killing by death receptor ligand TRAIL via BH3-only proteins Bik and Bim. *Mol Cancer Ther* **4**, 443–449 (2005).
132. Lopes, U. G., Erhardt, P., Yao, R. & Cooper, G. M. p53-dependent induction of apoptosis by proteasome inhibitors. *Journal of Biological Chemistry* **272**, 12893–12896 (1997).

133. Rivlin, N., Brosh, R., Oren, M. & Rotter, V. Mutations in the p53 Tumor Suppressor Gene: Important Milestones at the Various Steps of Tumorigenesis. *Genes Cancer* **2**, 466 (2011).
134. Cooper, G. M. Protein Sorting and Transport - The Endoplasmic Reticulum, Golgi Apparatus, and Lysosomes. (2000).
135. Vitale, A., Ceriotti, A. & Denecke, J. The Role of the Endoplasmic Reticulum in Protein Synthesis, Modification and Intracellular Transport. *J Exp Bot* **44**, 1417–1444 (1993).
136. Pelham, H. R. B. The retention signal for soluble proteins of the endoplasmic reticulum. *Trends Biochem Sci* **15**, 483–486 (1990).
137. Aronson, L. I. & Davies, F. E. DangER: protein ovERload. Targeting protein degradation to treat myeloma. *Haematologica* **97**, 1119 (2012).
138. Tilk, S., Frydman, J., Curtis, C. & Petrov, D. Cancers adapt to their mutational load by buffering protein misfolding stress. *Elife* **12**, (2023).
139. van Drie, J. H. Protein folding, protein homeostasis, and cancer. *Chin J Cancer* **30**, 124 (2011).
140. Nagaraj, N. S., Singh, O. V. & Merchant, N. B. Proteomics: a strategy to understand the novel targets in protein misfolding and cancer therapy. *Expert Rev Proteomics* **7**, 613 (2010).
141. Bertolotti, A., Zhang, Y., Hendershot, L. M., Harding, H. P. & Ron, D. Dynamic interaction of BiP and ER stress transducers in the unfolded-protein response. *Nature Cell Biology 2000 2:6* **2**, 326–332 (2000).
142. Shen, J., Snapp, E. L., Lippincott-Schwartz, J. & Prywes, R. Stable Binding of ATF6 to BiP in the Endoplasmic Reticulum Stress Response. *Mol Cell Biol* **25**, 921 (2005).
143. Kopp, M. C., Larburu, N., Durairaj, V., Adams, C. J. & Ali, M. M. U. UPR proteins IRE1 and PERK switch BiP from chaperone to ER stress sensor. *Nature Structural & Molecular Biology 2019 26:11* **26**, 1053–1062 (2019).
144. Vitale, M. *et al.* Inadequate BiP availability defines endoplasmic reticulum stress. *Elife* **8**, (2019).
145. Rozpędek, W. *et al.* The Role of the PERK/eIF2α/ATF4/CHOP Signaling Pathway in Tumor Progression During Endoplasmic Reticulum Stress. *Curr Mol Med* **16**, 533 (2016).
146. Harding, H. P., Zhang, Y., Bertolotti, A., Zeng, H. & Ron, D. Perk is essential for translational regulation and cell survival during the unfolded protein response. *Mol Cell* **5**, 897–904 (2000).
147. Hamanaka, R. B., Bennett, B. S., Cullinan, S. B. & Diehl, J. A. PERK and GCN2 contribute to eIF2α phosphorylation and cell cycle arrest after activation of the unfolded protein response pathway. *Mol Biol Cell* **16**, 5493–5501 (2005).
148. Teske, B. F. *et al.* The eIF2 kinase PERK and the integrated stress response facilitate activation of ATF6 during endoplasmic reticulum stress. *Mol Biol Cell* **22**, 4390–4405 (2011).
149. Jiang, H. Y. & Wek, R. C. Phosphorylation of the alpha-subunit of the eukaryotic initiation factor-2 (eIF2alpha) reduces protein synthesis and enhances apoptosis in response to proteasome inhibition. *J Biol Chem* **280**, 14189–14202 (2005).
150. Schröder, M. & Kaufman, R. J. The mammalian unfolded protein response. *Annu Rev Biochem* **74**, 739–789 (2005).

151. Hetz, C., Zhang, K. & Kaufman, R. J. Mechanisms, regulation and functions of the unfolded protein response. *Nature Reviews Molecular Cell Biology 2020 21:8* **21**, 421–438 (2020).
152. Hetz, C. The unfolded protein response: controlling cell fate decisions under ER stress and beyond. *Nature Reviews Molecular Cell Biology 2012 13:2* **13**, 89–102 (2012).
153. Obeng, E. A. *et al.* Proteasome inhibitors induce a terminal unfolded protein response in multiple myeloma cells. *Blood* **107**, 4907 (2006).
154. Brown, A. J. L. & Ish-Horowicz, D. Evolution of the 87A and 87C heat-shock loci in Drosophila. *Nature 1981 290:5808* **290**, 677–682 (1981).
155. Lindquist, S. The heat-shock response. *Annu Rev Biochem* **55**, 1151–1191 (1986).
156. PIRKKALA, L., NYKÄNEN, P. & SISTONEN, L. Roles of the heat shock transcription factors in regulation of the heat shock response and beyond. *FASEB J* **15**, 1118–1131 (2001).
157. Santoro, M. G. Heat shock factors and the control of the stress response. *Biochem Pharmacol* **59**, 55–63 (2000).
158. Bush, K. T., Goldberg, A. L. & Nigam, S. K. Proteasome inhibition leads to a heat-shock response, induction of endoplasmic reticulum chaperones, and thermotolerance. *J Biol Chem* **272**, 9086–9092 (1997).
159. Sha, Z. & Goldberg, A. L. Multiple myeloma cells are exceptionally sensitive to heat shock, which overwhelms their proteostasis network and induces apoptosis. *Proc Natl Acad Sci U S A* **117**, 21588–21597 (2020).
160. Ling, Y. H., Liebes, L., Zou, Y. & Perez-Soler, R. Reactive Oxygen Species Generation and Mitochondrial Dysfunction in the Apoptotic Response to Bortezomib, a Novel Proteasome Inhibitor, in Human H460 Non-small Cell Lung Cancer Cells. *Journal of Biological Chemistry* **278**, 33714–33723 (2003).
161. Maharjan, S., Oku, M., Tsuda, M., Hoseki, J. & Sakai, Y. Mitochondrial impairment triggers cytosolic oxidative stress and cell death following proteasome inhibition. *Scientific Reports 2014 4:1* **4**, 1–11 (2014).
162. Halasi, M. *et al.* ROS inhibitor N-acetyl-L-cysteine antagonizes the activity of proteasome inhibitors. *Biochemical Journal* **454**, 201–208 (2013).
163. Ughachukwu, P. & Unekwe, P. Efflux Pump-Mediated Resistance in Chemotherapy. *Ann Med Health Sci Res* **2**, 191 (2012).
164. Nakamura, T. *et al.* The mechanism of cross-resistance to proteasome inhibitor bortezomib and overcoming resistance in Ewing's family tumor cells. *Int J Oncol* **31**, 803–811 (2007).
165. Besse, A. *et al.* Carfilzomib resistance due to ABCB1/MDR1 overexpression is overcome by nelfinavir and lopinavir in multiple myeloma. *Leukemia* **32**, 391 (2018).
166. Chernykh, Y. & Golenkov, A. Effect of Expression of Multidrug Resistance Genes on Efficacy the Treatment of Multiple Myeloma By Proteasome Inhibitor. *Blood* **126**, 4859 (2015).
167. Rumpold, H. *et al.* Knockdown of PgP resensitizes leukemic cells to proteasome inhibitors. *Biochem Biophys Res Commun* **361**, 549–554 (2007).
168. Wu, Y. X., Yang, J. H. & Saitsu, H. Bortezomib-resistance is associated with increased levels of proteasome subunits and apoptosis-avoidance. *Oncotarget* **7**, 77622 (2016).

169. Öksüzoğlu, E. & Kozalak, G. Inhibition of apoptosis may lead to the development of bortezomib resistance in multiple myeloma cancer cells. *Turkish Journal of Biochemistry* **46**, 63–69 (2020).
170. Malek, M. A. Y. A. *et al.* Molecular chaperone GRP78 enhances aggresome delivery to autophagosomes to promote drug resistance in multiple myeloma. *Oncotarget* **6**, 3098–3110 (2014).
171. Besse, L. *et al.* A metabolic switch in proteasome inhibitor-resistant multiple myeloma ensures higher mitochondrial metabolism, protein folding and sphingomyelin synthesis. *Haematologica* **104**, e415 (2019).
172. Soriano, G. P. *et al.* Proteasome inhibitor-adapted myeloma cells are largely independent from proteasome activity and show complex proteomic changes, in particular in redox and energy metabolism. *Leukemia 2016 30:11* **30**, 2198–2207 (2016).
173. Roué, G. *et al.* The Hsp90 inhibitor IPI-504 overcomes bortezomib resistance in mantle cell lymphoma in vitro and in vivo by down-regulation of the prosurvival ER chaperone BiP/Grp78. *Blood* **117**, 1270–1279 (2011).
174. Ferguson, I. D. *et al.* Allosteric HSP70 inhibitors perturb mitochondrial proteostasis and overcome proteasome inhibitor resistance in multiple myeloma. *bioRxiv* 2020.04.21.052456 (2020) doi:10.1101/2020.04.21.052456.
175. Bao, W., Gu, Y., Ta, L., Wang, K. & Xu, Z. Induction of autophagy by the MG-132 proteasome inhibitor is associated with endoplasmic reticulum stress in MCF-7 cells. *Mol Med Rep* **13**, 796–804 (2016).
176. Wang, D. *et al.* Proteasome inhibition boosts autophagic degradation of ubiquitinated-AGR2 and enhances the antitumor efficiency of bevacizumab. *Oncogene 2019 38:18* **38**, 3458–3474 (2019).
177. Zhu, K., Dunner, K. & McConkey, D. J. Proteasome inhibitors activate autophagy as a cytoprotective response in human prostate cancer cells. *Oncogene* **29**, 451 (2010).
178. Driscoll, J. J. & Chowdhury, R. De. Molecular crosstalk between the proteasome, aggresomes and autophagy: Translational potential and clinical implications. *Cancer Lett* **325**, 147–154 (2012).
179. Chavda, S. J. *et al.* Autophagy Blockade Disrupts Myeloma Cell Recovery from Proteasome Inhibition and Enhances Apoptosis. *Blood* **138**, 1567–1567 (2021).
180. Vogl, D. T. *et al.* Combined autophagy and proteasome inhibition: A phase 1 trial of hydroxychloroquine and bortezomib in patients with relapsed/refractory myeloma. *Autophagy* **10**, 1380 (2014).
181. Bi, J. *et al.* Blocking autophagy overcomes resistance to dual histone deacetylase and proteasome inhibition in gynecologic cancer. *Cell Death Dis* **13**, (2022).
182. Dreger, H. *et al.* Protection of vascular cells from oxidative stress by proteasome inhibition depends on Nrf2. *Cardiovasc Res* **85**, 395–403 (2010).
183. Deng, X. *et al.* The Nrf2/PGC1α Pathway Regulates Antioxidant and Proteasomal Activity to Alter Cisplatin Sensitivity in Ovarian Cancer. *Oxid Med Cell Longev* **2020**, (2020).
184. Riz, I. *et al.* Noncanonical SQSTM1/p62-Nrf2 pathway activation mediates proteasome inhibitor resistance in multiple myeloma cells via redox, metabolic and translational reprogramming. *Oncotarget* **7**, 66360–66385 (2016).

185. Dolloff, N. G., Reyes, L., Smith, B., Langenheim, J. F. & Manevich, Y. Targeting Redox Overcomes Proteasome Inhibitor Resistance in Multiple Myeloma. *Blood* **126**, 1819 (2015).
186. Rosean, T. R. *et al.* Preclinical validation of interleukin 6 as a therapeutic target in multiple myeloma. *Immunol Res* **59**, 188 (2014).
187. Fan, J. L. *et al.* URI regulates tumorigenicity and chemotherapeutic resistance of multiple myeloma by modulating IL-6 transcription. *Cell Death & Disease 2014 5:3* **5**, e1126–e1126 (2014).
188. Brown, C. O. *et al.* Interleukin-6 counteracts therapy-induced cellular oxidative stress in multiple myeloma by up-regulating manganese superoxide dismutase. *Biochemical Journal* **444**, 515–527 (2012).
189. Voorhees, P. M. *et al.* Inhibition of Interleukin-6 Signaling with CNTO 328 Enhances the Activity of Bortezomib in Preclinical Models of Multiple Myeloma. *Clinical Cancer Research* **13**, 6469–6478 (2007).
190. Giannoni, P. & de Totero, D. The HGF/c-MET axis as a potential target to overcome survival signals and improve therapeutic efficacy in multiple myeloma. *Cancer Drug Resistance* **4**, 923 (2021).
191. Baljevic, M. *et al.* Phase II study of the c-MET inhibitor tivantinib (ARQ 197) in patients with relapsed or relapsed/refractory multiple myeloma. *Ann Hematol* **96**, 977 (2017).
192. Hov, H. *et al.* A Selective c-Met Inhibitor Blocks an Autocrine Hepatocyte Growth Factor Growth Loop in ANBL-6 Cells and Prevents Migration and Adhesion of Myeloma Cells. *Clinical Cancer Research* **10**, 6686–6694 (2004).
193. Moschetta, M. *et al.* Novel targeting of phospho-cMET overcomes drug resistance and induces antitumor activity in multiple myeloma. *Clin Cancer Res* **19**, 4371–4382 (2013).
194. Markovina, S. *et al.* Bortezomib-Resistant NF-κB Activity in Multiple Myeloma Cells. *Mol Cancer Res* **6**, 1356 (2008).
195. Yuan, T. *et al.* Inhibition of the PI3K/AKT signaling pathway sensitizes diffuse large B-cell lymphoma cells to treatment with proteasome inhibitors via suppression of BAG3. *Oncol Lett* **17**, 3719–3726 (2019).
196. Mimura, N. *et al.* Selective and potent Akt inhibition triggers anti-myeloma activities and enhances fatal endoplasmic reticulum stress induced by proteasome inhibition. *Cancer Res* **74**, 4458–4469 (2014).
197. Heinemann, L. *et al.* Inhibiting PI3K–AKT–mTOR Signaling in Multiple Myeloma-Associated Mesenchymal Stem Cells Impedes the Proliferation of Multiple Myeloma Cells. *Front Oncol* **12**, 874325 (2022).
198. Zhang, X. D. *et al.* Tight Junction Protein 1 Modulates Proteasome Capacity and Proteasome Inhibitor Sensitivity in Multiple Myeloma via EGFR/JAK1/STAT3 Signaling. *Cancer Cell* **29**, 639–652 (2016).
199. Gupta, V. A. *et al.* Bone marrow microenvironment–derived signals induce Mcl-1 dependence in multiple myeloma. *Blood* **129**, 1969–1979 (2017).
200. Harmer, D., Falank, C. & Reagan, M. R. Interleukin-6 Interweaves the Bone Marrow Microenvironment, Bone Loss, and Multiple Myeloma. *Front Endocrinol (Lausanne)* **9**, (2018).
201. Anderson, K. C. Targeted therapy of multiple myeloma based upon tumor-microenvironmental interactions. *Exp Hematol* **35**, 155–162 (2007).

202. Podar, K. & Anderson, K. C. The pathophysiologic role of VEGF in hematologic malignancies: therapeutic implications. *Blood* **105**, 1383–1395 (2005).
203. Giannoni, P. & de Totero, D. The HGF/c-MET axis as a potential target to overcome survival signals and improve therapeutic efficacy in multiple myeloma. *Cancer Drug Resistance* **4**, null (2021).
204. Hideshima, T., Mitsiades, C., Tonon, G., Richardson, P. G. & Anderson, K. C. Understanding multiple myeloma pathogenesis in the bone marrow to identify new therapeutic targets. *Nature Reviews Cancer 2007 7:8* **7**, 585–598 (2007).
205. Teramachi, J. *et al.* Pivotal Role of OCL-Derived IGF1 in Drug Resistance and Bone Destruction in MM. *Blood* **134**, 4336–4336 (2019).
206. Tagoug, I., de Chalon, A. S. & Dumontet, C. Inhibition of IGF-1 Signalling Enhances the Apoptotic Effect of AS602868, an IKK2 Inhibitor, in Multiple Myeloma Cell Lines. *PLoS One* **6**, e22641 (2011).
207. Herrero, A. B. *et al.* Effects of IL-8 Up-Regulation on Cell Survival and Osteoclastogenesis in Multiple Myeloma. *Am J Pathol* **186**, 2171–2182 (2016).
208. Chen, Z., Teo, A. E. & McCarty, N. ROS-induced CXCR4 signaling regulates mantle cell lymphoma (MCL) cell survival and drug resistance in the bone marrow microenvironment via autophagy. *Clinical Cancer Research* **22**, 187–199 (2016).
209. Azab, A. K. *et al.* CXCR4 inhibitor AMD3100 disrupts the interaction of multiple myeloma cells with the bone marrow microenvironment and enhances their sensitivity to therapy. *Blood* **113**, 4341–4351 (2009).
210. Yen, C. H. & Hsiao, H. H. NRF2 Is One of the Players Involved in Bone Marrow Mediated Drug Resistance in Multiple Myeloma. *International Journal of Molecular Sciences 2018, Vol. 19, Page 3503* **19**, 3503 (2018).
211. Farrell, M. L. & Reagan, M. R. Soluble and Cell-Cell-Mediated Drivers of Proteasome Inhibitor Resistance in Multiple Myeloma. *Front Endocrinol (Lausanne)* **9**, (2018).
212. Schwestermann, J., Besse, A., Driessen, C. & Besse, L. Contribution of the Tumor Microenvironment to Metabolic Changes Triggering Resistance of Multiple Myeloma to Proteasome Inhibitors. *Front Oncol* **12**, (2022).
213. Brandl, A. *et al.* Junctional adhesion molecule C expression specifies a CD138low/neg multiple myeloma cell population in mice and humans. *Blood Adv* **6**, 2195–2206 (2022).
214. Belloni, D. *et al.* Modeling multiple myeloma-bone marrow interactions and response to drugs in a 3D surrogate microenvironment. *Haematologica* **103**, 707–716 (2018).
215. Tamura, H. *et al.* Marrow stromal cells induce B7-H1 expression on myeloma cells, generating aggressive characteristics in multiple myeloma. *Leukemia* **27**, 464–472 (2013).
216. Khalife, J. *et al.* MiR-16 regulates crosstalk in NF-κB tolerogenic inflammatory signaling between myeloma cells and bone marrow macrophages. *JCI Insight* **4**, (2019).
217. Abdi, J., Rastgoo, N., Chen, Y., Chen, G. A. & Chang, H. Ectopic expression of BIRC5-targeting miR-101-3p overcomes bone marrow stroma-mediated drug resistance in multiple myeloma cells. *BMC Cancer* **19**, 1–12 (2019).
218. Gao, X. *et al.* Mechanism of exosomal miR-155 derived from bone marrow mesenchymal stem cells on stemness maintenance and drug resistance in myeloma cells. *J Orthop Surg Res* **16**, 1–13 (2021).
219. Wang, J. *et al.* Bone marrow stromal cell–derived exosomes as communicators in drug resistance in multiple myeloma cells. *Blood* **124**, 555–566 (2014).

220. Xu, H. *et al.* Exosome-Transmitted PSMA3 and PSMA3-AS1 Promote Proteasome Inhibitor Resistance in Multiple Myeloma. *Clin Cancer Res* **25**, 1923–1935 (2019).
221. Di Marzo, L. *et al.* Microenvironment drug resistance in multiple myeloma: emerging new players. *Oncotarget* **7**, 60698–60711 (2016).
222. Wu, F. *et al.* Signaling pathways in cancer-associated fibroblasts and targeted therapy for cancer. *Signal Transduction and Targeted Therapy 2021 6:1* **6**, 1–35 (2021).
223. Sakemura, R. *et al.* Targeting cancer-associated fibroblasts in the bone marrow prevents resistance to CART-cell therapy in multiple myeloma. *Blood* **139**, 3708–3721 (2022).
224. De Boeck, A. *et al.* Differential secretome analysis of cancer-associated fibroblasts and bone marrow-derived precursors to identify microenvironmental regulators of colon cancer progression. *Proteomics* **13**, 379–388 (2013).
225. Leung-Hagesteijn, C. *et al.* Xbp1s-Negative Tumor B Cells and Pre-Plasmablasts Mediate Therapeutic Proteasome Inhibitor Resistance in Multiple Myeloma. *Cancer Cell* **24**, 289–304 (2013).
226. Zang, M. *et al.* Cdc37 suppression induces plasma cell immaturation and bortezomib resistance in multiple myeloma via Xbp1s. *Oncogenesis 2020 9:3* **9**, 1–13 (2020).
227. Quwaider, D. *et al.* DEPTOR maintains plasma cell differentiation and favorably affects prognosis in multiple myeloma. *J Hematol Oncol* **10**, 1–12 (2017).
228. Orlowski, R. Z. Why Proteasome Inhibitors Cannot ERADicate Multiple Myeloma. *Cancer Cell* **24**, 275–277 (2013).
229. Downey-Kopyscinski, S. L. *et al.* Functional Interactions between Transcription Factors Involved in Myeloma Pathogenesis - Biological and Therapeutic Implications. *Blood* **134**, 315–315 (2019).
230. Guo, W. *et al.* Identification and Characterization of Multiple Myeloma Stem Cell-Like Cells. *Cancers (Basel)* **13**, (2021).
231. Huff, C. A. & Matsui, W. Multiple Myeloma Cancer Stem Cells. *J Clin Oncol* **26**, 2895 (2008).
232. Yang, Y. *et al.* Bruton tyrosine kinase is a therapeutic target in stem-like cells from multiple myeloma. *Cancer Res* **75**, 594 (2015).
233. Elbezanti, W. O. *et al.* Development of a novel Bruton's tyrosine kinase inhibitor that exerts anti-cancer activities potentiates response of chemotherapeutic agents in multiple myeloma stem cell-like cells. *Front Pharmacol* **13**, 894535 (2022).
234. Kraus, J. *et al.* The novel β2-selective proteasome inhibitor LU-102 decreases phosphorylation of I kappa B and induces highly synergistic cytotoxicity in combination with ibrutinib in multiple myeloma cells. *Cancer Chemother Pharmacol* **76**, 383–396 (2015).
235. Shabaneh, T. B. *et al.* Molecular Basis of Differential Sensitivity of Myeloma Cells to Clinically Relevant Bolus Treatment with Bortezomib. *PLoS One* **8**, 56132 (2013).
236. Weyburne, E. S. *et al.* Inhibition of the Proteasome β2 Site Sensitizes Triple-Negative Breast Cancer Cells to β5 Inhibitors and Suppresses Nrf1 Activation. *Cell Chem Biol* **24**, 218–230 (2017).
237. Britton, M. *et al.* Selective inhibitor of proteasome's caspase-like sites sensitizes cells to specific inhibition of chymotrypsin-like sites. *Chem Biol* **16**, 1278 (2009).
238. Geurink, P. P. *et al.* Incorporation of Non-natural Amino Acids Improves Cell Permeability and Potency of Specific Inhibitors of Proteasome Trypsin-like Sites. *J Med Chem* **56**, 1262 (2013).

239. Kumar, H. *et al.* secDrug: a pipeline to discover novel drug combinations to kill drug-resistant multiple myeloma cells using a greedy set cover algorithm and single-cell multi-omics. *Blood Cancer J* **12**, (2022).
240. Kuo, C. L., Collins, G. A. & Goldberg, A. L. Methods to Rapidly Prepare Mammalian 26S Proteasomes for Biochemical Analysis. *Methods Mol Biol* **1844**, 277 (2018).
241. Besche, H. C., Haas, W., Gygi, S. P. & Goldberg, A. L. Isolation of Mammalian 26S Proteasomes and p97/VCP Complexes Using the Ubiquitin-like Domain from HHR23B Reveals Novel Proteasome-Associated Proteins. *Biochemistry* **48**, 2538–2549 (2009).
242. Kisselev, A. F., Kaganovich, D. & Goldberg, A. L. Binding of Hydrophobic Peptides to Several Non-catalytic Sites Promotes Peptide Hydrolysis by All Active Sites of 20 S Proteasomes: EVIDENCE FOR PEPTIDE-INDUCED CHANNEL OPENING IN THE α-RINGS *. *Journal of Biological Chemistry* **277**, 22260–22270 (2002).
243. Britton, M. *et al.* Selective inhibitor of proteasome's caspase-like sites sensitizes cells to specific inhibition of chymotrypsin-like sites. *Chem Biol* **16**, 1278 (2009).
244. DeMartino, G. N. Purification of PA700, the 19S regulatory complex of the 26S proteasome. *Methods Enzymol* **398**, 295–306 (2005).
245. Dong, Y. *et al.* Cryo-EM structures and dynamics of substrate-engaged human 26S proteasome. *Nature* **565**, 49–55 (2019).
246. Saeki, Y., Isono, E. & Toh-E, A. Preparation of Ubiquitinated Substrates by the PY Motif-Insertion Method for Monitoring 26S Proteasome Activity. *Methods Enzymol* **399**, 215–227 (2005).
247. Gallastegui, N. & Groll, M. The 26S proteasome: assembly and function of a destructive machine. *Trends Biochem Sci* **35**, 634–642 (2010).
248. Bard, J. A. M. *et al.* Structure and Function of the 26S Proteasome. *https://doi.org/10.1146/annurev-biochem-062917-011931* **87**, 697–724 (2018).
249. Voges, D., Zwickl, P. & Baumeister, W. The 26S Proteasome: A Molecular Machine Designed for Controlled Proteolysis. *https://doi.org/10.1146/annurev.biochem.68.1.1015* **68**, 1015–1068 (2003).
250. Marshall, R. S. & Vierstra, R. D. Dynamic regulation of the 26S proteasome: From synthesis to degradation. *Front Mol Biosci* **6**, 40 (2019).
251. Bross, P. F. *et al.* Approval Summary for Bortezomib for Injection in the Treatment of Multiple Myeloma. *Clinical Cancer Research* **10**, 3954–3964 (2004).
252. Herndon, T. M. *et al.* U.S. Food and Drug Administration Approval: Carfilzomib for the Treatment of Multiple Myeloma. *Clinical Cancer Research* **19**, 4559–4563 (2013).
253. Shirley, M. Ixazomib: First Global Approval. *Drugs 2016 76:3* **76**, 405–411 (2016).
254. Balleari, E., Ghio, R., Falcone, A. & Musto, P. Possible Multiple Myeloma Dedifferentiation Following Thalidomide Therapy: A Report of Four Cases. *https://doi.org/10.1080/10428190310001617231* **45**, 735–738 (2009).
255. Leung-Hagesteijn, C. *et al.* Xbp1s-negative tumor B cells and pre-plasmablasts mediate therapeutic proteasome inhibitor resistance in multiple myeloma. *Cancer Cell* **24**, 289–304 (2013).
256. Zhou, G., Liu, Y., Zhang, B., Meng, F. & Liu, X. Expression of Bruton's Tyrosine Kinase in Multiple Myeloma. *Blood* **110**, 4751–4751 (2007).
257. Liu, Y., Dong, Y., Jiang, Q. L., Zhang, B. & Hu, A. M. Bruton's tyrosine kinase: potential target in human multiple myeloma. *Leuk Lymphoma* **55**, 177–181 (2014).

258. Yang, Y. *et al.* Bruton tyrosine kinase is a therapeutic target in stem-like cells from multiple myeloma. *Cancer Res* **75**, 594–604 (2015).
259. de Claro, R. A. *et al.* FDA Approval: Ibrutinib for Patients with Previously Treated Mantle Cell Lymphoma and Previously Treated Chronic Lymphocytic Leukemia. *Clinical Cancer Research* **21**, 3586–3590 (2015).
260. Dasmahapatra, G. *et al.* The Bruton tyrosine kinase (BTK) inhibitor PCI-32765 synergistically increases proteasome inhibitor activity in diffuse large-B cell lymphoma (DLBCL) and mantle cell lymphoma (MCL) cells sensitive or resistant to bortezomib. *Br J Haematol* **161**, 43–56 (2013).
261. Kraus, J. *et al.* The novel β2-selective proteasome inhibitor LU-102 decreases phosphorylation of I kappa B and induces highly synergistic cytotoxicity in combination with ibrutinib in multiple myeloma cells. *Cancer Chemother Pharmacol* **76**, 383–396 (2015).
262. Kisselev, A. F., Van Der Linden, W. A. & Overkleeft, H. S. Proteasome inhibitors: an expanding army attacking a unique target. *Chem Biol* **19**, 99–115 (2012).
263. Kisselev, A. F. Site-Specific Proteasome Inhibitors. *Biomolecules 2022, Vol. 12, Page 54* **12**, 54 (2021).
264. Mirabella, A. C. *et al.* Specific Cell-Permeable Inhibitor of Proteasome Trypsin-like Sites Selectively Sensitizes Myeloma Cells to Bortezomib and Carfilzomib. *Chem Biol* **18**, 608–618 (2011).
265. Britton, M. *et al.* Selective inhibitor of proteasome's caspase-like sites sensitizes cells to specific inhibition of chymotrypsin-like sites. *Chem Biol* **16**, 1278–1289 (2009).
266. Bard, J. A. M. *et al.* Structure and Function of the 26S Proteasome. *Annu Rev Biochem* **87**, 697–724 (2018).
267. Li, J. *et al.* Epidithiodiketopiperazines Inhibit Protein Degradation by Targeting Proteasome Deubiquitinase Rpn11. *Cell Chem Biol* **25**, 1350-1358.e9 (2018).
268. Li, J. *et al.* Capzimin is a potent and specific inhibitor of proteasome isopeptidase Rpn11. *Nat Chem Biol* **13**, 486–493 (2017).
269. D'Arcy, P. *et al.* Inhibition of proteasome deubiquitinating activity as a new cancer therapy. *Nat Med* **17**, 1636–1640 (2011).
270. Lee, B. H. *et al.* Enhancement of proteasome activity by a small-molecule inhibitor of USP14. *Nature* **467**, 179–184 (2010).
271. Inobe, T. & Genmei, R. Inhibition of the 26S proteasome by peptide mimics of the coiled-coil region of its ATPase subunits. *Biochem Biophys Res Commun* **468**, 143–150 (2015).
272. Lim, H. S., Cai, D., Archer, C. T. & Kodadek, T. Periodate-Triggered Cross-Linking Reveals Sug2/Rpt4 as the Molecular Target of a Peptoid Inhibitor of the 19S Proteasome Regulatory Particle. *J Am Chem Soc* **129**, 12936 (2007).
273. Sandu, C. *et al.* Thiostrepton interacts covalently with Rpt subunits of the 19S proteasome and proteasome substrates. *J Cell Mol Med* **19**, 2181–2192 (2015).
274. Shi, Y. *et al.* Ibrutinib inactivates BMX-STAT3 in glioma stem cells to impair malignant growth and radioresistance. *Sci Transl Med* **10**, (2018).
275. Kim, E. *et al.* Ibrutinib inhibits pre-BCR+ B-cell acute lymphoblastic leukemia progression by targeting BTK and BLK. *Blood* **129**, 1155–1165 (2017).
276. Dubovsky, J. A. *et al.* Ibrutinib is an irreversible molecular inhibitor of ITK driving a Th1-selective pressure in T lymphocytes. *Blood* **122**, 2539 (2013).

277. Kaptein, A. *et al.* Potency and Selectivity of BTK Inhibitors in Clinical Development for B-Cell Malignancies. *Blood* **132**, 1871–1871 (2018).
278. Di Paolo, J. A. *et al.* Specific Btk inhibition suppresses B cell– and myeloid cell–mediated arthritis. *Nature Chemical Biology 2010 7:1* **7**, 41–50 (2010).
279. Crawford, J. J. *et al.* Discovery of GDC-0853: A Potent, Selective, and Noncovalent Bruton's Tyrosine Kinase Inhibitor in Early Clinical Development. *J Med Chem* **61**, 2227–2245 (2018).
280. Chou, T. C. Drug combination studies and their synergy quantification using the Chou-Talalay method. *Cancer Res* **70**, 440–446 (2010).
281. Sato, K., Rajendra, E. & Ohta, T. The UPS: A promising target for breast cancer treatment. *BMC Biochem* **9**, 1–8 (2008).
282. Petrocca, F. *et al.* A Genome-wide siRNA Screen Identifies Proteasome Addiction as a Vulnerability of Basal-like Triple-Negative Breast Cancer Cells. *Cancer Cell* **24**, 182–196 (2013).
283. Mitsiades, N. *et al.* Molecular sequelae of proteasome inhibition in human multiple myeloma cells. *Proc Natl Acad Sci U S A* **99**, 14374–14379 (2002).
284. Wiita, A. P. *et al.* Global cellular response to chemotherapy-induced apoptosis. *Elife* **2013**, e01236–e01236 (2013).
285. Awasthi, N. & Wagner, B. J. Upregulation of Heat Shock Protein Expression by Proteasome Inhibition: An Antiapoptotic Mechanism in the Lens. *Invest Ophthalmol Vis Sci* **46**, 2082–2091 (2005).
286. Shah, S. P., Lonial, S. & Boise, L. H. When Cancer Fights Back: Multiple Myeloma, Proteasome Inhibition, and the Heat Shock Response. *Mol Cancer Res* **13**, 1163 (2015).
287. Bush, K. T., Goldberg, A. L. & Nigam, S. K. Proteasome inhibition leads to a heat-shock response, induction of endoplasmic reticulum chaperones, and thermotolerance. *J Biol Chem* **272**, 9086–9092 (1997).
288. Catley, L. *et al.* Aggresome induction by proteasome inhibitor bortezomib and alpha-tubulin hyperacetylation by tubulin deacetylase (TDAC) inhibitor LBH589 are synergistic in myeloma cells. *Blood* **108**, 3441–3449 (2006).
289. Mi, L., Gan, N. & Chung, F. L. Aggresome-like structure induced by isothiocyanates is novel proteasome-dependent degradation machinery. *Biochem Biophys Res Commun* **388**, 456 (2009).
290. Zhang, C. *et al.* Autophagic sequestration of SQSTM1 disrupts the aggresome formation of ubiquitinated proteins during proteasome inhibition. *Cell Death & Disease 2022 13:7* **13**, 1–15 (2022).
291. Cha-Molstad, H. *et al.* Amino-terminal arginylation targets endoplasmic reticulum chaperone BiP for autophagy through p62 binding. *Nat Cell Biol* **17**, 917–929 (2015).
292. Liu, W. J. *et al.* p62 links the autophagy pathway and the ubiqutin-proteasome system upon ubiquitinated protein degradation. *Cell Mol Biol Lett* **21**, 1–14 (2016).
293. Shim, S. M. *et al.* The endoplasmic reticulum-residing chaperone BiP is short-lived and metabolized through N-terminal arginylation. *Sci Signal* **11**, (2018).
294. Milan, E. *et al.* A plastic SQSTM1/p62-dependent autophagic reserve maintains proteostasis and determines proteasome inhibitor susceptibility in multiple myeloma cells. *Autophagy* **11**, 1161–1178 (2015).
295. Kumar, A. V., Mills, J. & Lapierre, L. R. Selective Autophagy Receptor p62/SQSTM1, a Pivotal Player in Stress and Aging. *Front Cell Dev Biol* **10**, 793328 (2022).

296. Sha, Z., Schnell, H. M., Ruoff, K. & Goldberg, A. Rapid induction of p62 and GABARAPL1 upon proteasome inhibition promotes survival before autophagy activation. *J Cell Biol* **217**, 1757–1776 (2018).
297. Kuusisto, E., Suuronen, T. & Salminen, A. Ubiquitin-Binding Protein p62 Expression Is Induced during Apoptosis and Proteasomal Inhibition in Neuronal Cells. *Biochem Biophys Res Commun* **280**, 223–228 (2001).
298. Sha, Z., Schnell, H. M., Ruoff, K. & Goldberg, A. Rapid induction of p62 and GABARAPL1 upon proteasome inhibition promotes survival before autophagy activation. *Journal of Cell Biology* **217**, 1757–1776 (2018).
299. Yang, H. *et al.* The role of cellular reactive oxygen species in cancer chemotherapy. *J Exp Clin Cancer Res* **37**, (2018).
300. Papa, L., Gomes, E. & Rockwell, P. Reactive oxygen species induced by proteasome inhibition in neuronal cells mediate mitochondrial dysfunction and a caspase-independent cell death. *Apoptosis* **12**, 1389–1405 (2007).
301. Lipchick, B. C., Fink, E. E. & Nikiforov, M. A. Oxidative stress and proteasome inhibitors in multiple myeloma. *Pharmacol Res* **105**, 210–215 (2016).
302. Park, W. H. & Kim, S. H. MG132, a proteasome inhibitor, induces human pulmonary fibroblast cell death via increasing ROS levels and GSH depletion. *Oncol Rep* **27**, 1284 (2012).
303. Pérez-Galán, P. *et al.* The proteasome inhibitor bortezomib induces apoptosis in mantle-cell lymphoma through generation of ROS and Noxa activation independent of p53 status. *Blood* **107**, 257–264 (2006).
304. Nikiforov, M. A. *et al.* Tumor cell-selective regulation of NOXA by c-MYC in response to proteasome inhibition. *Proc Natl Acad Sci U S A* **104**, 19488–19493 (2007).
305. Qin, J. Z. *et al.* Proteasome Inhibitors Trigger NOXA-Mediated Apoptosis in Melanoma and Myeloma Cells. *Cancer Res* **65**, 6282–6293 (2005).
306. Craxton, A. *et al.* NOXA, a sensor of proteasome integrity, is degraded by 26S proteasomes by an ubiquitin-independent pathway that is blocked by MCL-1. *Cell Death & Differentiation 2012 19:9* **19**, 1424–1434 (2012).
307. Baou, M. *et al.* Role of NOXA and its ubiquitination in proteasome inhibitor-induced apoptosis in chronic lymphocytic leukemia cells. *Haematologica* **95**, 1510–1518 (2010).
308. Magnaghi, P. *et al.* Covalent and allosteric inhibitors of the ATPase VCP/p97 induce cancer cell death. *Nat Chem Biol* **9**, 548–559 (2013).
309. Anderson, D. J. *et al.* Targeting the AAA ATPase p97 as an Approach to Treat Cancer through Disruption of Protein Homeostasis. *Cancer Cell* **28**, 653–665 (2015).
310. Skrott, Z. *et al.* Alcohol-abuse drug disulfiram targets cancer via p97 segregase adaptor NPL4. *Nature* **552**, 194–199 (2017).
311. Szczęśniak, P. P., Heidelberger, J. B., Serve, H., Beli, P. & Wagner, S. A. VCP inhibition induces an unfolded protein response and apoptosis in human acute myeloid leukemia cells. *PLoS One* **17**, e0266478 (2022).
312. Kors, S. Regulation of Proteasome Activity by (Post-)transcriptional Mechanisms. *Front Mol Biosci* **6**, 452008 (2019).
313. Lokireddy, S., Kukushkin, N. V. & Goldberg, A. L. cAMP-induced phosphorylation of 26S proteasomes on Rpn6/PSMD11 enhances their activity and the degradation of misfolded proteins. *Proc Natl Acad Sci U S A* **112**, E7176–E7185 (2015).

314. Chen, L. *et al.* Proteasome regulation by reversible tyrosine phosphorylation at the membrane. *Oncogene 2021 40:11* **40**, 1942–1956 (2021).
315. VerPlank, J. J. S. & Goldberg, A. L. Exploring the regulation of proteasome function by subunit phosphorylation. *Methods Mol Biol* **1844**, 309 (2018).
316. VerPlank, J. J. S. & Goldberg, A. L. Regulating Protein Breakdown Through Proteasome Phosphorylation. *Biochem J* **474**, 3355 (2017).
317. Ibtisam, I. & Kisselev, A. F. Recovery of proteasome activity in cells pulse-treated with proteasome inhibitors is independent of DDI2. *bioRxiv* 2023.08.03.550647 (2023) doi:10.1101/2023.08.03.550647.
318. Kisselev, A. F., Akopian, T. N., Castillo, V. & Goldberg, A. L. Proteasome Active Sites Allosterically Regulate Each Other, Suggesting a Cyclical Bite-Chew Mechanism for Protein Breakdown. *Mol Cell* **4**, 395–402 (1999).
319. Kisselev, A. F. *et al.* The caspase-like sites of proteasomes, their substrate specificity, new inhibitors and substrates, and allosteric interactions with the trypsin-like sites. *J Biol Chem* **278**, 35869–35877 (2003).
320. Deshmukh, F. K. *et al.* Allosteric regulation of the 20S proteasome by the Catalytic Core Regulators (CCRs) family. *Nature Communications 2023 14:1* **14**, 1–24 (2023).
321. Zeng, G. *et al.* Recent advances and future perspectives of noncompetitive proteasome inhibitors. *Bioorg Chem* **135**, 106507 (2023).
322. Osmulski, P. A. & Gaczynska, M. Rapamycin allosterically inhibits the proteasome. *Mol Pharmacol* **84**, 104–113 (2013).
323. Kisselev, A. F., Callard, A. & Goldberg, A. L. Importance of the Different Proteolytic Sites of the Proteasome and the Efficacy of Inhibitors Varies with the Protein Substrate *. *Journal of Biological Chemistry* **281**, 8582–8590 (2006).
324. Niewerth, D. *et al.* Antileukemic activity and mechanism of drug resistance to the marine Salinispora tropica proteasome inhibitor salinosporamide A (Marizomib). *Mol Pharmacol* **86**, 12–19 (2014).
325. Verbrugge, S. E. *et al.* Inactivating PSMB5 mutations and P-glycoprotein (multidrug resistance-associated protein/ATP-binding cassette B1) mediate resistance to proteasome inhibitors: ex vivo efficacy of (immuno)proteasome inhibitors in mononuclear blood cells from patients with rheumatoid arthritis. *J Pharmacol Exp Ther* **341**, 174–182 (2012).
326. Franke, N. E. *et al.* Impaired bortezomib binding to mutant β5 subunit of the proteasome is the underlying basis for bortezomib resistance in leukemia cells. *Leukemia* **26**, 757–768 (2012).
327. De Wilt, L. H. A. M. *et al.* Proteasome-based mechanisms of intrinsic and acquired bortezomib resistance in non-small cell lung cancer. *Biochem Pharmacol* **83**, 207–217 (2012).
328. Geurink, P. P. *et al.* Incorporation of non-natural amino acids improves cell permeability and potency of specific inhibitors of proteasome trypsin-like sites. *J Med Chem* **56**, 1262–1275 (2013).
329. Kerr, I. D. *et al.* Vinyl Sulfones as Antiparasitic Agents and a Structural Basis for Drug Design. *Journal of Biological Chemistry* **284**, 25697–25703 (2009).
330. Chaparro, J. D. *et al.* Two key cathepsins, TgCPB and TgCPL, are targeted by the vinyl sulfone inhibitor K11777 in in vitro and in vivo models of toxoplasmosis. *PLoS One* **13**, (2018).

331. Jílková, A. *et al.* Druggable Hot Spots in the Schistosomiasis Cathepsin B1 Target Identified by Functional and Binding Mode Analysis of Potent Vinyl Sulfone Inhibitors. *ACS Infect Dis* **7**, 1077–1088 (2021).
332. Palmer, J. T., Rasnick, D., Klaus, J. L. & Brömme, D. Vinyl Sulfones as Mechanism-Based Cysteine Protease Inhibitors. *J Med Chem* **38**, 3193–3196 (1995).
333. Kraus, M. *et al.* The novel β2-selective proteasome inhibitor LU-102 synergizes with bortezomib and carfilzomib to overcome proteasome inhibitor resistance of myeloma cells. *Haematologica* **100**, 1350–1360 (2015).
334. Mirabella, A. C. *et al.* Specific cell-permeable inhibitor of proteasome trypsin-like sites selectively sensitizes myeloma cells to bortezomib and carfilzomib. *Chem Biol* **18**, 608–618 (2011).
335. Besse, A. *et al.* Proteasome Inhibition in Multiple Myeloma: Head-to-Head Comparison of Currently Available Proteasome Inhibitors. *Cell Chem Biol* **26**, 340-351.e3 (2019).
336. Di Paolo, J. A. *et al.* Specific Btk inhibition suppresses B cell– and myeloid cell–mediated arthritis. *Nature Chemical Biology 2010 7:1* **7**, 41–50 (2010).
337. Gu, C. *et al.* BTK suppresses myeloma cellular senescence through activating AKT/P27/Rb signaling. *Oncotarget* **8**, 56858–56867 (2017).
338. Palazzo, A. F. & Gregory, T. R. The Case for Junk DNA. *PLoS Genet* **10**, e1004351 (2014).
339. Dai, X., Kaushik, A. C. & Zhang, J. The emerging role of major regulatory RNAs in cancer control. *Frontiers in Oncology* vol. 9 Preprint at https://doi.org/10.3389/fonc.2019.00920 (2019).
340. Huang, Z. hao, Du, Y. ping, Wen, J. tao, Lu, B. feng & Zhao, Y. snoRNAs: functions and mechanisms in biological processes, and roles in tumor pathophysiology. *Cell Death Discovery 2022 8:1* **8**, 1–10 (2022).
341. Williams, G. T. & Farzaneh, F. Are snoRNAs and snoRNA host genes new players in cancer? *Nat Rev Cancer* **12**, 84–88 (2012).
342. Bratkovič, T., Bozič, J. & Rogelj, B. Functional diversity of small nucleolar RNAs. *Nucleic Acids Res* **48**, 1627–1651 (2020).
343. Huang, Z. hao, Du, Y. ping, Wen, J. tao, Lu, B. feng & Zhao, Y. snoRNAs: functions and mechanisms in biological processes, and roles in tumor pathophysiology. *Cell Death Discovery 2022 8:1* **8**, 1–10 (2022).
344. Carlile, T. M. *et al.* Pseudouridine profiling reveals regulated mRNA pseudouridylation in yeast and human cells. *Nature* **515**, 143 (2014).
345. Zhang, M. *et al.* A snoRNA–tRNA modification network governs codon-biased cellular states. *Proc Natl Acad Sci U S A* **120**, e2312126120 (2023).
346. Huang, C. *et al.* A snoRNA modulates mRNA 3′ end processing and regulates the expression of a subset of mRNAs. *Nucleic Acids Res* **45**, 8647 (2017).
347. Ronchetti, D. *et al.* The expression pattern of small nucleolar and small Cajal body-specific RNAs characterizes distinct molecular subtypes of multiple myeloma. *Blood Cancer J* **2**, 96 (2012).
348. Chu, L. *et al.* Multiple myeloma-associated chromosomal translocation activates orphan snoRNA ACA11 to suppress oxidative stress. *Journal of Clinical Investigation* **122**, 2793–2806 (2012).
349. Zhang, Z. *et al.* Long non-coding RNA SNHG17 promotes lung adenocarcinoma progression by targeting the microRNA-193a-5p/NETO2 axis. *Oncol Lett* **22**, (2021).

350. Liu, X., Zhang, B., Jia, Y. & Fu, M. SNHG17 enhances the malignant characteristics of tongue squamous cell carcinoma by acting as a competing endogenous RNA on microRNA-876 and thereby increasing specificity protein 1 expression. *Cell Cycle* **19**, 711–725 (2020).
351. Xu, T. *et al.* Gene Amplification-Driven Long Noncoding RNA SNHG17 Regulates Cell Proliferation and Migration in Human Non-Small-Cell Lung Cancer. *Mol Ther Nucleic Acids* **17**, 405–413 (2019).
352. Wang, W., Yu, S., Li, W., Hu, H. & Zou, G. Silencing of lncRNA SNHG17 inhibits the tumorigenesis of epithelial ovarian cancer through regulation of miR-485-5p/AKT1 axis. *Biochem Biophys Res Commun* **637**, 117–126 (2022).
353. Bai, M. *et al.* Long Non-coding RNA SNHG17 Promotes Cell Proliferation and Invasion in Castration-Resistant Prostate Cancer by Targeting the miR-144/CD51 Axis. *Front Genet* **11**, 513149 (2020).
354. Chen, W. *et al.* LncRNA SNHG17 regulates cell proliferation and invasion by targeting miR-338-3p/SOX4 axis in esophageal squamous cell carcinoma. *Cell Death & Disease 2021 12:9* **12**, 1–10 (2021).
355. Chen, L. L., He, J., Qiu, X. T., Yu, J. & Wang, Z. M. The prognostic roles of long non-coding RNA SNHG17 in the patients with gastric cancer. *Eur Rev Med Pharmacol Sci* **23**, 1063–1068 (2019).
356. Yuan, J. *et al.* Stable gene silencing of cyclin B1 in tumor cells increases susceptibility to taxol and leads to growth arrest in vivo. *Oncogene 2006 25:12* **25**, 1753–1762 (2005).
357. Gong, J. *et al.* A Pan-cancer Analysis of the Expression and Clinical Relevance of Small Nucleolar RNAs in Human Cancer. *Cell Rep* **21**, 1968–1981 (2017).
358. Xu, L. *et al.* Distinct Profiles for Mitochondrial t-RNAs and Small Nucleolar RNAs in locally invasive and metastatic colorectal cancer. *Clinical Cancer Research* **22**, 773–784 (2016).
359. Rouillard, A. D. *et al.* The harmonizome: a collection of processed datasets gathered to serve and mine knowledge about genes and proteins. *Database* **2016**, (2016).
360. Ibáñez-Cabellos, J. S. *et al.* Acute depletion of telomerase components DKC1 and NOP10 induces oxidative stress and disrupts ribosomal biogenesis via NPM1 and activation of the P53 pathway. *Biochimica et Biophysica Acta (BBA) - Molecular Cell Research* **1867**, 118845 (2020).
361. Sharma, E., Sterne-Weiler, T., O'Hanlon, D. & Blencowe, B. J. Global Mapping of Human RNA-RNA Interactions. *Mol Cell* **62**, 618–626 (2016).
362. McGee, S. R. *et al.* Expansion and mechanistic insights into de novo DEAF1 variants in DEAF1-associated neurodevelopmental disorders. *Hum Mol Genet* **32**, 386 (2023).
363. Manne, U. *et al.* Altered subcellular localization of suppressin, a novel inhibitor of cell-cycle entry, is an independent prognostic factor in colorectal adenocarcinomas. *Clinical Cancer Research* (2001).
364. Martin, F. *et al.* Ribosomal 18S rRNA base pairs with mRNA during eukaryotic translation initiation. *Nature Communications 2016 7:1* **7**, 1–7 (2016).
365. Linxweiler, M., Schick, B. & Zimmermann, R. Let's talk about Secs: Sec61, Sec62 and Sec63 in signal transduction, oncology and personalized medicine. *Signal Transduction and Targeted Therapy 2017 2:1* **2**, 1–10 (2017).

366. Bolar, N. A. *et al.* Heterozygous Loss-of-Function SEC61A1 Mutations Cause Autosomal-Dominant Tubulo-Interstitial and Glomerulocystic Kidney Disease with Anemia. *The American Journal of Human Genetics* **99**, 174–187 (2016).
367. Tretter, T. *et al.* ERAD and protein import defects in a sec61 mutant lacking ER-lumenal loop 7. *BMC Cell Biol* **14**, 1–14 (2013).
368. Sundaram, A., Plumb, R., Appathurai, S. & Mariappan, M. The Sec61 translocon limits IRE1α signaling during the unfolded protein response. *Elife* **6**, (2017).
369. Drexler, H. C. A. Activation of the cell death program by inhibition of proteasome function. *Proc Natl Acad Sci U S A* **94**, 855–860 (1997).
370. Holley, C. L. *et al.* Cytosolic Accumulation of Small Nucleolar RNAs (snoRNAs) Is Dynamically Regulated by NADPH Oxidase. *J Biol Chem* **290**, 11741 (2015).
371. Roth, P. *et al.* EORTC 1709/CCTG CE.8: A phase III trial of marizomib in combination with temozolomide-based radiochemotherapy versus temozolomide-based radiochemotherapy alone in patients with newly diagnosed glioblastoma. *https://doi.org/10.1200/JCO.2021.39.15_suppl.2004* **39**, 2004–2004 (2021).
372. Study Details | Phase I Study of Marizomib + Panobinostat for Children With DIPG | ClinicalTrials.gov. https://clinicaltrials.gov/study/NCT04341311.
373. Hsu, H. C., Wang, J., Kjellgren, A., Li, H. & DeMartino, G. N. High-resolution structure of mammalian PI31–20S proteasome complex reveals mechanism of proteasome inhibition. *Journal of Biological Chemistry* **299**, 104862 (2023).
374. Rawson, S. *et al.* Yeast PI31 inhibits the proteasome by a direct multisite mechanism. *Nature Structural & Molecular Biology 2022 29:8* **29**, 791–800 (2022).
375. Lim, H. S., Archer, C. T. & Kodadek, T. Identification of a Peptoid Inhibitor of the Proteasome 19S Regulatory Particle. *J Am Chem Soc* **129**, 7750 (2007).
376. Lim, H. S., Cai, D., Archer, C. T. & Kodadek, T. Periodate-Triggered Cross-Linking Reveals Sug2/Rpt4 as the Molecular Target of a Peptoid Inhibitor of the 19S Proteasome Regulatory Particle. *J Am Chem Soc* **129**, 12936 (2007).
377. Yuan, T. *et al.* Inhibition of the PI3K/AKT signaling pathway sensitizes diffuse large B-cell lymphoma cells to treatment with proteasome inhibitors via suppression of BAG3. *Oncol Lett* **17**, 3719–3726 (2019).
378. Waxman, A. J. *et al.* Carfilzomib-Associated Cardiovascular Adverse Events: A Systematic Review and Meta-analysis. *JAMA Oncol* **4**, e174519–e174519 (2018).
379. Onoguchi-Mizutani, R. & Akimitsu, N. Long noncoding RNA and phase separation in cellular stress response. *The Journal of Biochemistry* **171**, 269–276 (2022).
380. Campos-Melo, D., Hawley, Z. C. E., Droppelmann, C. A. & Strong, M. J. The Integral Role of RNA in Stress Granule Formation and Function. *Front Cell Dev Biol* **9**, 621779 (2021).
381. Zhang, X. *et al.* Cell-Type-Specific Alternative Splicing Governs Cell Fate in the Developing Cerebral Cortex. *Cell* **166**, 1147-1162.e15 (2016).
382. Belluti, S., Rigillo, G. & Imbriano, C. Transcription Factors in Cancer: When Alternative Splicing Determines Opposite Cell Fates. *Cells* **9**, (2020).
383. Robak, P. *et al.* The Prognostic Value of Whole-Blood PSMB5, CXCR4, POMP, and RPL5 mRNA Expression in Patients with Multiple Myeloma Treated with Bortezomib. *Cancers (Basel)* **13**, 1–17 (2021).

Appendix: Supplementary Figures

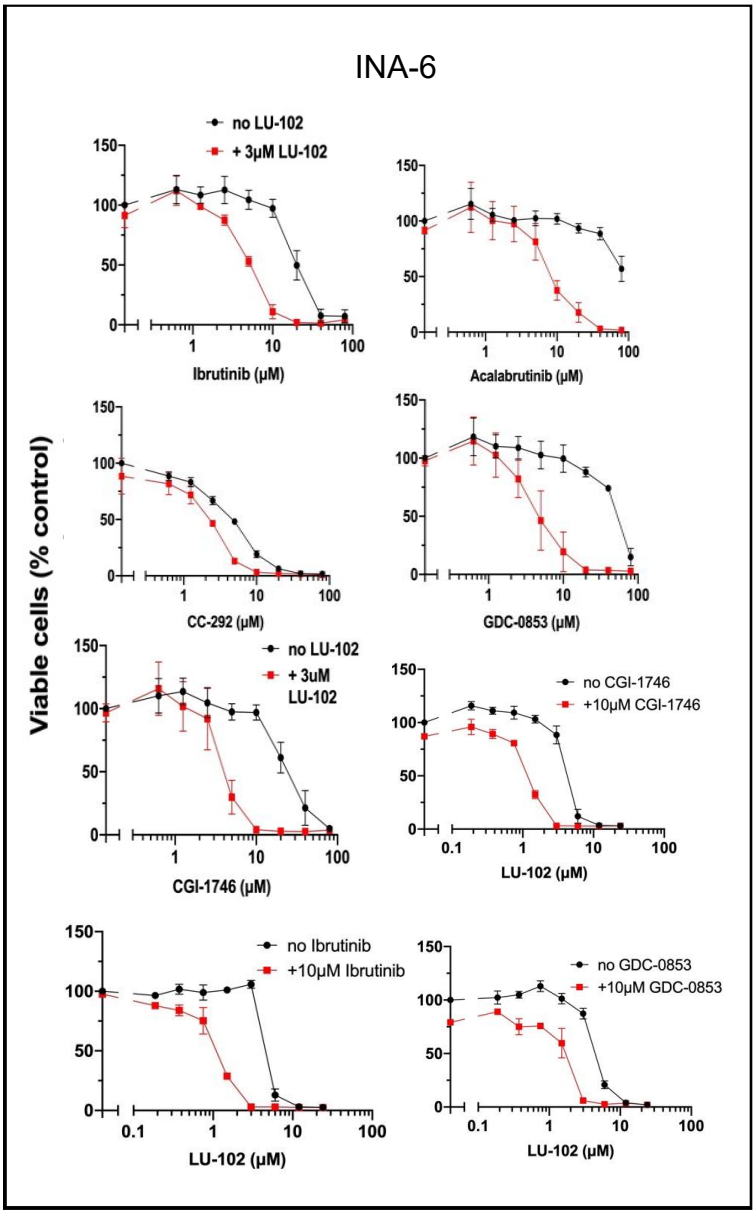

Figure S3. 1 Related to Fig. 3.1
Raw data for Fig. 3.1

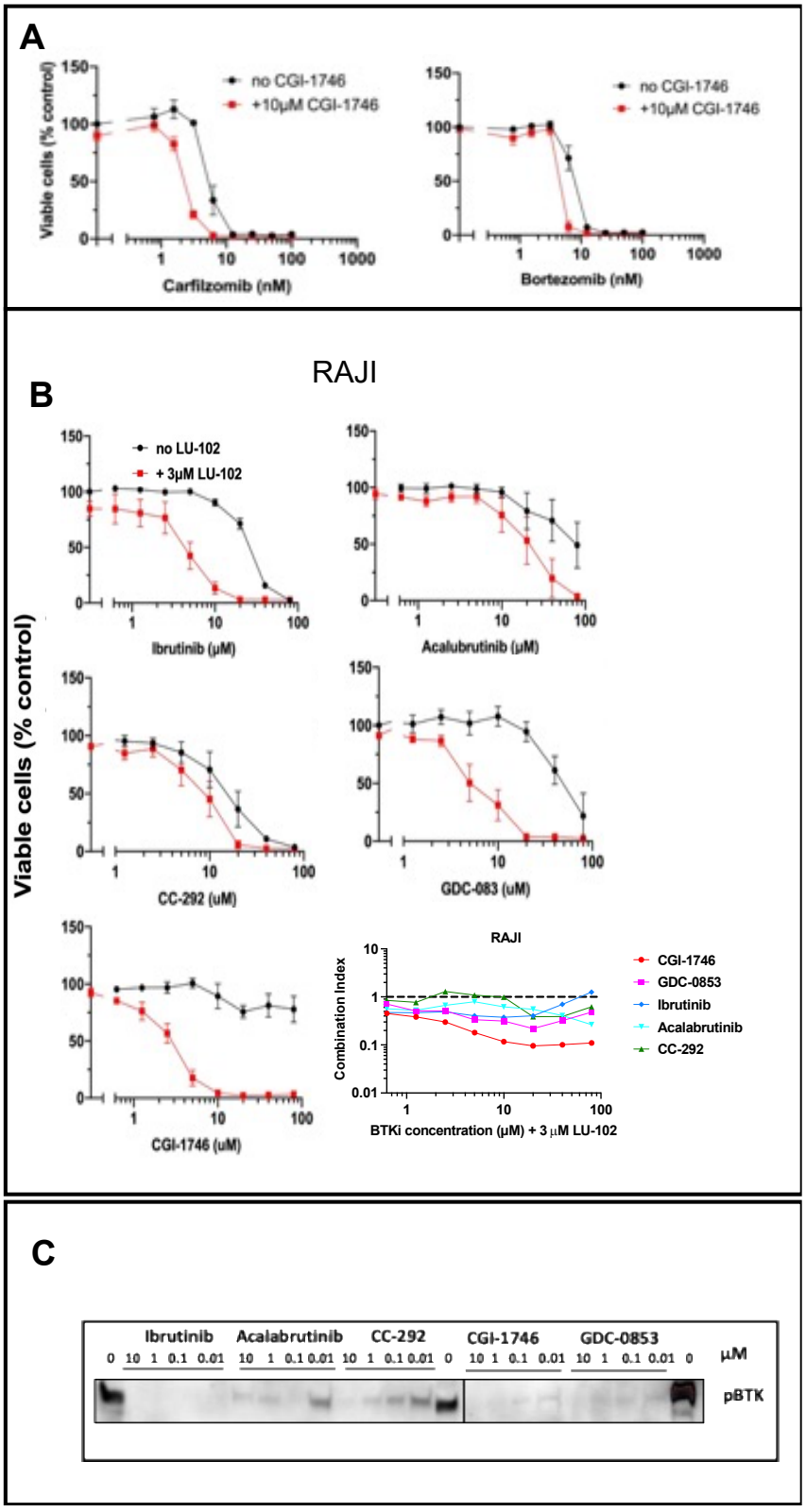

Figure S3. 2 Related to Fig. 3.2

(A) Raw data for Fig. 3.2a.
(B) BTK-expressing Burkitt's lymphoma cells, RAJI, were treated with BTK inhibitors (ibrutinib, acalabrutinib, CC-292, CGI-1746, and GDC-0853) alone and in combination with a sub-toxic dose of proteasome β2-site specific inhibitor, LU-102 at indicated concentrations for 48 hours, after which viability was determined by Alamar Blue dye conversion. Synergy was determined by combination index calculations using CalcuSyn (Synergy < 1, Antagonism > 1, Additive = 1).
(C) Western Blot shows that all BTK inhibitors tested inhibited BTK activity in RAJI cells treated for 2 hours at very low concentrations.

.

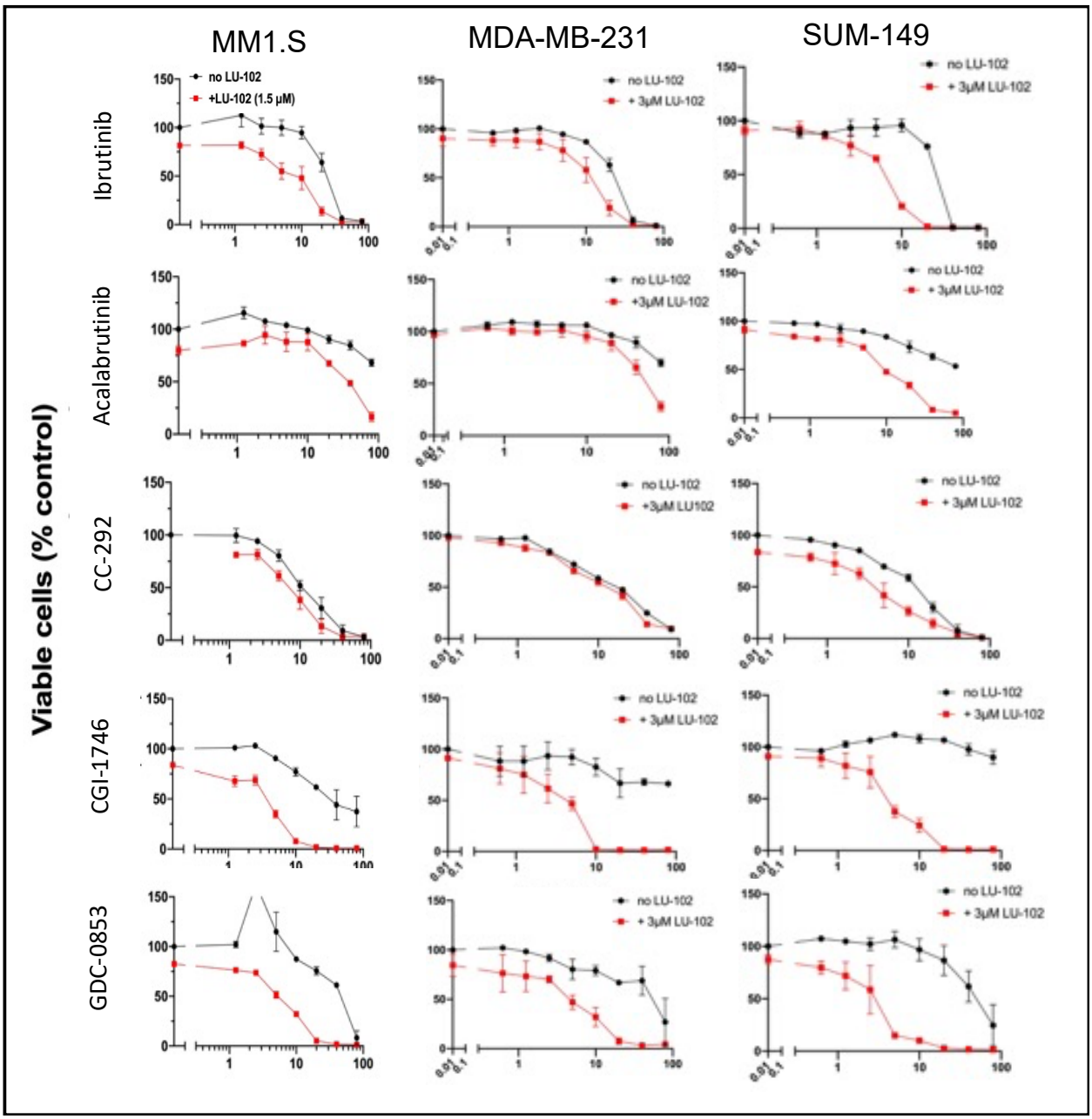

Figure S3. 3 Related to Fig. 3.3
Raw data for Fig. 3.3b.

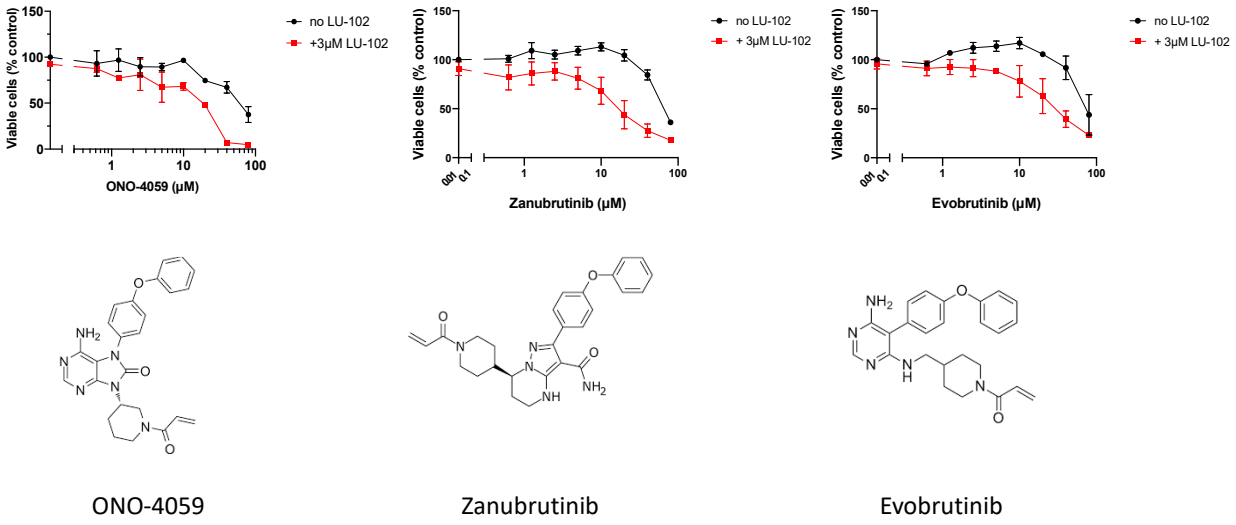

Figure S3. 4 Other BTK inhibitors synergize with LU-102.
Top: MDA-MB-231 cells treated with BTK inhibitors Zanubrutinib, and Evobrutinib, were tested in combination with 3 μM LU-102 for 48 hours and analyzed by Alamar Blue assay. Bottom: Structures of the BTK inhibitors used.

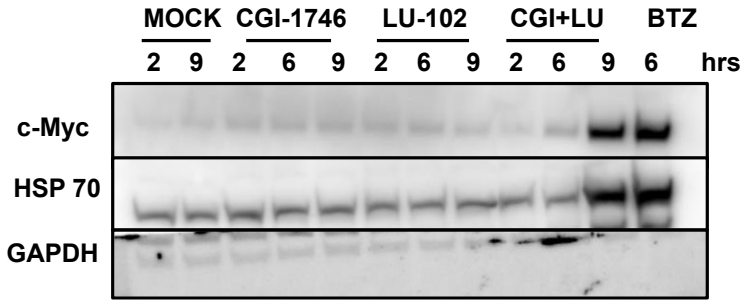

Figure S3. 5 c-Myc and HSP70 are upregulated upon treatment with a combination of CGI-1746 and LU-102.
MDA-MB-231 cells were treated with 20 μM CGI-1746, 3 μM LU-102, or 25 nM bortezomib. At the time points indicated, cells were harvested, and western blotting was performed to determine protein expression.

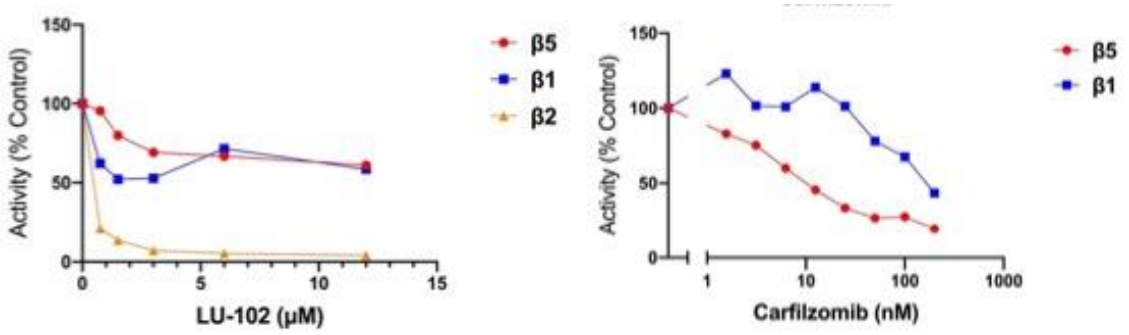

Figure S4. 1 LU-102 and Carfilzomib are specific for the β2 site and the β5 site of the proteasome, respectively, at low concentrations.
MDA-MB-231 cells were treated with the indicated concentrations of LU-102 (left) or carfilzomib (right) for 1 hour. Proteasome activity was determined by proteolytic cleavage of site-specific substrates.

Table S1 SNORA71D is the most upregulated transcript in cells treated with proteasome inhibitors.

Treatment	Gene Symbol	p-value	Fold Change
CGI-1746 vs MOCK	SNORA71D	2.79E-01	5.94
LU-102 vs MOCK	SNORA71D	2.36E-01	6.90
CGI+LU vs MOCK	SNORA71D	9.57E-02	13.87

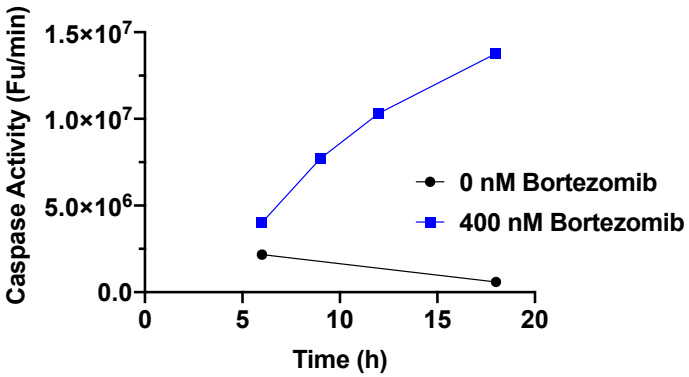

Figure S5. 1 Caspase activation in INA-6 cells upon bortezomib treatment.
INA-6 cells were pulse-treated with 400 nM bortezomib or DMSO. Cells were collected at time points after the start of treatment as indicated. Caspase activity was determined by cleavage of fluorescent substrate.